Structure and Dynamics of the Encephalomyocarditis virus Leader Protein in Deregulation of Host Nucleocytoplasmic Transport.

by

Valjean R. Bacot-Davis

A dissertation submitted in partial fulfillment of

the requirements for the degree of

Doctor of Philosophy

Microbiology

at the

University of Wisconsin-Madison

2014

Date of final oral examination: 07/30/14

The dissertation is approved by the following members of the Final Oral Committee:

Ann C. Palmenberg, Professor, Biochemistry
Katrina T. Forest, Professor, Bacteriology
Margaret J. McFall-Ngai, Professor, Medical Microbiology & Imunology
Robert F. Kalejta, Associate Professor, Molecular Virology and Oncology
Robert T. Striker, Associate Professor, Medical Microbiology & Immunology

Acknowledgements

Dr. Ann C. Palmenberg

For her constant support, advice, and guidance over my graduate school career.

Dr. Katrina Forest, Dr. Robert Kalejta, Dr. Margaret McFall-Ngai, Dr. Robert Striker,

For their critiques and recommendations that enhanced the quality of my research.

Dr. John Markley, Dr. Claudia Cornilescu, Dr. W. Milo Westler

For NMR training, advice, and collaboration on the structure of L_{MENGO} and Ran.

The Palmenberg Lab (current and past members); Marchel Hill, Dr. Holly Basta, Jessica Ciomperlik, Ryan Petty, Dr. Kelly Watters, Dr. Bradley Brown, Dr. Frederick Porter, Ashley Sacramo,

For camaraderie and being outstanding workmates.

Christa Lowe,

For her unfailing assistance, reassurance, fortitude, and love.

Table of Contents

Abstract

Structure and Dynamics of the Encephalomyocarditis virus Leader Protein in Deregulation of Host Nucleocytoplasmic Transport.

Valjean R. Bacot-Davis

Under the supervision of Professor Ann C. Palmenberg

At the University of Wisconsin-Madison

Determination of the 3D structural interfaces of diverse pathogen-host protein-protein interactions have elucidated many mechanisms involved in cellular biology and guided pharmacological drug development. Numerous virus families, including *Picornaviridae*, modulate the transport of proteins and RNA between the cytoplasm and nucleoplasm in order to inhibit the antiviral interferon (IFN) and NFκB pathways. Multiple studies have shown that the major immune modulatory functions of the Cardiovirus genus of *Picornaviridae* map to the activities of its Leader (L) protein. Nevertheless, the diverse activities attributed to L function have left its mechanism of action ambiguous. In this thesis, we sought to determine the structure of the L protein bound to the cellular factor Ran GTPase as well as the role of the L-Ran complex, L phosphorylation, and additional L binding partners in L coordinated deregulation of nucleocytoplasmic transport and nucleoporin hyperphosphorylation.

Mutagenesis and pulldown studies identified the L “hinge motif” (residues 31-41) in formation of the L-Ran interface. Further mutagenesis also identified the Ran GTPase C-terminus and acidic-tail as significant in L-Ran formation. Additionally, the L-Ran

complex accelerated L-directed hyperphosphorylation of the F-G nucleoporin Nup62, which correlates with host immune inhibition and increased viral replication.

Nuclear magnetic resonance was subsequently used to solve the three-dimensional structures of nucleotide-free Ran GTPase; Mengovirus L; Ran GTPase bound to Mengovirus L; Mengovirus L bound to Ran GTPase; and two phospho-isoforms of Mengovirus L, L1P and L2P. The three-dimensional structure of Ran GTPase revealed that, even in the absence of a guanosine nucleotide, Ran GTPase maintains a stable GDP-bound conformation. The three-dimensional structures of Mengovirus L revealed a largely flexible, random coil protein conformation, with the exception of a stable zinc-finger α-helix, which is crucial for proper L protein folding. L interactions with Ran GTPase stabilized the α-helix of the L zinc-finger, placed the L hinge motif (residues 29-41) in contact with the C-terminus of Ran GTPase, and also stabilized Ran GTPase into a -GTP core conformation. Phosphorylation of L Y_{41} and T_{47} caused an entropy transition in the L protein, increasing secondary structure stability of the L zinc-finger α-helix (α1), and enhancing L interactions with the export karyopherin, Crm1. Lastly, L was also found to interact directly with HRas GTPase, RanGAP and acts as a competitive binding inhibitor of RanBP1.

We propose that L-Ran interacts with various karyopherin β protein family members, such as Crm1, to select karyopherins carrying the ERK and RSK kinases. Here, this L-Ran-Karyopherin-ERK/RSK quaternary complex becomes localized around the nuclear pore complex due to L interactions with RanGAP. This L-directed mislocalization of the ERK and RSK kinases drives hyperphosphorylation of FG nucleoporins, resulting in the deregulation of innate immunity, and effective EMCV propagation.

List of Figures

List of Tables

Appendices

List of Abbreviations

aa	Amino acid
Ad	Adenovirus
ASA	Accessible surface area
BSA	Buried surface area
CA	Capsid
CAS	Cellular apoptosis susceptibility protein
CBB	Coomassie brilliant blue
cDNA	Complimentary DNA
CK2	Casein kinase 2
CNS	Central nervous system
CREB	cAMP response element binding protein
Crm1	Chromosome region maintenance 1
DE	Acidic-tail
EBOV	Ebola virus
EBV	Epstein-Barr virus
EMCV	Encephalomyocarditis virus
ERK	Extracellular signa-regulated kinases
F-G	Phenylalanine-glycine
FRET	Förster resonance energy transfer
GAP	GTPase-activating protein
GBL	Guanine-binding loop
GEF	Guanine nucleotide exchange factor
GI	Gastrointestinal
gRNA	Viral genomic RNA
HPLC	High-performance liquid chromatography
HPV	Human papilloma virus
HSQC	Heteronuclear single quantum coherence
HSV	Herpes simplex virus
HTLV	Human T-lymphotropic virus
IFN	Interferon
IFN I	Interferon type I
IP	Immunoprecipitation
IPTG	Isopropyl-ß-D-thiogalactopyranoside
ITC	Isothermal titration calorimetry
JNK	Jun amino-terminal kinase
K_D	Dissociation constant
Kpn	Karyopherin
L	Leader
L0P	Unphosphorylated Leader
L1P	Leader incubated with CK2
L2P	Leader incubated with CK2 and SYK
LMP1	Latent membrane protein 1
MAPK	Mitogen-activated protein kinases

MEK	MAP kinase
MKK	MAP kinase kinase
MS	Mass spectrometry
NA	Neuraminidase
NCT	Nucleocytoplasmic transport
NES	Nuclear export signal
NFκB	Nuclear factor kappa-light-chain-enhancer of activated B cells
NLS	Nuclear localization signal
NMR	Nuclear magnetic resonance
NOESY	Nuclear Overhauser effect
NP	Nucleoporin
NPC	Nuclear pore complex
nsp	Non-structural protein
NTF2	Nuclear transport factor 2
Nup	Nucleoporin
PB1	Ribonuclear protein 2
PIC	Pre-integration complex
PKC	Protein Kinase C
PKR	Protein Kinase R
pL	Phosphorylated Leader
PT	Post-transfection
PTM	Posttranslational modification
RanBP1	Ran binding protein 1
RanBP2	Ran binding protein 2
RCC1	Regulator of chromosome condensation 1
RMSD	Root-mean-square deviation
SAFV	Human Saffold virus
SARS-CoV	Severe acute respiratory syndrome coronavirus
Sw	Switch
SYK	Spleen tyrosine kinase
TKR	Tyrosine kinase receptor
TMEV	Theiler’s encephalomyelitis virus
TOCSY	Total correlated spectroscopy
VEEV	Venezuelan equine encephalitis virus
VSV	Vesicular stomatitis virus
WT	Wild-type

Chapter 1.

Introduction.

The virus family *Picornaviridae*

Picornaviruses are an extensive family of animal pathogens with a positive-sense, single-stranded RNA genome ranging in size from 7.0 (*Tremovirus*) -9.7 kb (*Megrivirus*) (1-4). There are currently 26 genera in the picornavirus family: *Aphthovirus* (FMDV), *Aquamavirus* (Aquamavirus A), *Avihepatovirus* (Duck hepatitis virus), *Avisivirus* (Avisivirus A), *Cardiovirus* (EMCV), *Cosavirus* (Human cosavirus), *Dicipivirus* (Cadicivirus A), *Enterovirus* (Rhinovirus), *Erbovirus* (Equine rhinitis B virus), *Gallivirus* (Gallivirus A), *Hepatovirus* (Hepatitis A virus), *Hunnivirus* (Hunnivirus A), *Kobuvirus* (Aichi virus), *Megrivirus* (Melegrivirus A), *Mischivirus* (Mishivirus A), *Mosavirus* (Mosavirus A), *Oscivirus* (Oscivirus A), *Parechovirus* (Human parechovirus), *Pasivirus* (Pasivirus A), *Passerivirus* (Passerivirus A), *Rosavirus* (Rosavirus A), *Salivirus* (Salivirus A), *Sapelovirus* (Porcine sapelovirus), Senecavirus (Seneca valley virus), *Teschovirus* (Porcine teschovirus), and *Tremovirus* (Avian encephalomyelitis virus)(5)(Table 1-1). The genome is divided into three sections: the 5'untranslated regions (5'UTR), the coding region, and the 3'untranslated region (3'UTR), which contains a poly(A) tail of several dozen adenosines. The picornavirus 5'UTR contains an internal ribosome entry site (IRES), which is a highly structured RNA segment of hundreds of nucleotides that mediates cap-independent translation of viral proteins. The 5' and 3' UTRs contain *cis*-elements that aid viral replication and RNA translation,

whereas the coding region is one long, open reading frame that directs ribosome synthesis of a large viral polyprotein that becomes co- and post-translationally processed into functional, mature viral proteins.

The picornavirus polyprotein encodes 11-14 mature protein products categorized into three sub-regions: P1, P2, and P3. The P1 region codes the viral structural proteins, which include the capsid polypeptides VP4, VP2, VP3, and VP1 (in this order). P2 contains the 2A, 2B, 2B* and 2C proteins, with various functions such as vesicle formation and inhibition of host translation. P3 encodes the 3A, 3B, 3C, and 3D proteins, which are involved in RNA replication, proteolytic processing of the viral polyprotein, and progeny release. Some picornavirus genera also encode a protein before the P1 region known as the Leader (L) protein, involved in inhibition of the host immune response and shut-off of host (m^7GpppN) cap-dependent translation. Many viral proteins are poly-functional, as protein labor division comes at a cost due to the instability of a large RNA genome as well as the high error rate inherent to RNA-dependent polymerases.

The *Cardio-, Aphtho-, Erbo-, Kobu-, Sapelo-*, *Seneca-* and *Teschovirus*es encode a Leader (L) protein preceding the P1 region. The aphthovirus and sapelovirus L proteins are papain-like proteases (L^{pro}) that release themselves from the viral polypeptide (L/P1 junction), and cleave eIF4G in order to inhibit cap-dependent translation. During the initiation of picornavirus polyprotein translation, the P1 region is rapidly released either by a ribosome skipping mechanism (*Cardio-, Aphtho-, Erbo-,* and *Teschovirus*es), or due to the proteolytic activity of 2A itself [$2A^{pro}$] (*Enteroviruses*) (6, 7). The functions of the 2B and 2C proteins are not well characterized in many species, but in some, are

involved in calcium signaling, vesicle formation, and inhibition of secretory pathways (8). 3A interacts with PI4KIIIβ as well as the golgi adaptor protein acyl coenzyme A (acyl-CoA) to obstruct intracellular transport (9, 10). 3B (Vpg) primes and protects the virus genome. $3C^{pro}$ is a trypsin-like protease that carries out the majority of processing cleavages of the picornavirus polyprotein. Finally, the 3D protein is the viral RNA-dependent RNA polymerase, which localizes to virus-induced membrane compartments where it replicates viral genomic RNA.

Receptor expression is a major determinant to virus-tissue tropism. The capsid binds a host receptor on the plasma membrane resulting in endocytosis of the virus particle, RNA delivery into the cytoplasm, and ribosome recruitment for viral protein synthesis (11). Membrane-bound replication complexes sequester double-stranded RNA products away from host innate pattern recognition receptors (PRRs). After RNA replication, hundreds of viral progeny particles assemble and are released by cellular lysis. However, should an anti-viral state become triggered, various picornavirus proteins (L, 2A, and 3C) have anti-host properties that limit this response, and have therefore been designated as “viral security proteins” (12) (Fig. 1-1).

The burden of picornavirus infection on animal and human health is billions of dollars world-wide, with the human rhinovirus costing the US economy $40 billion per year, and FMDV outbreaks costing the UK 3.1 billion £ per year (13). Picornavirus molecular studies have also led to vaccine developments (polio) and characterizations of host cellular pathways as a result of virus-host interactions. Furthermore, the Seneca valley virus (*Senecavirus*) and Poliovirus (*Enterovirus)* are currently in clinical trial as oncolytic

viruses (14); and the ability of several picornavirus proteins to target nucleocytoplasmic transport (L and $2A^{pro}$) have potentials in cancer therapy.

Nucleocytoplasmic Transport

Eukaryotic cells have specialized compartments known as organelles dedicated to particular cellular functions, such as metabolism (mitochondria), protein synthesis (endoplasmic reticulum), protein post-translational modification (endoplasmic reticulum and Golgi apparatus), and DNA transcription (nucleus). These organelles help to alleviate the smaller surface-to-volume ratio of eukaryotic cells in comparison to their prokaryotic counterparts. However, because these organelles are enclosed by a membrane lipid bilayer, energy-dependent, regulated transport is required to maintain an open and coordinated cellular system. As its name suggests, the nucleus (Greek: *caryon*) is the most distinguished, as well as conspicuous, organelle of the eukaryotic cell. The nucleus holds the cellular genomic DNA in a nucleoplasm separate from cellular contents in the cytoplasm. The nucleoplasm is connected to the cytoplasm by a massive, selectively permeable, 125 MDa protein complex known as the nuclear pore complex (NPC).

The bidirectional transport of molecules in and out of the nucleoplasm and cytoplasm is a continuous and rapid process, with one NPC capable of mediating 1,000 transport processes per second. With an average of 3,000 NPCs in a cellular nucleus, this amounts to 3 million nucleocytoplasmic transport events per second per cell (15). The NPC is composed of over 100 different proteins known as nucleoporins (Nups) in 8-fold

octagonal symmetry that allow hydrophilic molecules smaller than 9 nm to passively diffuse. The majority of protein and protein-RNA cargos larger than 40 kDa are restricted by the pores and require an energy gradient to actively drive their final localizations. The NPC has three domains: (1) cytoplasmic filaments (Nup358, Nup214, Nup98); (2) central channel (Nup62, Nup98, Rae1, Nup45, Nup54, Nup58); and (3) nuclear basket (Nup98, Rae1, Nup153, TPR, Nup50). Many Nups contain Phenylalanine-glycine (F-G) repeats, which are natively unfolded hydrophobic domains that directly contribute to NPC cargo selectivity (16). FG-Nups have differing distributions of three types of FG clusters: Phenylalanine-Glycine (F-G), Glycine-Leucine-Phenylalanine-Glycine (GLFG) or Phenylalanine-any-Phenylalanine-Glycine (FXFG). Well-characterized FG-Nups include Nup358, Nup214, Nup153, Nup98, Nup62, Nup58, Nup54, and Nup45 (Fig. 1-2).

Proteins containing short peptide sequences, typically 4-8 positively charged amino acids, known as *nuclear localization signals* (NLS) are recognized by receptors (importin karyopherins) and efficiently targeted to the cellular nucleus. In contrast, proteins containing short peptide sequences, typically 15 leucine-rich amino acids, known as *nuclear export signals (*NES) are transported and accumulate in the cellular cytoplasm (17-20). NES and NLS cargos are correctly delivered to their appropriate sub-cellular locations by interactions with dozens of proteins involved in nucleocytoplasmic transport. These proteins include the small GTPase Ran and its effectors RanGAP, RCC1, karyopherin receptors (importins and exportins), Ran binding proteins (RanBP1, RanBP2), CAS and NTF2 (21, 22). Ran cycling and its coordination by various cellular effectors and protein receptors will be further discussed.

Ran GTPase and Ran Effectors.

The *Ras*-related Nuclear protein, Ran, is a member of the small GTPase *Ras* superfamily. The three-dimensional protein structure of the *Ras* superfamily consists of an anti-parallel β-sheet core surrounded by α-helices. The Ras GTPase superfamily is divided into 5 branches based on both functionality and sequence: Ras, Rho, Rab, Ran, and Arf. These small GTPases function by binding a GTP nucleotide followed by catalyzing its hydrolysis into GDP through a binary molecular switch mechanism, where the GTP-bound form is the active "on" configuration, and the GDP-bound form is the inactive "off" configuration (23). The *Ras* superfamily share conserved protein motifs known as G boxes, which are involved in guanosine nucleotide binding and GDP/GTP sensor switching: G1, GXXXXGKS/T; G2, T; G3, DXXGQ/H/T; G4, T/NKXD; and G5, C/SAK/L/T (24, 25). The G1 (also known as the P-loop or Walker A motif), G2, and G3 boxes interact with the β and γ-phosphate atoms of GTP and GDP, and the G4 and G5 boxes are involved in guanine base recognition. Two protein domains undergo the most drastic structural changes associated with the protein's GTP-bound or GDP-bound state. These domains are called the switch I and switch II regions, and are also involved in reorienting residues that interact with Ran effector proteins and modulating Ran activity (26).

Ran GTPase is a 24 kDa protein of 216 amino acids that provides the energy gradient to drive the nuclear import and export of cargo molecules (proteins and RNA) in a process known a nucleocytoplasmic transport (NCT) (27). Ran GTPase functions

as a regulator of NCT over a spatial gradient, where Ran-GTP is concentrated in the nucleoplasm, and Ran-GDP in the cytoplasm. Importin proteins carrying NLS-cargos interact directly with the FG-repeats of Nups, and as they cross the NPC, Ran-GTP binds the importin receptor to dissociate the complex and deliver the NLS-cargo effectively into the nucleoplasm. The import process is a reversible reaction, and without Ran-GTP-importin associations, the complex diffuses back into the cytoplasm and results in failed NLS cargo delivery (25, 28). Similarly, NES-cargo bind exportin protein and Ran-GTP, and exportins interact directly with FG-Nups to carry the complex into the cytoplasm. Once in the cytoplasm, Ran-GTP hydrolysis into Ran-GDP strongly favors protein complex dissociation and effective delivery of the NES-cargo into the cytoplasm. The intrinsic GTPase activity of Ran is very slow, but Ran GTPase binding proteins and effectors maintain the Ran GDP/GTP concentrations that facilitate cycling and coordinate NCT (29). In addition to containing the G boxes, switch I and switch II domains, Ran GTPase is unique among the Ras GTPase superfamily in that it contains a C-terminal acidic tail (^{211}DEDDDL^{216}), and a basic patch region (^{139}HRKK^{142}). The acidic tail stabilizes Ran-GDP and interacts with various effectors using a C-terminal switch mechanism (30, 31).

The Ran Guanine Exchange Factor (GEF) known as RCC1 and the Ran GTPase-Activating Protein (GAP) referred to as RanGAP, maintain Ran GDP/GTP cycling. RCC1 is tethered to chromatin in the nucleus. RCC1 uses a β hairpin wedge (residues 146-156) to interact with the Ran GTPase P-loop and switch II region, resulting in the dissociation of GDP in exchange for GTP to generate Ran-GTP. RCC1-facilitated nucleotide exchange is a reversible reaction, but because GTP nucleotide levels are

higher in the nucleus, the Ran-GTP concentration gradient is highest in the nucleoplasm. In contrast, once Ran-GTP exits the nucleus, Ran-GTP interacts with its coactivators, RanGAP and Ran binding protein 1 (RanBP1). Jointly, RanGAP and RanBP1 stimulate the intrinsic hydrolase activity of Ran, converting Ran-GTP to Ran-GDP. The sumolylation of RanGAP concentrates the protein to the cytoplasmic fibrils on the NPC, where it binds directly to Ran binding protein 2 (RanBP2), also known as Nup358. The Nup358-RanGAP-RanBP1 complex maintain segregated, cytoplasmic Ran-GDP levels. The exclusive Ran GTPase import factor, NTF2, binds and brings Ran-GDP back into the nucleus for RCC1 interactions and maintenance of the cellular Ran GDP/GTP cycle.

Ran interacts with numerous receptors (importins, exportin, and transportins) that belong to the karyopherin protein families (from the Greek *karyon-pherein*, meaning nucleus-to carry to or from) (32). The Karyopherin β (Importin β) family includes prominent members such as CRM1 (Exportin 1), CAS (Exportin 2), Importin β, and Karyopherin β (33) (34). The Karyopherin α (Importin α) family includes many Importin α (Karyopherin α) proteins (35). Importin and many Transportin proteins recognize and bind the NLS peptide sequence of a cargo molecule. Once bound to their appropriate cargo, members of the Karyopherin family interact directly with FG-Nups of the NPC to carry out NCT(34) (Fig. 1-3).

Kinetic studies have been used to model the temporal sequence of NCT: (1) Firstly, karyopherin (importin) receptors interact with their NLS cargo with a very high affinity (Importin β-cargo dissociation constant (K_D) of 0.5-50nM) (36). (2) The heterodimer or heterotrimer importin-NLS complex is dissociated by the higher affinity of the importin

for nucleoplasmic Ran-GTP (K_D of 0.23-270nM) (37). (3) The Ran-GTP gradient is maintained in the nucleus through Ran-RCC1-chromatin generation of Ran-GTP (Ran-RCC1 K_D of 13-18 μM) (38). (4) The Ran-GTP-exportin-NES trimer crosses the NPC where cytoplasmic RanBP1 has a higher affinity for Ran-GTP over cytoplasmic Ran-GDP (Ran-GTP-RanBP1 K_D of 0.6nM versus Ran-GDP-RanBP1 of K_D of 4.6μM) (39). (5) RanGAP co-activates Ran-GTP hydrolysis to generate Ran-GDP, where RanGAP is 3.5-fold more efficient at generating Ran-GDP in conjunction with RanBP1 (Ran-GAP-BP1 K_D of 2μM) than without (Ran-GAP K_D of 7μM) (40). (6) Following Ran-GTP hydrolysis into Ran-GDP, the exportin-Ran-NES trimeric complex dissociates, releasing the NES cargo, and thereby completing the export process (34).

Cardioviruses

The Cardiovirus genus of Picornaviridae consists of two species: *Encephalomyocarditis virus* (EMCV) and *Theilovirus*. The EMCV species has a single serotype, a wide host range, and hundreds of different strains have been globally isolated (EMCV R, EMCV D, EMCV Mengo M); however, the majority of EMCV infections are isolated to the rodent population (41). The *Theilovirus* species currently contains three serotypes: *Theiler's murine encephalomyelitis virus* (TMEV), *Vilyuisk human encephalomyelitis virus* (VHEV), and human *Saffold virus* (SAFV). Although the natural hosts of Cardioviruses are mice, the novel human SAFV has been associated with gastroenteritis and paralysis (42, 43). Cardioviruses replicate in the gastrointestinal (GI) tract and transmit along the fecal-oral route. Cardiovirus infection can lead to

encephalomyelitis, chronic demyelinating disease resembling multiple sclerosis, and death (44). The amino acid sequence of EMCV and TMEV are 50% identical, with capsid identity being slightly higher at 62% (45).

Picornaviruses have four types of IRES structures that differ in secondary structure: Type I (*Enteroviruses*-Polio, Enterovirus 71), Type II (*Aphthoviruses*-FMDV, *Cardioviruses*-EMCV, TMEV), Type III (*Hepatoviruses*-Hepatitis A virus), and Type IV (*Teschoviruses*-porcine teschovirus). The type II IRES of picornaviruses relies on particular host proteins for translational efficiency: Polypyrimidine tract-binding protein (PTB), Neural polypyrimidine tract-binding protein (nPTB), Lupus autoantigen (La), and Poly(A)-binding protein (PABP). The type I IRES of picornaviruses, such a poliovirus, require additional translation factors, such as Nucleolin, Upstream of N-ras (Unr), and Poly(rC)-binding protein 1,2 (PCBP1, 2). PABP is required for normal translation initiation of capped mRNAs while noncanonical translation factors (PTB, La, PCB, Unr, Nucleolin) have more diverse cellular localizations and functions, such as nuclear splicing of pre-mRNAs (PTB), or RNA stabilization (La) (46).

Cardioviruses can replicate in a variety of different cells and tissue types, including macrophages and endothelial cells. *EMCV* currently appears to have a broader host range than *TMEV* species, even thought EMCVs only comprise one serotype (45). EMCV uses the VCAM-1 receptor expressed on vascular endothelial cells to initiate infection (47). Although the receptor for TMEV has not been determined, TMEV is believed to use a 34 kDa entry receptor, perhaps glycoprotein PO, and at least one co-receptor with a sialic acid moieties, such as integrin avβ3, for cellular entry (48, 49).

Picornavirus persistence has been linked to viral protein expression, cell cycle, and receptor expression (50).

The Cardiovirus polyprotein undergoes release of the P1 region by a ribosomal skipping mechanism after translation of the 2A protein, followed by a cleavage cascade carried out by the viral 3C protease ($3C^{pro}$) to generate 12-14 final protein products. Intermediate protein complexes have a short half-life, and many have specialized cellular functions (51). Their genome organization is evolutionarily conserved, with the accessory L protein followed by the capsid proteins (1A, 1B, 1C, and 1D), commonly known as VP4, VP2, VP3, and VP1, respectively. Encoded downstream of the structural proteins are the non-structural viral proteins: 2A, 2B, 2C, 3A, 3B, 3C, and 3D. The precursor of VP4 and VP2 is VP0, which undergoes its final cleavage step during capsid assembly using 60 capsid subunits for final virion infectivity and stability (52). Alternate start codons due to leaky ribosomal scanning and frameshifting among certain Cardiovirus species can generate L* (TMEV-DA) and 2B* (EMCV) proteins (53, 54). L* frameshifting has been postulated to play a regulatory role during viral infection in TMEV-DA persistence(55-57) (Fig. 1-4).

TMEV is classified into two subgroups: highly virulent GDVII and persistent TO. The GDVII subgroup includes the GDVII and FA stains, while the TO subgroup contains the DA, BeAn, TO, WW, Yale, and various other strains (58). The GDVII subgroup is highly virulent and causes symptoms resembling poliomyelitis in mice followed by death due to encephalomyelitis. GDVII neuropathology includes destruction of the spinal chord and motor neurons. In cell culture, the GDVII strains have larger plaque sizes in BHK-21 cells than do TO strains. In contrast, TO subgroups usually cause a biphasic disease

during mice infection. The first symptoms range from none to flaccid paralysis. Three weeks later, an inflammatory demyelinating disease develops that peaks at 6 weeks and continues for the remainder of the life of the mouse. The virus persists in microglia and oligodendrocytes of the central nervous system. Mice genetics are important in determining disease progression, with major histocompatibility complex (MHC) H-2 class I ($CD8^+$ and IFN-γ genes) being an important determinant of susceptibility to TMEV (59-61).

EMCV was first isolated from rodents in 1940 (Jungeblut and Sanders 1940) and later in 1945 from a captive male gibbon that died of pulmonary edema and myocarditis. The Mengovirus strain of EMCV was isolated in 1948 in Uganda from a captive rhesus monkey that developed hind limb paralysis, and serotyping determined that Mengovirus was in the same species as EMCV (62). The EMCV genome is 7.8 kb and covalently linked to the viral protein VPg (3B) at the 5' end. Upstream of the EMCV 5'UTR is a poly(C) tract of ~150 nucleotides whose length plays a critical role in EMCV pathogenesis (63). *Theiloviruses* do not have a poly (C) tract in their 5'UTR. Interestingly, *Apthoviruses* contain a poly (C) tract, so *Theiloviruses* either lost their poly (C) tract, or EMCV and *Apthoviruses* independently evolved these motifs. After internalization of the EMCV particle using the VCAM-1 host receptor, polyprotein translation commences (2.5-3 hours). Replication (3-4 hours), encapsidation, and cell lysis (4-6 hours) release viral progeny to continue replication in new hosts cells. EMCV virulence is not only determined by the length of the poly(C) tract, but also directed by several viral proteins: L, L*, 2A, and 2B*. The roles of the L, L*, and 2A proteins during EMCV infection will be discussed at length (62).

Saffold virus (SAFV) is a novel human Cardiovirus member of the *Theilovirus* species that was discovered in 2007 when isolated from children presenting symptoms of gastroenteritis, flaccid paralysis, and respiratory illness (42). While SAFV has not been decidedly associated with human disease, limited studies have associated it with serious illness in children, including meningitis, myocarditis, and encephalitis (64). Currently, eight genotypes of SAFV have been isolated, and their seroprevalences appear to be worldwide (SAFV-1, SAFV-2, SAFV-3, etc.) (65, 66).

The Cardiovirus L protein has become known as a "viral security protein", in that it is not absolutely required for viral replication but its inhibition of the innate immune response greatly enhances viral propagation. Thus, the major function of L is to counteract host anti-viral defenses. L is an 8kDa (EMCV L 67 amino acids; Theilovirus L 76 amino acids), highly acidic protein with an atypical amino-terminal zinc-finger (CHCC motif), and a carboxyl-terminal acidic motif enriched with D-E acidic residues. The EMCV and Theilovirus L proteins only share 35% amino acid identity (67). This lack of identity is due to two additional C-terminal motifs in the Theilovirus L protein downstream of its acidic motif: a Serine/Threonine-rich motif, and a Theilo motif (68). This configuration suggests that the N- and C-terminal domains cooperate for L activity. The EMCV L protein can be phosphorylated on residues T_{47} and Y_{41}, while the *Theilovirus* L proteins are likely phosphorylated at different sites using different kinases (69-71). Whereas the Cardiovirus L does not have direct enzymatic activity, it inhibits NCT and IFN production by binding directly to Ran-GTPase, inducing the hyperphosphorylation and sequential inactivation of Nups, and obstructing stress granule formation (72-78). It has been hypothesized that the EMCV and Theilovirus L

protein diverged to carry out the same activities at different rates, thus becoming optimized to use similar species host factors (67).

The persistent TMEV TO subgroup encodes a frame-shifted L protein called L*, which is absent in the highly virulent TMEV GDVII subgroup. L* has therefore been implicated as functioning in TMEV TO persistence, although its role in persistence remains controversial (55-57, 79, 80). L* is a 156 amino acid protein translated from an AUG start-codon 13 nucleotides downstream of the L initiation codon ending in the VP2-encoding region (81). This AUG in the GDVII subgroup has been substituted with ACG. L* is required for TMEV infection of macrophages and is solely expressed in neurons during the acute stage of infection (53, 82-84). This differential expression based upon cell type is believed to allow TMEV to evade the host immune response in macrophages, followed by initiating subsequent recurring infections in nearby neurons, leading to demyelination and MS-like symptoms in mice infected with the TMEV TO subgroup.

The 2A protein is a secondary Cardiovirus “security protein” (12). 2A is a 17kDa, 143 amino acid, highly basic protein (pI 10.3). However, unlike the *Enterovirus* genus, the *Cardiovirus* 2A protein has no proteolytic activity. The 2A-2B polyprotein junction is not proteolytically processed in *Cardioviruses*, but is released by a novel ribosome skipping mechanism induced by the NPG(P) peptide sequence in C-terminus of the 2A protein (85). This sequence is thought to either causes the ribosome to stall and not form a peptide bond with the Proline-tRNA, or to allow a water molecule to attack the weak peptide bond once formed. The activity of the *Cardiovirus* 2A protein has been associated with the shut-off of host protein synthesis (86). Several mechanisms have

been characterized for 2A inhibition of host mRNA translation: (1) induction of 4E-BP1 hypophosphorylation to reduce the assembly of eukaryotic initiation factors, (2) 2A interactions with eIF4E between 2A residues 126-136, which negatively affects the assembly of cap-dependent translation machinery, (3) associations with nascent ribosomal subunits in the nucleoli due to the 2A-NLS, and (4) 2A-40S ribosomal subunit associations (87-91). 2A also interacts non-specifically with RNA, but this function in *Cardiovirus* infection has not been well characterized (92, 93). Although 2A is not required for viral replication *in vivo* as well as *in vitro*, 2A is important for virulence and pathogenicity, aiding in viral subversion of the host immune response. The EMCV 2A protein also inhibits apoptosis by suppressing cleavage of Caspase-3 using an as yet characterized mechanism (93).

Virus modulation of nucleocytoplasmic trafficking

As obligate intracellular parasites, numerous viruses modulate and exploit host cell machineries to carry out productive infectious cycles. Some viruses disrupt the nuclear envelope in order to gain access to cellular factors, obstruct innate immune activation, or enter the nucleus as a necessary step in their replication cycle.

Members of *Orthomyxoviridae*, such as influenza A, are unusual RNA viruses in that they conduct their replication and transcription in the nucleus. Influenza A ribonucleoprotein genome segments are imported into the nucleus using the classical importin α/β karyopherin heterodimer because the influenza virus nucleoprotein (NP) and ribonucleoprotein 2 (PB2) proteins have a NLS (94-96). Other host factors involved

in influenza A genomic import and export include importin β (karyopherin β), Crm1, NXF1, Nup98, and Nup153 (97) (98) (99). Crm1 plays a role in ribonucleoprotein genome export following replication, outcompeting host cargos with NESs for Crm1 binding (100). Influenza A also down regulates Nup98 and sequesters Rae1 to prevent the export of host mRNAs that could illicit an anti-viral immune response (IRF-1 and MHC I) (101).

Vesicular stomatitis virus (VSV), a relative of the rabies virus, is a member of the negative-sense, single stranded RNA *Rhabdoviridae* virus family. During VSV replication in the cytoplasm, the matrix (M) protein interacts directly with Rae1-Nup98 of the NPC. This M-Rae1-Nup98 complex inhibits host transcription by mechanically blocking the nuclear export of host mRNA. IFN-β, IL-6, and c-Jun mRNAs are induced by VSV infection, but nearly 100% of these induced transcripts become trapped in the nucleus due to the VSV M protein (102, 103). Interestingly, the M protein appears to selectively inhibit the export of host transcripts, as housekeeping genes such as actin are not blocked during VSV infection. As such, the VSV M protein is a greatly advantageous “security protein” that alters cellular transcription to the advantage of the virus.

The severe acute respiratory syndrome coronavirus (SARS-CoV) is a positive-sense RNA virus and a member of the *Coronaviridae* family. SARS-CoV specifically targets the host protein, signal transducer and activator of transcription 1 (STAT1), for inactivation. STAT1 is a cytoplasmic interferon transcription factor that becomes activated when host pattern recognition receptors (PRRs) recognize pathogen associated molecular patterns (PAMPs) displayed on intracellular pathogens. When

STAT1 becomes activated, it translocates into the nucleus and binds to interferon-stimulate response elements (ISRE) found in the promoter region of interferon (IFN)-inducible genes residing along different chromosome regions (104). The C-terminus of the protein product of the SARS-CoV open reading frame 6 (ORF6) blocks the nuclear import of STAT1 (105). ORF6 sequesters Karyopherins α1 and β1 on the ER/Golgi membranes such that STAT1 cannot interact with these NCT receptors for import (106). In this way, SARS-CoV modulates NCT to inhibit the host immune response and enhance viral replication and progeny production.

HRas and Mitogen-Activated Protein Kinases

Ras proteins are members of the Ras superfamily of small guanosine triphosphates (GTPases), which are responsible for regulating cellular division, differentiation, proliferation, growth, and death, by cycling between a GDP-bound inactive and a GTP-bound active state (107). The four different Ras isoforms, H-Ras, N-Ras, K-Ras4A, and KRas4B, have distinct cellular localizations where they are regulated by RasGEFs and RasGAPs to activate the Raf-MEK-ERK Mitogen-activated protein kinase (MAPK) cascade (108-113).

The cellular (*c*) *c*-H-Ras protein is regulatable homolog of the Harvey (Ha) rat sarcoma virus, v-Ha-ras, which is constitutively active and drives tumorigenesis in infected rats (114). HRas activation at the plasma membrane (PM) is mediated by the Shc-Grb2-Sos complex (Shc-Grb2-Sos). Shc (Src homologous and collagen) is an adaptor protein that interacts with the phosphotyrosine of activated receptor tyrosine

kinases (RTKs) at the cell surface. Shc recruits Grb2 (Growth factor receptor binding protein 2) that recruits RasGEF Son of sevenless (Sos). Sos activates HRas localized to the PM to initiate a downstream MAPK phosphorylation cascade (Shc-Grb2-Sos). HRas activation at the Golgi and the ER is mediated by Ca^{2+} activated cytoplasmic RasGEFs (RasGRP1/2 and CAPRI) that initiate the same downstream MAPK phosphorylation cascade (Ca^{2+}-RasGRP1/2-CAPRI).

MAPKs are an ancient eukaryotic, integrated serine/threonine/tyrosine protein kinase network that coordinates cellular responses to diverse stimuli. The three best-characterized MAPK pathways are ERK, p38, and JNK. ERK, p38, and JNK have different biological signaling consequences as well as divergent downstream substrates and gene targets (Fig. 1-5). ERK MAPK has two major isoforms, ERK1 (MAPK3) and ERK2 (MAPK1). Upstream MAP2Ks, MEK1/2 (MAP2K1 and MAP2K2), activate ERK by phosphorylating ERK1 residues T_{202} and Y_{204} and ERK2 residues T_{185} and Y_{187}. Proximally, the RAF MAPK3K (Raf-1) is recruited and activated by phosphorylation on S_{338} by the GTP-bound form of Ras GTPase. RAF contributes to MEK1/2 activation (S_{218}/S_{222} or S_{222}/S_{226} phosphorylation), and then MEK1/2 activates ERK 1/2. ERK phosphorylates and activates the RSK kinase (RSK1/2/3), which phosphorylates Activating Transcription Factors (ATF1/4) and Activator Protein 1 (AP-1) transcription factors. Inactive ERK is cytoplasmic, and is sequestered with MEK, which has a NES that keeps MEK actively exported from the nucleus (115). Upon ERK phosphorylation and dimerization, the ERK-MEK complex is disrupted and ERK translocates into the nucleus (116). It is important to note that although ERK1/2 does not contain a recognizable NLS, ERK nuclear translocation occurs using importin-7 (117). However,

another ERK, ERK5, contains both an NLS and a NES (118). A novel ERK1/2 NLS could become displayed following dimerization, or a tertiary binding partner could be involved (119). ERK downstream targets include the p90 ribosomal s6 kinase (p90RSK) and transcription factors involved in ribosome biogenesis, increased tRNA and rRNA synthesis, higher translation efficiency (RNA Pol III-TFIIIB phosphorylation), inflammatory cytokine activation (TNF, IL-1β, IL-10), cellular growth, and proliferation (Fig. 1-5 and Fig. 1-6).

p38 has 4 isoforms: α (MAPK14), β (MAPK11), γ (MAPK12), δ (MAPK13) (120). p38 is activated by the MAP2Ks MKK3 (MAP2K3), MKK6 (MAP2K6), and to a lesser extend, by MKK4 (MAP2K4) (121, 122). p38 becomes activated through phosphorylation in response to stress triggers including cytokines, osmotic shock, lipopolysaccharide (LPS), or UV light. Activated p38 induces downstream DNA damage genes such as p53 and Activating transcription factor proteins 1, 2, and 6 (ATF-1/2/6); inflammatory cytokines (IL-1, TNF- and IL-6); and gene products involved in differentiation, autophagy, and apoptosis (120, 123, 124). The kinetics of p38 MAPK activation are balanced by the duration of upstream signals as well as phosphatases such as phosphoprotein phosphatase 1 (PP1), protein phosphatase-2A (PP2A), and MAPK-specific protein tyrosine phosphatases (PTPs) (125, 126).

The Jun N-terminal kinase (JNK) MAPK pathway is the least well understood of the MAPK family. There are three JNK isoforms: JNK1 (MAPK8), JNK2 (MAPK9), and JNK3 (MAPK10) (127). JNK is pivotal in regulating the apoptosis and NFκB pathways. The tumor necrosis factor α (TNFα) receptor at the PM, or caspase 8 through mitochondrial signaling activate the MAPK3K protein, MEKK1. MEKK1 phosphorylates

MAP2K proteins MKK4/7, and MKK4/7 phosphorylates various JNK isoforms. Phosphorylated JNK also up-regulates inflammatory cytokines involved in immune activation (IL-12, IL-2, IL-6), activates the p53 “tumor suppressor” protein, and regulates *c*-Jun cell cycle progression. NFκB is a protein complex of transcription factors that becomes phosphorylated in response to extracellular stimuli and act as a negative regulator of JNK. In this way, JNK and NFκB regulate one another to control cell survival and death (128-132).

Picornavirus Deregulation of Nucleocytoplasmic Transport

Only the *Aphthovirus* and *Erbovirus* genera of *Picornaviridae* encode a Leader (L) protein with proteolytic activity (133, 134). The aphthovirus L^{pro} is a papain-like cysteine protease that down-regulates cap-dependent mRNA translation by proteolytic cleavage of the eukaryotic initiation factor 4G (eIF4G) protein (135). The erbovirus L^{pro} (ERBV L^{pro}) is also a papain-like cysteine protease, but only shares 18% amino acid identity with the *Aphthovirus* FMDV L^{pro}, and is also predicted to have a different structure (136, 137). The erbovirus L^{pro} does not induce cleavage of eIF4G or inhibit cap-dependent translation, and its function remains unclear (134). The *Cardiovirus* L protein is not a protease, and its cellular activities in regards to the deregulation of NCT by inducing F-G Nup hyperphosphorylation (Nup214, Nup153, Nup98, and Nup62) and interacting with Ran GTPase have been discussed. It is interesting to note that the Cardiovirus L protein (67-76 amino acids) is more efficient at inhibiting type I IFN (IFN-α/β) than the FMDV L^{pro} (173-201 amino acids) despite its lack of inherent enzymatic (138).

Among the *Enterovirus* genus of *Picornaviridae*, the poliovirus and rhinovirus $2A^{pro}$ targets eIF4G for cleavage, much like the *Aphthovirus* L^{pro}, in order to inhibit host capped mRNA translation and reduce activation of the anti-viral IFN response (139, 140). In addition to cap-dependent mRNA translation inhibition, the $2A^{pro}$ of poliovirus and rhinovirus also targets F-G Nups 153, 98, and 62 for degradation (140-142). F-G Nup cleavage by $2A^{pro}$ prevents the export of nascent mRNAs, and Nup98 cleavage specifically interferes with the IFN-γ anti-viral immune response. The $2A^{pro}$ of Enterovirus 71 (EV71) also targets Nup62 for degradation and NCT inhibition (143). It can therefore be concluded that proteolytic Nup processing appears to be a conserved mechanism of the Enterovirus $2A^{pro}$ to modulate the host immune response in favor of viral replication.

The Enterovirus $3C^{pro}$ (Poliovirus, Rhinovirus, Coxsackie B virus) is targeted to the NPC in its precursor form, 3CD, due to the NLS of 3D (144, 145). The poliovirus $3C^{pro}$ also targets the host TATA-binding protein (TBP), effectively suppressing cellular RNA polymerase II-mediate transcription during infection. The rhinovirus $3C^{pro}$ can degrade host FG-Nups 153, 214, and 358 (146). In conjunction with the $2A^{pro}$, this $3C^{pro}$–mediated degradation of Nups modifies nuclear membrane permeability to mislocalize nuclear proteins (La, PTB, PCBP1/2, Nucleolin) involved in IRES-mediated translation, and disrupt the host innate immune response (IFN, PRRs) (46, 146, 147).

The Cardiovirus 2A protein has no proteolytic activity like the Enterovirus 2A protein, sharing < 20% amino acid identity (21.74% amino acid identity between Poliovirus 1 2A and EMCV 2A alone). However, both the Enterovirus and the Cardiovirus 2A proteins are involved in the inhibition of cap-dependent host translation. The Cardiovirus 2A

protein accomplishes this due to 2A-40S associations and 2A-induced hypophosphorylation of 4E-BP1, a eukaryotic suppressor of cap-dependent translation (88, 92, 148). These results suggest different mechanisms of action of the Cardiovirus and Enterovirus 2A proteins, targeting similar translation and transcription pathways in order to enhance viral replication and abolishment of host immune activation.

Comprehensively, the biochemical and structural studies we conducted on the Cardiovirus L protein and its various binding partners support a model for L activity where L interacts with a Ran-Karyopherin complexes to recruit ERK and RSK kinases in order to trigger nucleoporin hyperphosphorylation and disrupt nucleocytoplasmic transport. L localization appears to be critical for L activity while high concentrations can overcome this inhibition. **Here, we predict that the L zinc-finger interacts with ERK and RSK kinase cargo molecules, while the L hinge motif, acidic motif, and phosphorylated residues enhance L-Ran-Crm1 complex formation, with L-RanGAP maintaining L-Nup localization in order to magnify these phosphorylation events.**

Thesis Preview

The Cardiovirus L protein disrupts nucleocytoplasmic transport by inducing the hyperphosphorylation of nucleoporin proteins as well as by interacting with the cellular trafficking molecule Ran GTPase. However, the importance of L-Ran interactions and the mechanism of nucleoporin hyperphosphorylation remained ill defined. **In this thesis, I investigated the changes in L interactions with viral and host cellular factors in order to determine the role of these complexes in L-induced deregulation of nucleocytoplasmic transport and nucleoporin hyperphosphorylation.** In Chapter 2, I performed mutagenesis and chemical amino acid modifications on the L and Ran proteins to determined L-Ran residues required for L-Ran interactions. Chapter 3 details the first solution structure of Ran GTPase using NMR. Chapter 4 describes the determination of the three-dimensional solution structure of the L-Ran complex using NMR as well as the effects of L phosphorylation on L protein folding, activity, and binding partner recruitment during infection. For Chapter 5, I determined the biological relevance of L-HRas interactions juxtaposed with L-Ran, L-2A, and L-RanGAP complexes for L activity during infection.

Picornaviridae			
Virus (type member)	**Disease**	**Genera**	**No.**
Foot-and-mouth disease virus	Foot-and-mouth disease	*Aphthovirus*	1
Aquamavirus A	Seal picornavirus	*Aquamavirus*	2
Duck hepatitis virus	Duck hepatitis, death	*Avihepatovirus*	3
Avisivirus A	Turkey gastrointestinal disease	*Avisivirus*	4
Encephalomyocarditis virus	Encephalomyocarditis	*Cardiovirus*	5
Human cosavirus	Gastroenteritis	*Cosavirus*	6
Cadicivirus A	Canine virus	*Dicipicirus*	7
Rhinovirus	Common cold	*Enterovirus*	8
Equine rhinitis B virus	Horse respiratory disease	*Erbovirus*	9
Gallivirus A	Chicken and Turkey virus	*Gallivirus*	10
Hepatitis A virus	Hepatitis A	*Hepatovirus*	11
Hunnivirus A	Cattle virus	*Hunnivirus*	12
Aichi virus	Gastroenteritis	*Kobuvirus*	13
Melegrivirus A	Avian hepatitis	*Megrivirus*	14
Mischivirus A	Bat virus	*Mischivirus*	15
Mosavirus A	Rodent and bird virus	*Mosavirus*	16
Oscivirus A	Wild bird death	*Oscivirus*	17
Human parechovirus	Gastroenteritis	*Parechovirus*	18
Pasivirus A	Swine virus	*Pasivirus*	19
Passerivirus A	Wild bird death	*Passerivirus*	20
Rosavirus A	Rodent and human virus	*Rosavirus*	21
Salivirus A	Gastroenteritis	*Salivirus*	22
Porcine sapelovirus	Respiratory, neurological disorders	*Sapelovirus*	23
Seneca Valley virus	Neuroendocrine oncolytic virus	*Senecavirus*	24
Porcine teschovirus	Fatal pig encephalomyelitis	*Teschovirus*	25
Avian encephalomyelitis virus	Avian encephalomyelitis	*Tremovirus*	26

Table 1-1. Picornaviridae. Representative viruses for each genus of the Picornavirus family.

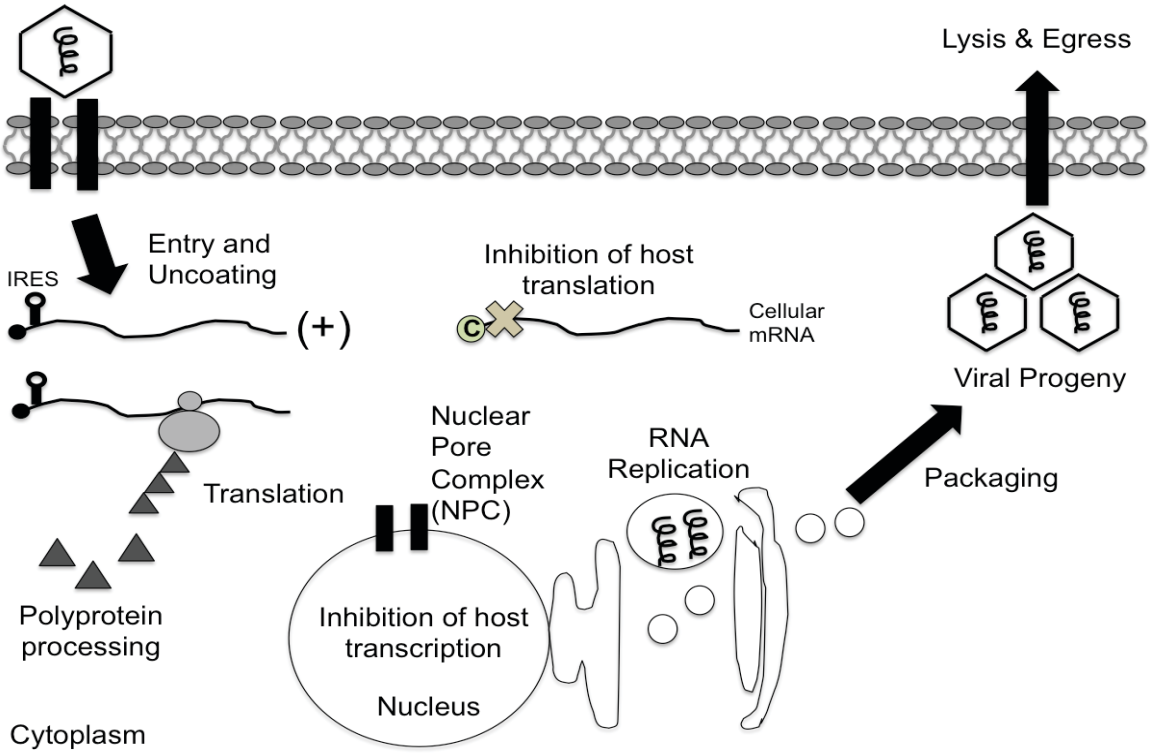

Figure 1-1. Replication cycle of a picornavirus. Capsid interactions with a host receptor result in receptor-mediated endocytosis and the delivery of the viral RNA into the cytoplasm. The IRES element recruits ribosomes for viral polyprotein translation. Non-structural viral proteins process the polyprotein into mature products and modulate host immunity by inhibiting host transcription and translation. RNA replication occurs inside of re-arranged membrane envaginations, and a switch occurs to initiate viral particle assembly. Cellular lysis releases progeny to infect neighboring cells.

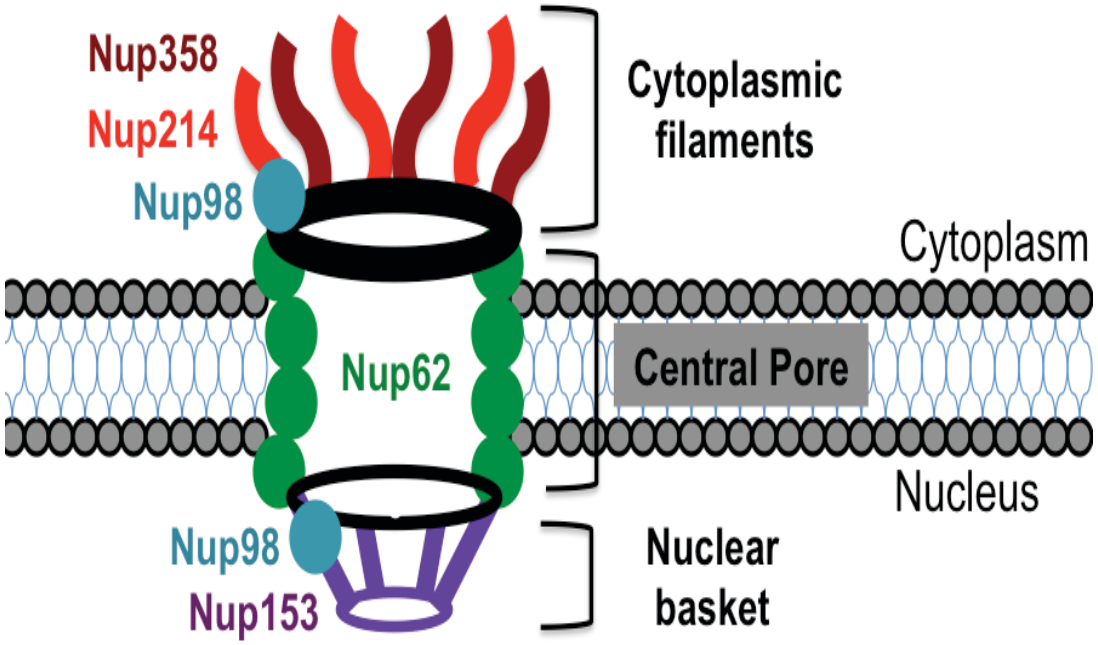

Figure 1-2. Configuration of the nuclear pore complex. The eukaryotic nuclear pore complex (NPC) is organized into 3 domain: nuclear basket, central pore, and cytoplasmic filaments. Disorganized phenylalanine(F)-glycine(G) repeats interact and select which large macromolecules can cross the semi-permeable barrier for correct sub-cellular localization to the cytoplasm or nucleus. Various FG nucleoporins that form the NPC as well as their domain localizations are indicated.

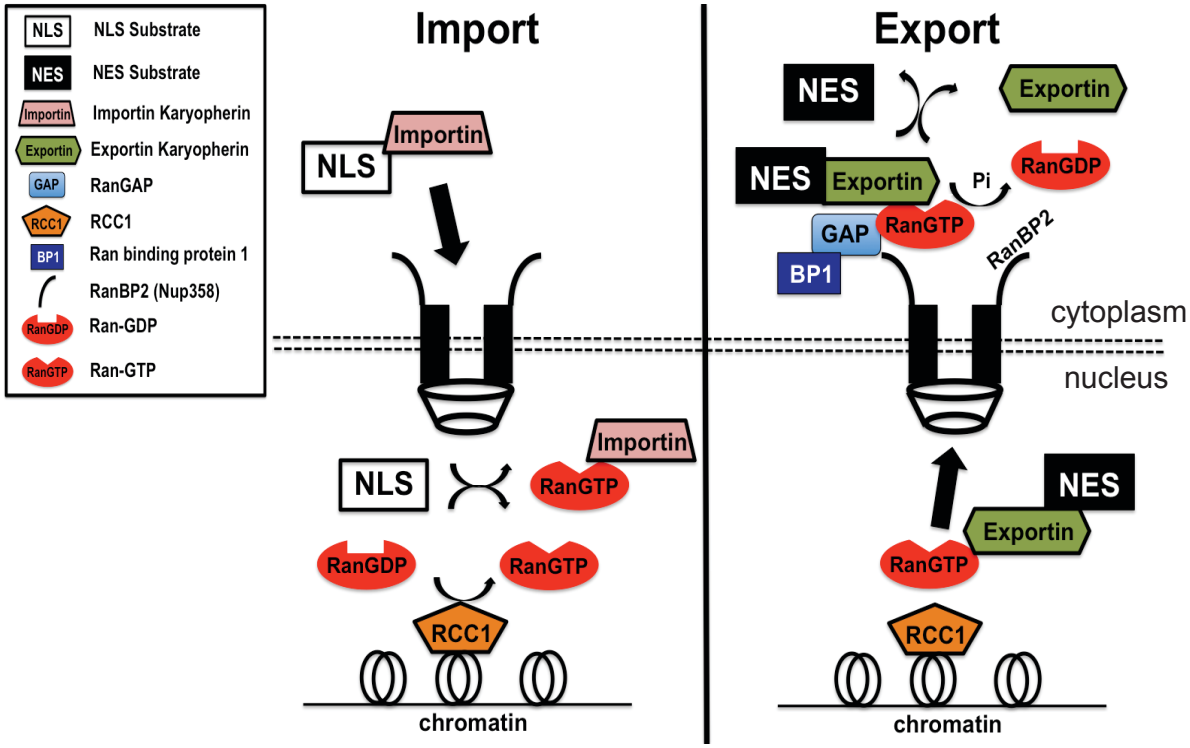

Figure 1-3. Ran GTPase-mediated nucleocytoplasmic transport.

Importins recognize the nuclear localization signal (NLS) of macromolecules and traffic them to the nucleus where Ran-GTP dissociates the complex for nuclear delivery. Exportins recognize macromolecules with a nuclear export signal (NES), and interacts with the NPC to deliver the NES cargo to the cytoplasm. Ran-GTP hydrolysis by RanGAP-RanBP1 dissociates the Ran-GTP-Exportin-NES complex for final NES delivery into the cytoplasm.

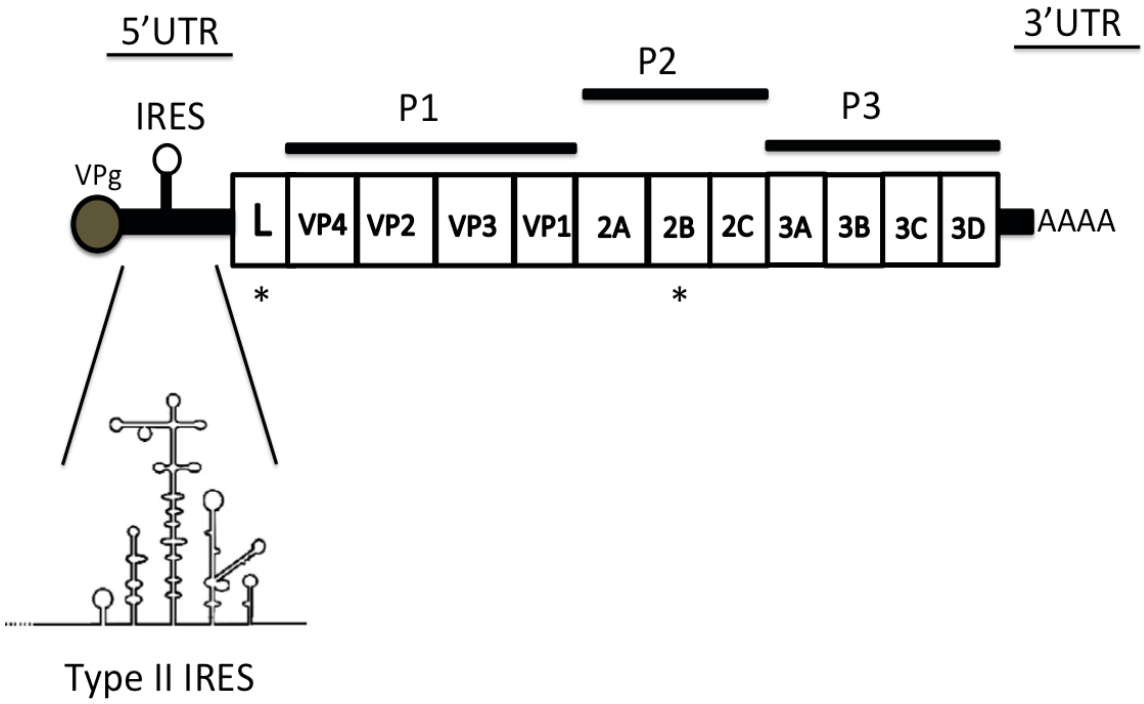

Figure 1-4. Cardiovirus genome. Schematic organization of the cardiovirus genome. The 5'UTR contain a " type II" internal ribosome entry site (IRES) that recruis ribosomes for polyprotein translation. The long open reading frame encodes 14 mature viral proteins. The 3'UTR contains a polyadenylated tail for RNA stability, transcription, and translation.

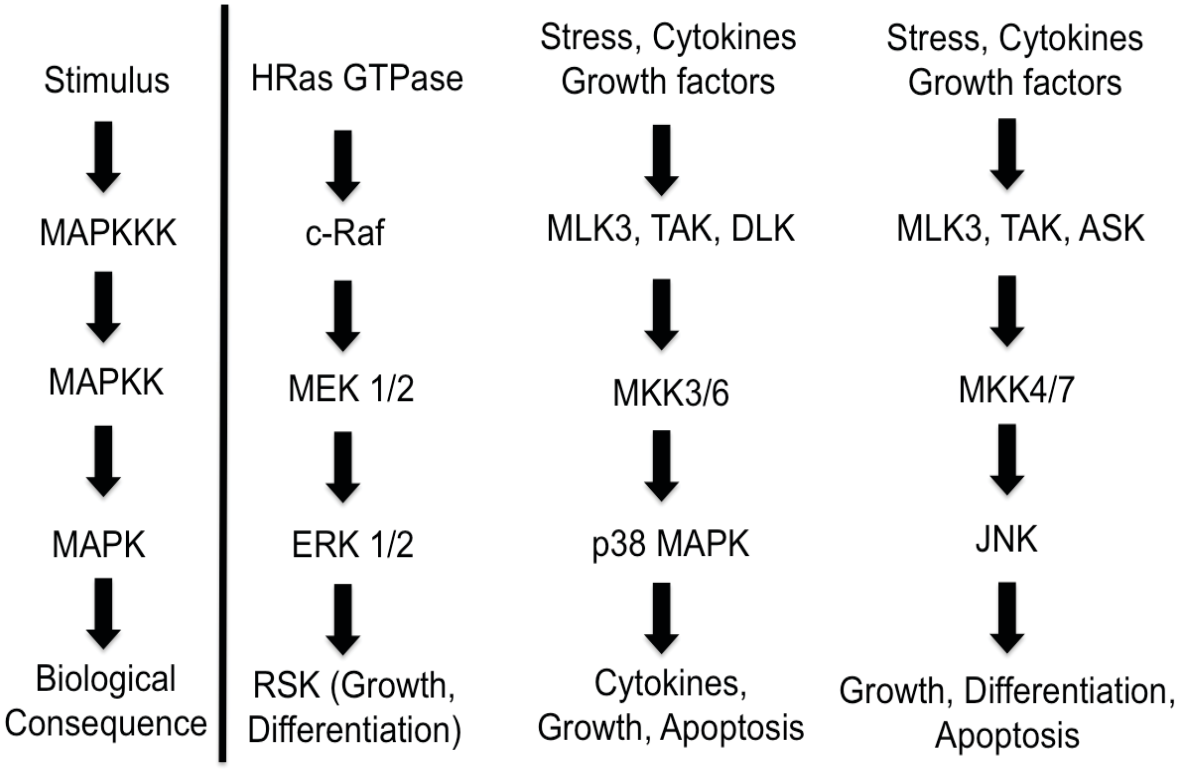

Figure 1-5. Mitogen-activated protein kinase pathways. The three mitogen-activate protein kinase (MAPK) pathways are indicated: ERK, p38, and JNK. Arrows indicate the sequential phosphorylation events of each signaling cascade. Cross talk between each pathway has been eliminated for simplicity.

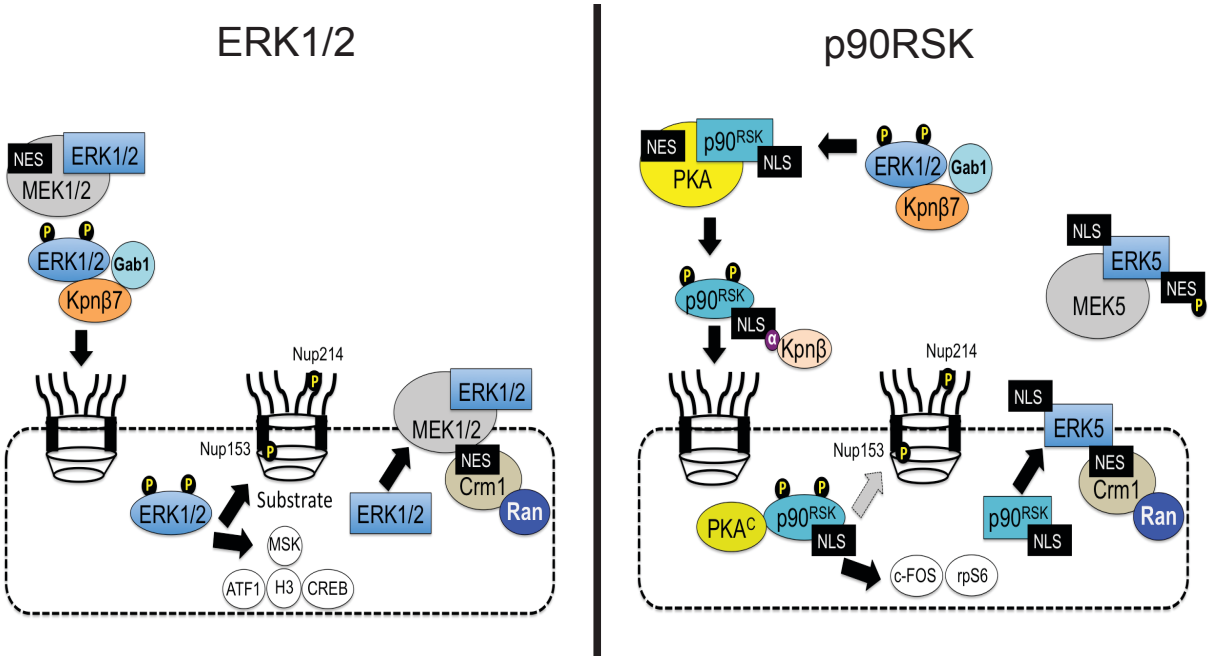

Figure 1-6. ERK and p90RSK nucleocytoplasmic trafficking. Activation of ERK and p90RSK kinases by sequential phosphorylation events result in their relocalization from the cytoplasm to the nucleoplasm. Binding partners involved in ERK and p90RSK transport, subcellular localization, and gene modulation are noted.

Chapter 2.

Encephalomyocarditis virus Leader protein hinge domain is responsible for interactions with Ran GTPase

Published in: *Virology*, Volume 443, pages 177-85 (2013)

Studies were performed by Valjean R. Bacot-Davis.

ABSTRACT

Encephalomyocarditis virus (EMCV), a *Cardiovirus*, initiates its polyprotein with a short 67 amino acid Leader (L) sequence. The protein acts as a unique pathogenicity factor, with anti-host activities which include the triggering of nuclear pore complex hyperphosphorylation and direct binding inhibition of the active cellular transport protein, Ran GTPase. Chemical modifications and protein mutagenesis now map the reactive binding domain to the L hinge-linker region, and in particular, to amino acids 35-40. Large deletions affecting this region were shown previously to diminish Ran binding. New point mutations, especially K35Q, D37A and W40A, preserve the intact L structure, abolish Ran binding and are deficient for nucleoporin (Nup) hyperphosphorylation. Ran itself morphs through multiple configurations, but reacts most effectively with L when in the GDP format, preferably with an empty nucleotide binding pocket. Therefore, L:Ran binding, mediated by the linker-hinge, is a required step in L-induced nuclear transport inhibition.

BACKGROUND

The *Picornaviridae* comprise a family of non-enveloped, positive-sense, single-stranded RNA viruses. The genomes encode long open reading frames translated into single polyproteins which are processed nascently and post-translationally into functional viral components (149). Isolates in the Cardioviruses genus are subdivided into two species. Theiler's murine encephalomyelitis virus (TMEV) is a *Theilovirus*, while encephalomyocarditis virus (EMCV) is the type member of the *Encephalomyocarditis virus* species. A close relative Mengo, differs from EMCV only by an average of 3.6 % identity at the amino acid level (150). All cardiovirus polyproteins begin with short N-terminal Leader (L) sequences, without homologs in any other viral or cellular genomes. The L proteins of EMCV (~67 amino acids) and TMEV (~76 amino acids) share about 35% identity, including common zinc-finger and acidic domains. The length differences come from an added C-terminal domain in the TMEV, rich in Ser-Thr, that is characteristic and species-specific (68). During infection with all these viruses, L acts as a potent, novel virulence factor capable of repressing host antiviral responses such as interferon type I synthesis, apoptosis, mRNA production, host translation, and nucleocytoplasmic trafficking (NCT). The collective mechanisms are poorly understood, but clearly involve extensive nuclear pore complex (NPC) rearrangements through abnormal hyperphosphorylation. This process alone, directly or indirectly, is the probable cause for all L-induced anti-host responses (72, 73, 76, 138, 148, 151-153).

Other RNA viruses also inhibit NCT, promoting high viral yields when the cell becomes incapable of trafficking anti-viral molecules to their active locations. Commonly

though, suppressive NCT mechanisms target specific nucleoporin proteins (Nups) by binding inhibition (e.g. rhabdovirus M protein), proteolysis (e.g. polio and rhinovirus 2A protein), or masquerade as a dominant transport karyopherin (e.g. HIV rev protein) (154). The Cardiovirus L proteins uniquely induce Nup hyperphosphorylation (e.g. Nup62, Nup153, and Nup214) (76) (74). Presumably, the consequent Nup charge change prevents most karyopherin-cargo complexes from entering or leaving the nucleus (155). L binding to Ran GTPase has been implicated in this process of L-induced NCT inhibition (72).

Ran is one of the most abundant proteins in cells with an estimated 10^7 copies (156). In the cytoplasm, near the NPC, effector proteins Ran GAP 1 (29, 157) and Ran binding protein 1 (Ran BP1) (158) interact to accelerate Ran's intrinsically slow GTPase activity, converting Ran GTP to Ran GDP. In the GDP form, Ran cannot bind import karyopherins, and thus promotes alternative karyopherin interactions with cargo, readying them for import via the Nups in the NPC. In the nucleus, Ran GDP is exchanged for GTP, a process facilitated by RCC1, a chromatin-bound helper factor (159). Nuclear Ran GTP displaces newly arrived imported cargos from karyopherin complexes, completing the import process. The Ran GTP:karyopherin units consequently cycle back to the cytoplasm, promoting protein and mRNA export (160).

The EMCV and Mengo L proteins have short amino-terminal zinc-finger domains, dominant carboxy-terminal acidic domains and flexible hydrophobic hinge regions linking these segments (Fig. 2-1A). The NMR structure of the Mengo L zinc-finger and hinge region is published (161)[PDB: 2BAI]. The full NMR structure was also recently completed (Fig. 2-1B) and is being prepared for submission [Supplementary file 1; PDB

ID: 2M7Y; BMRB ID: 19084; Cornilescu, C.C., personal communication]. Cardioviruses from other species (i.e. TMEV) encode similar L domains, but are extended by C-terminal Ser-Thr rich segments (77). The current study was aimed at determining which of the EMCV L domains influence interactions with Ran, and which if not participating in binding, might therefore be available to other (phosphatase or kinase) partners. Moreover, since free nucleotides, either as GTP or GDP, are known to be inhibitory to L:Ran binding unless RCC1 is present (162), the preferred configurational format of Ran captured by this binding, if indeed there is one, needed to be better defined. These points are important mechanistically because EMCV L is reported to localize to the nuclear envelope during infection (72), and it has been unclear whether cardioviruses use a specific form of Ran solely to achieve this localization, or instead are dependent on the consequent Ran functional inhibition as a trigger for Nup hyperphosphorylation.

RESULTS

L:Ran Binding with Described L Mutations. The influence of previously described L mutations on Ran binding was examined with GST pull-down assays. Endogeneous Ran from HeLa cytosol (Fig. 2-2A) and bacterially expressed, human, recombinant His-Xp-Ran (Fig. 2-2B) were equivalently extracted with GST-L, GST-L_{C19A}, and GST-L_{4D4A}, but not with the deletion protein, GST-$L_{\Delta A}$. One-dimensional proton NMR analysis [see Supplementary file 2] showed that C_{19}A (zinc-finger region) and ΔA (missing residues 37-59) both caused misfolding of L, especially as evident from the amide and aromatic portions of the spectra. But C_{19}A and the properly folded 4D4A, nevertheless still bound

efficiently to Ran. GST-L_{4D4A} has four charge changes in the acidic domain ($D_{48}A$, $D_{51}A$, $D_{52}A$, and $D_{55}A$). Therefore, within this panel, the L zinc-finger, the acidic domain, and the overall conformation of L were apparently not contributing essential binding parameters. Only full removal of the acidic domain ($\Delta_{37\text{-}59}$), with part of the adjoining hinge linker, affected the pull down of Ran.

Chemical modification of GST-L. Chemical modification of specific amino acid types can help identify reactive interfaces. Accordingly, GST-L was treated with seven well-defined modifying agents, using concentrations known to confine the reactions to a particular cohort of amino acids (163-165) (166). Since L is small, with a restricted residue composition, a change in the GST(-L) to (His-Xp-)Ran Western signal ratio after pull down, particularly at low IC_{50} for the modifying agent, might be expected to highlight reactive participants.

As an example, pre-incubation of GST-L with DCCD (167) inhibited subsequent formation of L:Ran complexes with an IC_{50} of 11 nM (Fig. 2-3A) [see Supplementary file 3]. GST-L was still readily extracted from beads, but it no longer brought down His-Xp-Ran, suggesting a component of the L binding domain probably contains at least one functionally important aspartate or glutamate residue(s) in a hydrophobic environment (163). The only L carboxy groups which meet these criteria are D_{37}, E_{38}, and E_{39}. Consistent with the $L_{\Delta A}$ and L_{4D4A} mutational results, each of these is in the hinge region, next to the acidic domain.

Protein modification by *TNBS (*Fig. 2-3B) or DIDS (Fig. 2-3C) discriminate respectively between lysines in hydrophilic and hydrophobic environments (168, 169).

The L moiety of GST-L has only two lysines, K_{21} and K_{35}, which exist respectively (and fortuitously) in hydrophilic and (strong) hydrophobic environments. Like DCCD, protein treatment with DIDS eliminated Ran pull down at a very low IC_{50} (0.2 nM). TNBS treatment required concentrations of at least 0.025% (IC_{50} 0.012%) to reduce Ran binding to 55% [see Supplementary file 3]. This differential implicates K_{35} (via DIDS) in L:Ran interactions, but does not preclude additional weaker contributions from K_{21} (via TNBS).

EMCV L has a single tryptophan (W_{40}). At an appropriate pH, NBS reacts with this type of amino acid by oxidizing the nitrogen of the pyrrole ring (170). Treatment of GST-L over a 4 log concentration range, eventually dropped Ran binding activity to 10% (Fig. 2-3D). But even the lowest tested concentrations were still quite active (0.1 μM, 84%). Given the reasonably low overall IC_{50} (370 μM) [see Supplementary file 3] it likely that W_{40} is sited within or near the Ran binding interface.

Reactions to modify cysteine (C_{10}, C_{19}, C_{22}) and arginine (R_{28}), using NEM (171) or PG (172) were significantly less effective. NEM reduced Ran binding to 30%, but required an IC_{50} of 0.75 mM (Fig. 2-3E) [see Supplementary file 3]. The three Cys residues in the L sequence are conformational, holding the zinc ion in the amino-terminal finger. R_{28} is at the base of this finger. PG modification had an IC_{50} of 3.2 mM (Fig. 2-3F) [see Supplementary file 3]. While Ran binding participation by these residues cannot be excluded, again, the data do not place them, or the zinc-finger, as the most obvious choice for the interface.

The final tested compound, DEPC reacts with histidyl residues (173, 174). GST-L has only one His (H_{12}), aiding the three cysteines, in zinc binding. Even modest

treatment (10 mM) of GST-L with DEPC, eliminated the GST signal, let along the Ran signal, indicating gross misfolding of the total protein, to the extent it could no longer react with glutathione beads. With an estimated IC_{50} of 5 mM, the DEPC experiment must be classified as indeterminate, and cannot confirm or deny H_{12} participation in Ran interactions (Fig. 2-3G) [see Supplementary file 3].

These initial chemical modification experiments were performed to identify protein regions of interest to target for L protein mutagenesis and binding studies. Enhanced characterization of the chemically modified GST-L by mass spectrometry was precluded by the lack of trypsin cleavage sites within L (2x only) and the inability of the resultant large fragments of low pI (3.8) to resolve by this method (175, 176). While the modifications could have been repeated using GST-Ran or L without its GST, in the absence of effective, confirmatory mass spec protocols, these directions were deferred in favor of a mutagenesis approach with better specificity.

Mutagenesis of GST-L. The previous results suggested the L zinc-finger and the acidic domains were probably less important Ran binding targets than residues in the hinge linker, especially within central segment, K_{35} to W_{40}. Eighteen new point mutations were engineered into GST-L, nine of which focused on residues 35 to 40 (Fig. 2-1A). For each of these nine, His-Xp-Ran binding was severely diminished (Fig. 2-4A) with the most potent constructions ($K_{35}A$, $K_{35}Q$, $D_{37}A$, $W_{40}A$, $W_{40}V$) having virtually no pull-down capacity. Sequence rather than conformation caused these effects, because when $K_{35}Q$, $D_{37}A$, and $W_{40}A$ were probed by NMR proton analyses, the spectra coincided with the wild-type L, indicating properly folded proteins [see Supplementary file 2]. However,

that $C_{19}A$, even when misfolded could still react with His-Xp-Ran, is consistent with a binding, dependent more properly, on a defined, linear segment of L, than on a topologically constrained structure. Clearly, the L hinge residues K_{35}, D_{37}, and W_{40} must lie at the heart of this required segment. Mutations in intermediate residues, $Y_{36}F$, $E_{38}A$ and $E_{39}A$, reduced Ran binding to 45%, 47% and 23%, respectively. If not primary contacts for the interaction, these amino acids must certainly contribute to the required linear segment.

To ensure that other regions of L behaved differently, nine additional point mutations outside the hinge region, were created and tested. GST-L T_3A, T_4A, T_9A, $T_{15}A$, confirmed the $C_{19}A$ results, in that none of these zinc-finger region changes reduced Ran binding (Fig. 2-4C). $Y_{27}F$ and $Y_{32}F$ on the amino side of the hinge-linker, and $Y_{41}F$, $T_{47}E$, and $T_{47}A$ on the carboxyl side likewise did not affect Ran binding. In the L structure, Y_{41} delineates the carboxyl edge of the hinge domain. T_{47} is in the acidic domain, abutting the β-loop encompassing the 4D4A residues. As with the hinge-domain panel, NMR confirmed these proteins were properly folded [see Supplementary file 2] but whenever the locale was outside of residues 33-40, the proteins could react with and pull down Ran.

L Mutations and Nup Phosphorylation. During infection, an L:Ran interaction is one of several steps contributing to Nup hyper-phosphorylation(74). Regardless of mechanistic order, if L:Ran binding is required within this path, inhibitory interface mutations should manifest in defective Nup phosphorylation. Using recombinant GST-L (and derivatives), isolated nuclei (Nup targets) and cytosol (Ran and kinase source),

incorporation of radiolabel into Nup62, as measured by fold increase over background (i.e. GST signal) was indeed diminished by each of the altered hinge domain protein mutations (Fig. 2-4C&D). Hinge mutations with the strongest Ran binding effects (i.e. K_{35}, D_{37}, W_{40} sites) reduced phosphorylation to background levels. Intervening locations where substitution still allowed a partial Ran binding (Y_{36}, E_{38}, E_{39}), correspondingly reduced Nup62 phosphorylation by only 40-60%. The inhibition by these three sites was never absolute. Mutations at T_3, T_4, T_9, T_{15}, C_{19}, Y_{27}, Y_{32}, Y_{41}, and T_{47}, or collectively at D_{48}A, D_{51}A, D_{52}A, and D_{55}A (i.e. 4D4A) gave proteins that bound Ran effectively, and all these except C_{19}A and 4D4A, were able to trigger Nup62 phosphorylation. The requirement for the zinc finger (i.e. C_{19}) and acidic domain (4D4A) at mechanistic steps subsequent to Ran binding has been documented before (74).

Ran Mutations and GST-L Binding. The Ran requirements for L interactions are more complicated to map because native Ran (216 amino acids) is larger than L and it readily switches among GDP, GTP and unbound nucleotide conformers, depending upon available guanosine nucleotide phosphate (GNP) concentrations or co-factors. However, known Ran mutations have been characterized (177), which limit GTP hydrolysis and/or nucleotide exchange, to the effect that recombinant isolates are locked into nucleotide independent states, mimicking GTP (G_{19}V, L_{43}E, Δ_{DE}) or GDP (Q_{69}L) conformers. Ran T_{24}N has a reduced affinity for guanine nucleotides and is found equivalently in GDP-bound or nucleotide-free states *in vivo* (178). The Δ_{DE} deletion is in a C-terminal (D_{211}EDDDL$_{216}$), defining a tail segment that influences the format of the GNP binding pocket (179).

In previous experiments, GST-L binding to $T_{24}N$ and $L_{43}E$ forms of His-Ran were measured by Coomassie staining after pull down (72). Both structural mimics bound to L, but it required a higher molar ratio of $L_{43}E$ (GTP form) to achieve saturation. Using more sensitive Western assays and a larger panel of Ran proteins (Fig. 2-5), the effect was repeated in that Ran GTP mimics ($G_{19}V$ and $L_{43}E$) each had reduced GST-L binding (to 75% and 60%), relative to His-Xp-Ran, while the Ran GDP mimics ($T_{24}N$ and $Q_{69}L$) and unbound mimic ($T_{24}N$) were extracted more efficiently (116% and 203%), to the point where they were actually more effective than the unmodified protein. Only the deleted Ran (Δ_{DE}) was unreactive with GST-L.

These particular Ran mimics assume their respective conformations regardless of whether bound nucleotides are co-isolated during recombinant expression. To test whether nucleotides themselves contributed to GST-L interactions, His-Xp-Ran and His-Ran_{Q69L} were stripped with EDTA, and then incubated with ATP, GTP or GDP (Fig. 2-6). HPLC after dialysis confirmed that the pockets were now empty (no nucleotide, ATP) or appropriately filled with GDP or GTP (data not shown). GST-L binding was sensitive to this treatment. The empty pocket Ran forms were pulled down effectively and equivalently for wild type and $Q_{69}L$. Loaded pockets, especially with GTP, bound less well, reducing the GST-L interactions to virtually zero. Both tested Rans when loaded with GDP, bound GST-L better than when loaded with GTP, although even $Q_{69}L$ (plus GDP) only restored binding to 60% of that for either empty pocket.

Chemical Modification of Ran. Although Ran is too large for a detailed chemical mapping, it was still of interest to see if reactions with the standard compounds would

impact L binding. At concentrations effective for GST-L modification, His-Xp-Ran remained soluble after reaction with all reagents, but each sample now had reduced affinity in the pull down assays [see Supplementary file 4]. DEPC (His), DIDS (hydrophobic Lys) and PG (Arg) gave more severe reductions than DCCD (Asp/Gly), NEM (Cys), NBS (Trp) and TNBS (hydrophilic Lys). The results suggest that in addition to the C-tail of Ran, whose deletion (Δ_{DE}) was restrictive to GST-L binding, an additional (presumed) surface patch with Arg, Lys and His residues contribute to the contact itself, or to the Ran conformation that allows optimal L interaction.

DISCUSSION

Before this study, it was known that EMCV L could interact tightly with Ran GTPase, but it had not been established that single point mutagenic interference with this binding would lead directly to failure of Nup phosphorylation. The experiments here establish that connection and moreover, point to the flexible L linker-hinge region K_{35} to W_{40} as the likely Ran contact segment. All other Cardioviruses, including the Theiloviruses, conserve the character of this linker, including absolute conservation of residues D_{37}, E_{49} and W_{40} (67). Mutations interfering with the EMCV L zinc-finger ($C_{19}A$) or acidic domain (4D4A) still bound Ran even when 1-D proton analyses showed the protein was completely misfolded (e.g. $C_{19}A$). Therefore it is probably the linker segment and not its conformation, which are important here. If true, this finding implies that the L acidic domain and zinc-finger do not make important contacts with Ran and perhaps are

otherwise available for tertiary interactions, for example, with the kinases (or phosphatases) that ultimately carry out Nup phosphorylation.

During infection or when incubated with cytoplasmic extracts, native and recombinant EMCV/Mengo L is slowly and sequentially phosphorylated at T_{47} and Y_{41} (69, 70, 148). Point mutations at either site reduce virus viability (69, 70, 148), but for reasons unknown, relative to the Nup phosphorylation pathway. Y_{41} borders the hinge domain. T_{47} is in the acidic domain. In the absence of any other factors, or any L phosphorylation, His-Xp-Ran and GST-L obviously react. It is probable these natural L modifications serve in some regulatory capacity at a late-infection mechanistic step, subsequent to Ran binding. When the other binding partners of L (or L:Ran) are finally identified, the role of L phosphorylations is sure to become clear, but they are not a requirement for Ran binding.

The Ran requirements for L binding are more difficult to define. The K_D of L:Ran, measured at ~3 nM by surface plasmon resonance (SPR) is extraordinarily tight and virtually non-dissociable (162). Under the 2 hr reaction conditions described here (no RCC1), about half of the added GST-L reacts with and pulls down His-Xp-Ran (162). When assessed as the ratio of Ran (mAb) to GST (mAb) pixels in Western assays, this value was defined in these experiments, as “100%“ (e.g. Fig. 2-2). If RCC1 were to be added, it would work to increase Ran flexibility, allowing it to morph through multiple conformers and readily exchange nucleotides with the solvent. Importantly, RCC1 does not facilitate morphing or GNP exchange with the mutant forms of Ran. Since comparative binding with locked Ran conformers was a goal of the current study, RCC1 was not included, and the reaction extent (% Ran bound) measured an experimentally

determined surrogate, proportional to binding affinities at equilibrium rather than saturation. Although ideally, one would like to determine relative SPR K_D values for the full panel of L and Ran mutations, this is technically impractical even if the reactions (other than wild type), could be driven to saturation. Rather, as used here, the next most sensitive measure of affinity was the L:Ran ratios using the GST signal as a proxy for L. Within these parameters, the binding proved sensitive to conformers of Ran, with the GDP mimics ($T_{24}N$ and $Q_{69}L$) outperforming the GTP mimics ($G_{19}V$, $L_{43}E$, Δ_{DE}) and even the wild type protein (in the absence of RCC1). But filling the Ran GNP pockets of even the best mimic ($Q_{69}L$) with any nucleotide, even if it was GDP, reduced the L binding affinity. Therefore, Ran in the GDP conformation, but with an empty GNP pocket, is the preferred partner for L. RCC1, if it were present, would work to provide catalytic aid to this binding by accelerating the Ran morphing rate, and facilitating release of any bound nucleotides, increasing the proportion of empty GNP pockets.

As an approximation of whether these binding ideas were structurally feasible, PDB files for RanGDP [PDB: 1K5G] and 5 NMR variants of Mengo L were submitted to the GRAMM-X protein docking server and asked to interact into the 10 best (each) minimum energy conformations without any specified constraints. The “best” model, consistent with each L conformer (E_{total} -2134.97 Kcal/M) surpassed all others by at least 100 Kcal/M (Fig. 2-1D). It placed the L hinge domain into a hydrophobic cleft surrounded by the carboxyl-terminus of Ran (F_{176} to M_{189}), opposite the nucleotide binding pocket. When probed by PDBePISA for specific interface information all iterations of the model placed L_{34}, K_{35}, D_{37}, and E_{38} of L within 2-4 Å of a Ran contact face (variously) including loops H_{30}-E_{34}, L_{50}-H_{53}, E_{175}-M_{179} lining the Ran hydrophobic

cleft. L W_{40} had additional potential for tight stacking interactions in some of the models. The model is consistent with the above chemical and mutagenic mapping of L, predicting interaction via the hinge domain, and specifically implicates L residues 35-40. When placed this way, L masks the Ran BP1 binding site, but not those of RCC1, Ran GAP or various karyopherins, which interact on other Ran faces (Fig. 2-1C) (30, 180, 181). In agreement with *in vivo* evidence that native L:Ran complexes sometimes include Ran GAP and importin β, but never Ran BP1 (72), the model suggests that L may out-compete Ran BP1 for Ran C-tail interactions, or share an overlapping binding site on the core of Ran.

The tested Ran point mutations all map internally to the P-loop and Switch regions (I & II) controlling GTP/GDP protein conformation (25, 182, 183). In the GDP form preferred by L, the acidic C tail of Ran, -DEDDDL^{216} participates in and is required for Ran BP1 interactions (Fig. 2-1C). The orientation of the C-tail is influenced by the bound GNP, and by an extraordinary basic patch, ^{139}HRKK, nearby on the Ran surface (179, 181). Were this tail to assume a similar configuration during L binding, as depicted in the model (Fig. 2-1D), or if C tail truncation forced a Ran GTP conformer, its deletion should be inhibitory, as was observed in the pull downs (Fig. 2-5). Chemical alteration of any residue in the basic patch (e.g. Supplementary file 4) should have a similar effect. The Ran structure in this region is highly susceptible to the format of the bound nucleotide (GTP, GDP or empty), and the orientation of Ran C-tail relative to the basic patch is also crucially dependent upon that nucleotide. These parameters can readily explain why excess free nucleotides can inhibit L:Ran formation unless conformer preference, facilitated by RCC1, drives Ran into the GDP format, regardless of

nucleotide (162). While any such model generated by a computer obviously needs to be interpreted with a great deal of caution, if this one is even partially true (an authentic structure determination is underway), it predicts extensive hydrophobic and hydrophilic interactions between L and Ran, that would be very tight without requiring either zinc finger or acidic domain contacts. Ran, once bound to L would be nucleotide independent in its conformation, and unable to undergo normal cycling. The next step in Nup phosphorylation would presumably be the recruitment of kinases (e.g. ERK1 or p38), anchored to the NPC by L:Ran, to carry out the direct modifications.

CONCLUSIONS

The EMCV Leader protein hinge domain is the major facilitator of L interactions with Ran GTPase. Prevention of stable L:Ran complex formation by protein mutagenesis inhibits successive Nup phosphorylation, as triggered by the presence of L *in vitro* and *in vivo*. Therefore, L:Ran complex formation is a requisite step in L-dependent anti-host activities. The studies show L associates most readily with Ran in a GDP conformation, preferably with an empty nucleotide binding pocket. The virtually irreversible tightness of this reaction suggests the EMCV Leader might be a useful inhibitory reagent in other investigations on Ran or related nuclear transport mechanisms.

METHODS

Plasmids. Recombinant plasmids encoding the EMCV L protein linked to N-terminal GST tags have been reported (72). Eighteen additional plasmids with single point mutations were constructed using 2-step PCR procedures [see Supplementary file 5 and Supplementary file 6]. Bacterial plasmids encoding 6-His-Xpress tagged human Ran GTPase (His-Xp-Ran) and 6-His tagged human Ran $Q_{69}L$ (His-Ran_{Q69L}) were gifts from Mary Dasso (National Institutes of Health, Bethesda, MD). Plasmids linking human Ran mutant sequences to an N-terminal GST tag ($G_{19}V$, $T_{24}N$, $L_{43}E$, and deletion Δ_{DE}, 211-216), were gifts from Ian Macara (University of Virginia, Charlottesville, VA), and previously described (177) [see Supplementary file 5]. All plasmid insert sequences were verified by Sanger techniques.

Protein expression in *E. coli* and purification. Recombinant GST-L plasmids were transformed into *E. coli* BL21 (DE3) cells, grown then expressed in media containing $ZnCl_2$ (25μM). The protein was harvested then purified on GSTrap FF columns (GE Healthcare). For recombinant Ran, the respective plasmids were transformed into BL21 cells, grown and expressed without $ZnCl_2$. The protein was harvested on GSTrap FF columns or HisTrap FF nickel columns, as appropriate. GST tags were removed ($G_{19}V$, $T_{24}N$, $L_{43}E$, Δ_{DE}), before elution, by reacting the columns with 10 units of PreScission protease (2 days, 4°C, GE Healthcare). The cleaved Ran was further purified by gel filtration using Sephacryl S-100 columns. The protein nomenclature used here indicates whether the GST, His or His-Xp tags were present on recombinant Ran or L.

GST-L Pull-down Assays. HeLa cells (ATCC CRL-1958) were grown in suspension (37°C; 5% CO_2) in modified Eagle's medium supplemented with 10% calf serum. After collection, the cells were lysed by sonication for whole cell extracts, or clarified (16,100 x g, 20 min) after sonication for cell cytosol, then stored (-80°C for up to 30 days) before use. For endogenous Ran pull-down experiments, the extracts were supplemented with Triton X-100 (0.5%) then incubated with glutathione-Sepharose 4B beads (30µl, 50% slurry, GE Healthcare) pre-reacted with GST (2.2 µg) or with GST-L proteins. Bound proteins were resolved by SDS-PAGE and visualized by Western assays.

For binding studies with Ran, the proteins (10.5 µg His-Xp-Ran, His-Ran_{Q69L} or mutated Ran after GST tag removal) were added to glutathione-Sepharose 4B beads pre-reacted with GST, GST-L or its mutant derivatives. The molar ratio during incubation was 4:1 (Ran:L) in PBS buffer (500 mM NaCl, 2.7 mM KCl, 100 mM Na_2HPO_4, 2 mM KH_2PO_4, 0.02% Triton X-100). The beads were washed, and the proteins resolved by SDS-PAGE, then visualized by Western assays or staining (Coomassie Brilliant Blue R-250, Thermo Scientific). The percentage of bound Ran was calculated after densitometry (Total Lab-TL 100, Sigma-Aldrich), relative to control bands (wild type or untreated Ran). Inhibitory concentrations (IC_{50}) were determined by linear plots in Excel [see Supplementary file 3] (184).

Chemical Modification of Proteins. Before chemical modification, GST-L (3 mg) was dialyzed (10 mM Bis-Tris propane, pH 7.4, 50 mM NaCl, 2 mM DTT) then collected after anion exchange using a Mini Macro-Prep High Q cartridge (Bio-Rad) over a twenty column volume salt gradient (50 - 500 mM NaCl), removing inadvertent translation

truncation products. Modification of selective residues was carried out while the protein was bound to glutathione-Sepharose beads, using the following compounds, concentrations and buffers: 0- 500 μM dicyclohexylcarbodiimide (*DCCD) or* 0-1 mM N-ethyl maleimide (*NEM*, in 50 mM HEPES, pH 7.0, 33 mM sorbitol), 0-10 mM diethylpyrocarbonate (*DEPC*, in 50 mM MOPS, pH 7.4, 33 mM sorbitol), 0-1 mM N-bromosuccinimide (*NBS*, in 50 mM Tris, pH 7.4, 33 mM sorbitol), 0-5 mM phenylglyoxal (*PG*), 0-2 mM 4,4′-diisothiocyanatostilbene-2,2′-disulfonic acid disodium salt hydrate (*DIDS*), 0-1% 2,4,6-trinitrobenzenesulfonic acid (*TNBS, in* 50 mM HEPES, pH 8.0, 33 mM sorbitol) according to standard procedures (163, 185, 186). The modified bead-bound protein was washed 3 times before pull-down assays with (unmodified) His-Xp-Ran. Ran modifications, used similar reactions, except the His-Xp-Ran (10.2 mg) was in solution, and then dialyzed (3x) against buffer before testing in pull-down assays with (unmodified) GST or GST-L.

Western Analyses. Protein samples were separated on SDS-PAGE gels (187), transblotted onto membranes (Immobilon-P, Millipore), and probed with primary antibodies against the carboxyl-terminus of human Ran (goat polyclonal IgG, C-20; Santa Cruz Biotech, 1:5000), the amino-terminus of human Ran (goat polyclonal IgG, N-19; Santa Cruz Biotech, 1:5000), GST (mouse monoclonal IgG; Novagen, 1:10000), Nup62 (mouse monoclonal IgG C-9; Santa Cruz Biotech, 1:2,500), or Phe-Gly containing Nups (mouse monoclonal IgG mAb414; Covance,1:5000). After membrane washing, either rabbit anti-goat horseradish peroxidase (*HRP*, Sigma-Aldrich; #A5420, 1:5000) or goat anti-mouse HRP (Sigma-Aldrich; #A2554, 1:5000) was added as the

secondary antibody. Reagents for chemiluminescence were added (GE Healthcare, Amersham ECL Prime; or Thermo Scientific, Pierce ECL) as per manufacturer's instructions and signals were detected with a CCD camera (Fotodyne, Inc) or X-ray film (Fujifilm).

Nup Phosphorylation. HeLa cells grown in suspension (above) were washed with PBS, lysed in RSB buffer (10 mM Tris, pH 7.5, 100 mM NaCl, 2.5 mM $MgCl_2$, 35 µg/ml digitonin) and fractionated (2000 x *g,* 8 min). The pellet, containing nuclei, was washed (RSB buffer), re-suspended, and then recollected (once at 2,000 x *g,* 8 min, and 3x at 60 x *g* for 5 min). Labeling reactions (500 µl) contained nuclei (4.5 mg), HeLa cytosol (300 µl/4.5 mg), γ-^{32}P-ATP (100 µCi) , GTP (100 µM), and recombinant GST, or various GST-L proteins (3 µg). After incubation with L (45 min, 37°C), the nuclei were lysed in RIPA buffer by needle aspiration. Monoclonal mAb414 (1:5,000) was cross-linked to protein G beads (20 µl, GE Healthcare) then incubated with the nuclei lysates (4 hrs, 4°C). Pelleted beads were washed, boiled, resolved by SDS-PAGE, and the proteins visualized by Western blot (mAb to Nup62) or autoradiography with densitometry using a Typhoon imager (GE Healthcare).

Protein Docking Simulation. PDB files for the Mengo L NMR structure models 1, 2, 5, 10, 17 [Supplementary file 1; PDB ID: 2M7Y] and human Ran GDP [PDB: 1K5G] (188) were submitted to the GRAMM-X Protein-Protein Docking web server (189, 190).

Recombinant Ran Nucleotide Format. Recombinant His-Xp-Ran and His-Ran_{Q69L} (20 µg) in exchange buffer (1 mL, 50 mM Tris, pH 8, 100 mM KCl, 5 mM EDTA, 1 mM DTT) were incubated (1 hr, 25°C) with ATP, GDP or GTP (20 mM), then transferred to ice after addition of $MgCl_2$ (5 mM). The samples were dialyzed (3x, 20 mM HEPES, pH 7.5, 150 mM KCl, 5 mM $MgCl_2$, 2 mM DTT) using Amicon Ultracentrifuge devices (Millipore) before the nucleotide(s) bound to Ran were confirmed by HPLC chromatography (191). The same nucleotide-loaded Ran samples were used in GST-L pull-down assays (above).

One-Dimensional Proton NMR. The GST tags were removed from GST-L proteins by on-column digestion. The proteins were collected after gel-filtration, treated with EDTA (50 µM), then dialyzed (24 hrs) to facilitate refolding (20 mM HEPES, pH 7.0, 100 mM NaCl, 0.04% NaN_3, 5 mM DTT, 25 µM $ZnCl_2$). After a final dialysis (omitting $ZnCl_2$), D_2O was added (to 10%) and the samples were concentrated (to 0.5 mM). 1-D proton spectra (64 transients) were collected at 25°C on a Bruker AVIII-600 MHz Avance console with a WATERGATE water suppression protocol. The data were processed and analyzed by NMRPipe (Frank Delaglio, NIH). The integrity and activity of L preparations were confirmed before and after NMR by SDS-PAGE fractionation and their ability to induce Nup62 hyperphosphorylation (as above).

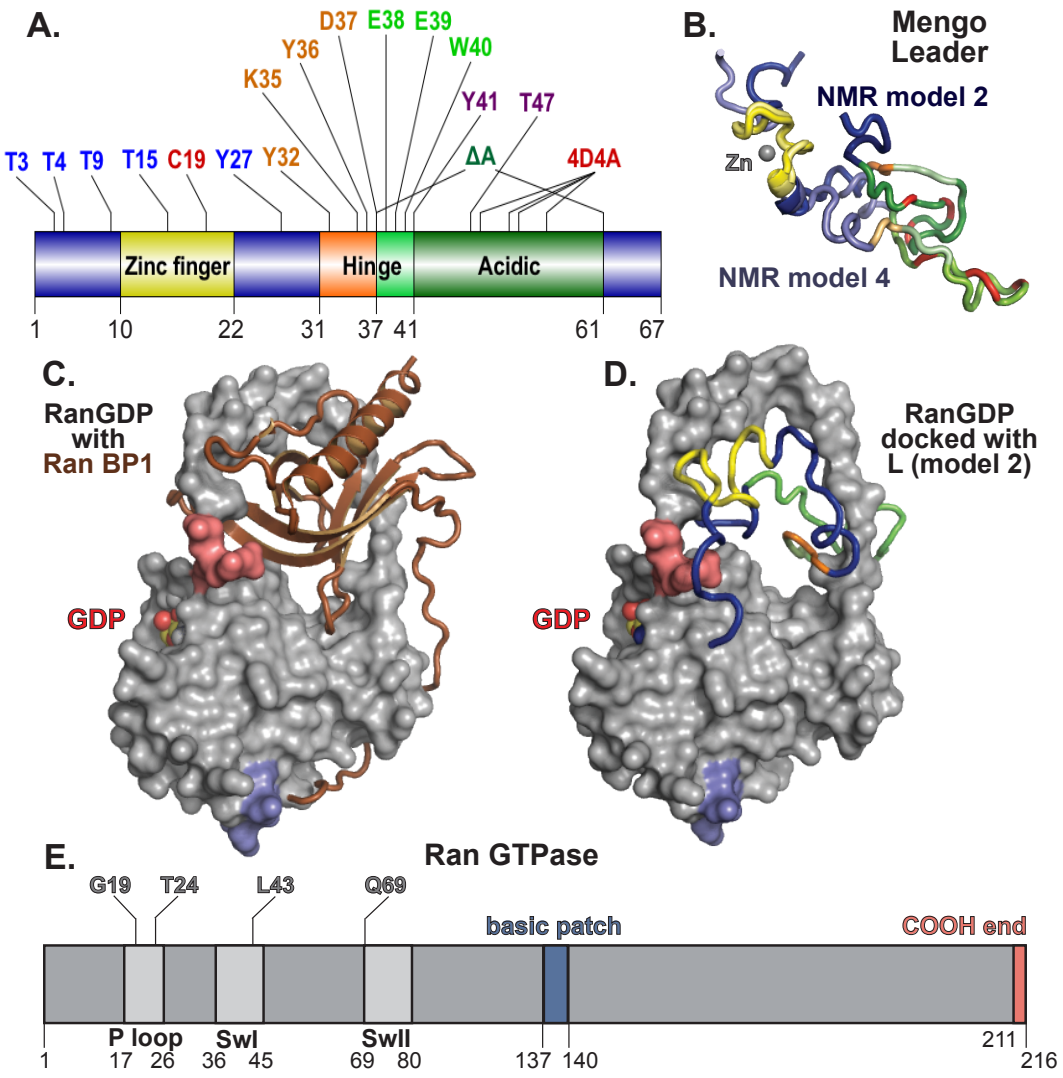

Figure 2-1. Schematic and structural representation of the L protein and L bound to Ran GTPase. (A) L protein domain organization and residue mutations used in this study. The zinc-finger domain, hinge domain, and acidic domain are shown in yellow, orange-lime, and lime-forest-green, respectively. (B) The full structure of the mengo L protein was determined by NMR1 [PDB: 2M7Y]. Two conformational isomers are shown with domains colored to match (A). (C) Structure of the Ran GDP: Ran BP1 protein complex as determined by crystallography [PDB:1K5G]. (D) The pdb files of mengo L [PDB: 2M7Y] and Ran GDP [1K5G] were loaded and docked into a protein complex by the Vakser Lab's GRAMM-X Protein-Protein docking web server. L is predicted to occupy similar sites on Ran as Ran BP1.

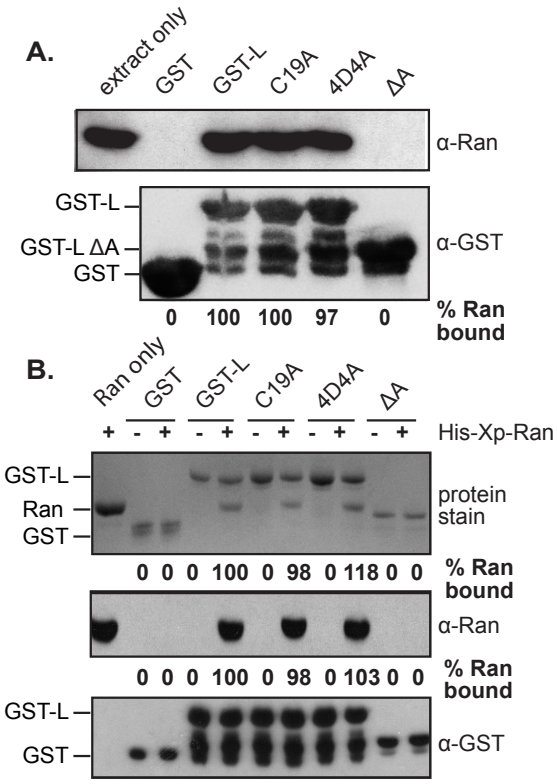

Figure 2-2. Mutations within the acidic domain of Leader preclude interaction with endogenous and recombinant Ran GTPase. (A) HeLa cellular extracts or (B) recombinant wtRan GTPase (His-Xp-Ran) were incubated with glutathione beads preincubated with GST, GST-L wt, GST-L C19A, GST-L 4D4A, or GST-L ΔA. Ran GTPase was not observed to precipitate in complex with GST-L ΔA as indicated in the last lane of the α-Ran western blots (A & B) as well as by the last lane of the total protein stain (B).

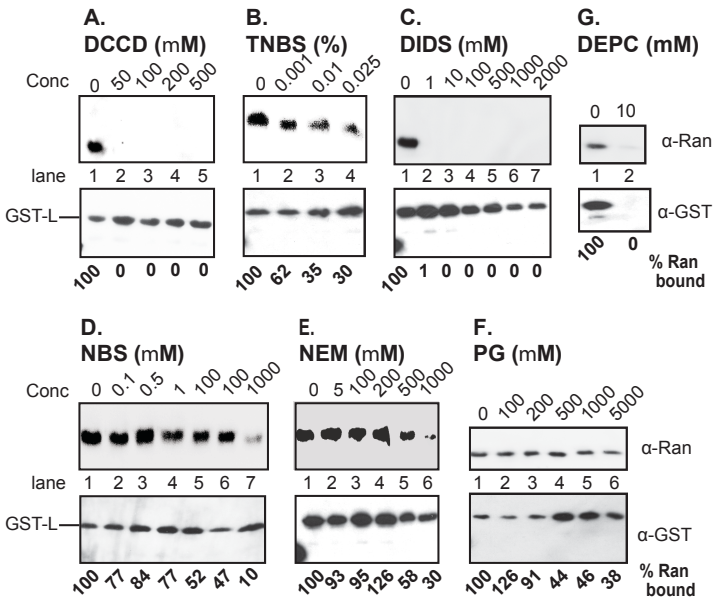

Figure 2-3. Chemical modifications of specific Leader residues inhibit Leader-Ran complex interactions. GST-L wt EMCV was incubated with 7 amino acid modifying compounds: (A) DCCD, (B) TNBS, (C) DIDS, (D) NBS, (E) NEM, (F) PG, (G) DEPC. The compounds were removed by washing before modified GST-L wt EMCV was incubated with wtRan GTPase (His-Xp-Ran). The Ran:L bound ratio for each lane was quantified by densitometry. DCCD, DIDS, and NBS were most inhibitory to the formation of the L-Ran complex, as compared to each compound's IC50 value for a known protein-protein interaction in the literature. N, N'-Dicyclohexylcarbodiimide (DCCD); 2,4,6-trinitrobenzenesulfonic acid (TNBS); 4,4'-Diisothiocyano-2,2'-stilbenedisulfonic acid (DIDS); N-Bromosuccinimide (NBS); N-ethyl maleimide (NEM); Phenylglyoxal (PG); Diethylpyrocarbonate (DEPC).

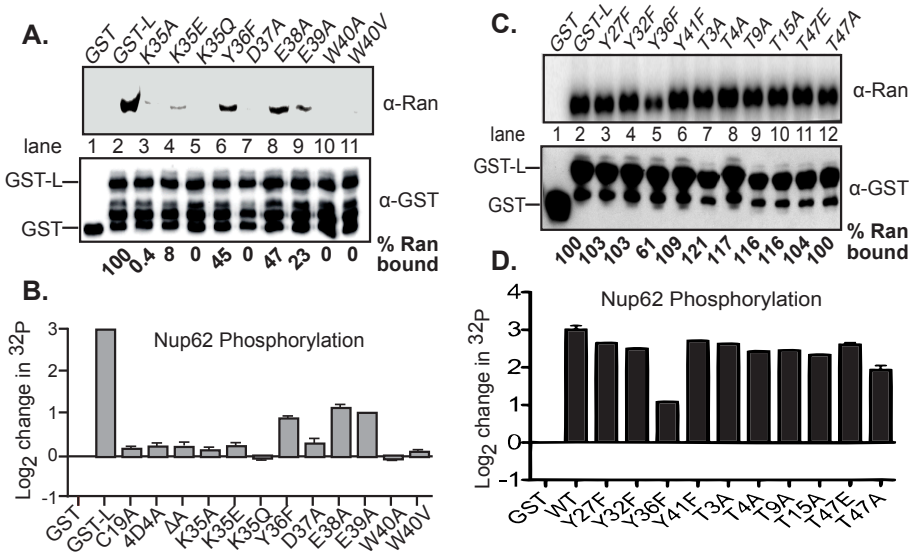

Figure 2-4. The hinge domain of Leader interactions with recombinant wtRan GTPase and enhances Leader-induced Nup62 phosphorylation. (A) Recombinant wtRan GTPase (His-Xp-Ran) was incubated with glutathione beads pre-incubated with GST, GST-L wt, K35A, K35E, K35Q, Y36F, D37A, E38A, E39A, W40A, or W40V. The protein complexes were precipitated and the ratio of Ran:L was quantified by densitometry. Lanes 5, 7, 10, and 11 demonstrate that L EMCV point mutations K35Q, D37A, W40A, and W40V are the most-inhibitory protein mutations for L:Ran binding activity. (B) HeLa cell nuclei were isolated and incubated with HeLa cytosol containing γ-32P ATP and GST or GST-L wt, K35A, K35E, K35Q, Y36F, D37A, E38A, E39A, W40A, or W40V. Nup62 was immunoprecipitated and Nup62 phosphorylation was determined by phosphorscreen detection of γ-32P incorporation. γ-32P was normalized to input Nup62 by densitometry. Log2 fold-change in Nup62 γ-32P incorporation was graphed with GST normalized to zero. (C) Recombinant wtRan GTPase (His-Xp-Ran) was incubated with glutathione beads pre-incubated with GST, GST-L wt, Y27F, Y32F, Y36F, Y41F, T3A, T4A, T9A, T15A, T47E, and T47A. The ratio of Ran:L was quantified by densitometry. Lane 5 demonstrates that L Y36F is the most-inhibitory of the L-T/Y protein mutations, at facilitating L:Ran binding activity. (D) HeLa cell nuclei were isolated and incubated with HeLa cytosol containing γ-32P ATP and GST or GST-L wt, Y27F, Y32F, Y36F, Y41F, T3A, T4A, T9A, T15A, T47E, and T47A. Nup62 phosphorylation was determined as before.

Figure 2-5. The acidic tail and residue Q69 of Ran GTPase facilitate Ran-Leader binding activity. (A) WT His-Xp, G19V, T24N, L43E, ΔDE, or Q69L recombinant Ran GTPase [loaded with GDP from bacterial expression] were purified and (B) incubated with GST or GST-L wt. Protein complexes were precipitated and the ratio of Ran:L was determined by densitometry. Lane 10 indicates that Ran acidic-tail protein mutation, Ran ΔDE, is completely inhibited for L-binding activity, while lane 12 shows that Ran Q69L exhibits enhanced L-binding activity. Wild type (WT).

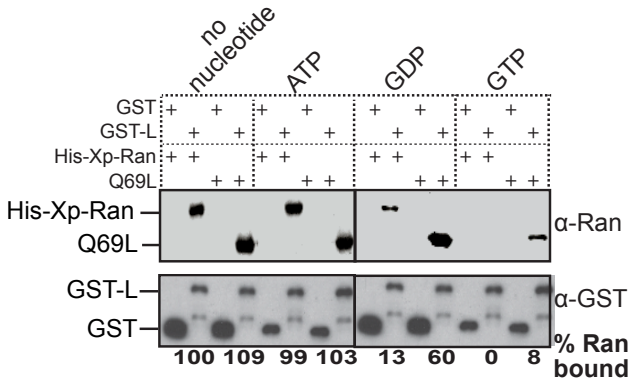

Figure 2-6. The nucleotide state of Ran GTPase influences Ran-Leader binding activity. wtRan (His-Xp-Ran) or Ran Q69L were pre-loaded with no nucleotide, ATP, GDP, or GTP by EDTA-facilitated exchange. Preloaded Ran samples were tested for L-binding activity under the same exogenous buffer conditions used in their loading. Ran GTPase displayed inhibited L-binding activity in the presence of exogenous GDP (lanes 10 and 12) and to a greater degree, in the presence of exogenous GTP (lanes 14 and 16). Ran Q69L was less inhibited by exogenous GDP and GTP than was wtRan GTPase (His-Xp-Ran). Wild type (WT).

Chapter 3.

Nuclear Magnetic Resonance Structure of Ran GTPase Determines C-terminal Tail Conformational Dynamics.

To be submitted to the *Journal of Biomolecular NMR*.

Studies were performed by Valjean R. Bacot-Davis

ABSTRACT

The nuclear pore complex (NPC) serves as a selective channel for large macromolecules to cross the nuclear envelope for functional cellular localization. The gradient of the small Ras-related nuclear GTPase, Ran GTPase, plays a crucial role in directing nucleocytoplasmic transport (NCT) in eukaryotic cells. Ran GTPase interacts with transport receptors based upon allosteric binding to GTP or GDP, which leads to a switch in protein conformation between an active and inactive state. The atomic GDP/GTP-bound conformational changes of Ran GTPase have been diligently characterized by crystallography. However, no NMR assignments have been reported for Ran GTPase. We solved the nucleotide-free conformational state of *H. sapiens* Ran GTPase (PDB ID: 2MMC and BMRB ID: 19852), characterized as sharing great similarity with the GDP-bound conformation (RMSD: 0.217-0.229) over that of the GTP-bound conformation (RMSD: 0.642-0.734), excluding minor changes in the switch I region (residues 40-43) and full resolution of the amino- and carboxyl-termini. Furthermore, resolution of the distinctive acidic tail motif, ^{211}DEDDDL^{216}, now provides

direct structural confirmation that this tail interacts with the Ran GTPase ^{139}HRKK^{142} basic patch in order to destabilize GTP-binding and stabilize GDP-binding. These NMR analyses confirm currently accepted structural mechanisms for Ran nucleotide exchange and effector binding (RanGAP, RanBP1, Exportin 1) based upon changes in the Ran GTPase switch I, switch II and acidic tail domains, further predicting that the C-terminus of Ran GTPase interacts directly with the nucleosome as well as RCC1 when undergoing GDP-GTP nucleotide exchange.

INTRODUCTION

Small GTPases are a family of G-proteins that can bind and hydrolyze guanosine triphosphate (GTP) into guanosine diphosphate (GDP). The RAS protein superfamily of small GTPases, named for the RAS oncogene, coordinate central signal transduction and protein trafficking pathways crucial for vast processes in cellular biology (26, 192). The superfamily is subdivided into six families: Rho, Ras, Rab, Arf, Sar, and Ran (26). The activities of the RAS superfamily are regulated by a switch mechanism, cycling between an active GTP-conformation, and an inactive GDP-conformation. Numerous upstream and downstream effector proteins regulate these GTPase activities, but the two main effectors are guanine nucleotide exchange factors (GEFs), and GTPase-activating proteins (GAPs). GEF binding induces molecular structural changes that facilitate the exchange of GDP for GTP. Inversely, GAP binding stimulates the intrinsic GTPase activity of these proteins to catalyze GTP hydrolysis into a GDP-bound, inactive state.

The RAS protein family shares protein homology involved in nucleotide binding and hydrolysis capabilities. The G1 box (also known as the P-loop or Walker A motif) [aaaaGxxxxGKS/T, where a = L, I, V, or M; and x-any amino acid] can recognize the purine and phosphate moiety of GDP/GTP (182, 193, 194). The G2 box acts as a sensor that changes conformation depending upon the protein's GDP/GTP bound state, whereas the G3 box (Walker B motif) helps coordinate nucleotide association with a Mg^{2+} ion (193). The G4 box distinguish the guanosine ring from that of adenosine (ATPases), and the G5 box [bbE(A/C/S/T)SA(K/L)] makes indirect contacts with the guanosine ligand.

Two protein domains of the Ras superfamily undergo major structural changes when the small GTPases are GDP- or GTP-bound: the switch I domain (aa. 32-40 for Ran GTPase) and the switch II domain (aa. 60-76 for Ran GTPase). Changes in the switch domains are known to affect the binding affinities of GTPase effector proteins such as GEFs and GAPs. For example, the α2 helix of switch II is involved in GEF recognition (195) and changes in the switch I region can inhibit GAP binding (196).

The consequence of eukaryotic cell compartmentalization is the requirement of energy-dependent, regulated transport of macromolecules across membrane barriers. The eukaryote nucleus is a membrane-enclosed organelle that retains the majority of cellular genomic DNA in a nucleoplasm dissociated from the cellular cytoplasm. The vertebrate NPC is a ~125 megaDaltons (MDa) amalgamation of 30 different proteins known as nucleoporins (Nups) (197). The Nups of the NPC function as a selective barrier, associating directly with transport receptor-cargo complexes larger that 40kDa that must cross the nuclear pore envelope for their appropriate cellular localization.

Many Nups contain disordered phenylalanine (F) and glycine (G) repeating regions (F-G repeats), which interact directly with transport proteins known as Karyopherins [Importin α-Importin β heterodimer, Transportin 1, or Exportin 1 (Crm1)] that are associated with their corresponding cargo molecules (198-200).

The small GTPase called Ras-related nuclear protein (Ran) provides the energy that coordinates trafficking of the majority of macromolecules across the nuclear envelope between the cytoplasm and the nucleoplasm. Ran-GTP is found in a higher concentration in the cellular nucleus, and this Ran-GDP/Ran-GTP concentration gradient across the nuclear envelope helps provides the energy for the nuclear import and export of these receptor-cargo complexes. The rate limiting step in nuclear import and export, also known as nucleocytoplasmic transport (NCT), is the exchange of Ran-GDP for Ran-GTP. Ran is unique among the Ras GTPase superfamily in that it only has one core GEF protein, Regulator of chromosome condensation 1 (RCC1), which facilitates the exchange of Ran-GDP to Ran-GTP. Importin-β has been described as an additional Ran GEF, but these studies are limited (201). RCC1 is tethered to chromatin inside the nucleus, and creates a higher concentration gradient of Ran-GTP in the nucleus because local GTP concentrations are higher in the nucleoplasm (202-205) (206, 207). RanGAP and Ran binding protein 1 (RanBP1) aid catalysis of Ran-GTP to Ran-GDP in the cytoplasm. As RanGAP is tethered to Nup358 on the cytoplasmic filaments of the NPC by sumoylation, RanBP1 binds to Ran-GTP, increasing the protein's intrinsic GTPase activity, while RanGAP also binds to stimulate Ran-GTP hydrolysis by forming the RanGAP-Ran-GTP-RanBP1 trimeric protein complex. Once

Ran-GTP is hydrolyzed to Ran-GDP, the nuclear transport factor 2 (NTF2) protein translocates Ran-GDP back into the nucleus for the cycle to repeat (208, 209).

MATERIALS AND METHODS

Plasmid. The plasmid encoding Hexa-His-Xpress tagged human Ran GTPase (pHis-Xp-Ran) was a gift from Mary Dasso (National Institutes of Health, Bethesda, MD).

Labeled Ran sample preparation. [U–^{15}N, U-^{13}C]-Ran GTPase was overexpressed in BL-21 (DE3) cells transformed with pHis-Xp-Ran, and grown at 30°C in [^{15}N, ^{13}C] M9 medium (42.3mM Na_2HPO_4, 22.0 mM KH_2PO_4, 8.5 mM NaCl, 18.3 mM $^{15}NH_4Cl$, 2 mM $MgSO_4$, 0.1 mM $CaCl_2$, 0.2% ^{13}C -D-glucose w/v, 50 µg/ml ampicillin, pH 7.3) induced with IPTG at a final concentration of 1 mM. Bacteria were harvested after 5-6 hours growth and purified as previously described (210). [U–^{15}N, U-^{13}C]-Ran was treated with 5mM EDTA (30 minutes, 25°C) and dialyzed (2 hours, 25°C) into 2L of final NMR buffer [20mM HEPES (pH 7.4), 100mM KCl (99.9% purity), 2mM $MgCl_2$ (99.9% purity), 2mM DTT, and 0.04% NaN_3], followed by dialysis into fresh NMR buffer over night at 4°C. Ran-bound nucleotide was determined by HPLC as previously described (191).

Structure determination by NMR Spectroscopy. Experimental pulse sequences were executed from the Biomolecular NMR pulse program catalogue using Topspin software (Bruker, version 2.0). [^{1}H–^{15}N] HSQC, [^{1}H-^{13}C] HSQC, HBHA(CO)NH, CBCA(CO)NH, HNCACB, C(CO)NH, HC(CO)NH, HC(C)H-TOCSY, 3D ^{15}N-NOESY (t_{mix} = 150 ms), 3D

^{13}C-NOESY(t_{mix} = 140 ms), and ^{31}P experiments were recorded in sample buffer supplemented with 10% $^{2}H_20$. Data were collected on 0.5mM [U–^{15}N, U–^{13}C]-His-Xp-Ran (25°C, 280µl, 5 mm Shigemi tube) using a Bruker AVIII-600 MHz spectrometer equipped with a ^{1}H, ^{13}C, ^{15}N, ^{31}P three-axis gradient cryogenic probe. NMRPipe software was used to process the raw NMR data (211). Backbone and side-chain residues were assigned manually using CARA (cara.nmr-software.org) (212) and SPARKY analysis software (213). TALOS+/RAMA+ were used to generate dihedral angle constraint files (214) for input into CYANA (215) for CYANA structure calculations.

RESULTS

Purification of His-Xp-Ran GTPase (Ran) recombinant protein. His-tagged ^{15}N/^{13}C Ran GTPase was purified using nickel sepharose affinity chromatography and imidazole gradient elution. Gel filtration followed to remove high molecular weight impurities. Ran was treated with EDTA and then dialyzed into NMR buffer to carry out final NMR experiments. Ran GTPase purity, size, and reactivity were confirmed by SDS-PAGE using Coomassie brilliant blue or immunoblot with α-Ran specific antibodies (Fig. 3-1).

NMR structure of Ran GTPase. The P loop domain of Ran GTPase, shown in red, coordinates the di- and tri-phosphate atoms of the GDP and GTP. Four additional regions of Ran GTPase alter configuration dependent upon the nucleotide-bound state of Ran GTPase: the switch I region colored in yellow-orange, the switch II region colored in green, the basic patch colored in blue, and the acidic, C-terminal tail colored

in purple (Fig. 3-2A). The 10 lowest-energy structures of Ran GTPase, *gray*, were superimposed using the backbone atom coordinates for residues 1-216 to generate a conformer root mean square average (RMSD) of 0.155 Å (PDB ID: 2MMC and BMRB ID: 19852) (Fig. 3-2B). The overall structure of nucleotide-free Ran GTPase consists of 12 α-helices and 7 β-sheets (Fig. 3-2C). The 7 anti-parallel β-sheets associate through hydrogen bonding to form the central core of Ran GTPase. The acidic tail domain of Ran GTPase forms a α-helix (α12) that interacts directly with the α-helical basic patch domain (α8) of Ran GTPase (Fig. 3-2D). Distinct Ran GTPase secondary structural elements were colored as follows: α-helices (red), β-sheets (purple), random-coil (gray) (Fig. 3-2E).

Summary of structural statistics for Ran GTPase. The quality of the structures of Ran GTPase as solved by NMR were analyzed in terms of restraint violations using the TALOS+, RAMA+ and CYANA software programs (211 2763) (215). 50 initial structures of Ran GTPase were generated using CYANA, with the final 10 included as output files. 99.1% of Ran GTPase backbone atoms were in most favored positions, with none in disallowed regions (Table 3-1).

HPLC analysis of Ran-EDTA nucleotide exchange. Ran GTPase was treated with EDTA and loaded with 20mM of GTP, GDP, or GMP. Nucleotide exchange was stabilized by 5mM $MgCl_2$, and the nucleotide-bound state of Ran GTPase was evaluated by HPLC as previously described (191). Exchange buffer was used as an internal control for guanosine nucleotide absorption levels (Fig. 3-3A). Ran GTPase

treated with EDTA-only demonstrated negligible levels of bound-GDP as carried over from bacterial expression, while the majority of EDTA-treated Ran GTPase was nucleotide-free (Fig 3-3B). Ran GTPase treated with EDTA and then incubated against GTP, GDP, or GMP followed by 5mM $MgCl_2$ were analyzed by HPLC. HPLC verified that these Ran GTPase exchange reactions resulted in > 95% of Ran GTPase in a –GTP (Fig. 3-3C), -GDP (Fig. 3-3D), or –GMP (Fig. 3-3E) bound conformation.

NMR structure of Ran GTPase. The 2D [^{15}N, ^{1}H]-HSQC spectrum of Ran GTPase displayed well-resolved resonances (Fig. 3-4A). Backbone assignments were obtained manually by cross-referencing the 2D [^{15}N, ^{1}H]-HSQC of Ran GTPase with the 3D HNCACB, 3D CBCA(CO)NH, 3D ^{15}N-NOESY and 3D ^{13}C-NOESY spectra of Ran GTPase using CARA software analysis to verify connectivities (Fig. 3-4B). Backbone assignments were assigned for 216 (83%) of the 259 residues.

TALOS+ Ran GTPase secondary structure. TALOS+ software was used to generate Ran GTPase secondary structure predictions from NMR chemical shift assignments and dihedral angle constraints. TALOS+ predictions agreed with the secondary structure previously determined for the crystal structure of Ran GTPase in its GDP-bound conformation (PDB ID: 3GJ0). Artificial Neural Network (ANN)-predicted secondary structure probabilities were determined using Random coil index-sigma squared (RCI-S^2) values, where alpha-helix (rmagenta), random coil, and beta-sheet (cyana) scores are -1.00, 0.00, and 1.00 respectively. Graph amplitudes correspond to backbone protein motions correlated to RCI-order parameters (S^2) (Fig. 3-5).

Backbone phi-psi torsional angles. Main-chain dihedral angles for the structure of Ran GTPase as solved by NMR were plotted using the Visual Molecular Dynamics (VMD) program. 99.1% (214 residues) of Ran GTPase amino acids were in most favored regions with the remaining 0.9% (2 residues) in additionally favored regions (Fig. 3-6).

Ran GTPase NMR structural comparison with Ran-GDP and Ran-GTP. The NMR structure of Ran GTPase (PDB ID: 2MMC and BMRB ID: 19852) was aligned and compared to 23 reported crystal structures of Ran GTPase deposited in the protein data bank. The NMR structure of Ran GTPase was more structurally similar to Ran-GDP, notably when aligning the switch I, switch II, and acidic tail domains (Table 3-2). Compared to Ran-GDP, the NMR structure of Ran GTPase also exhibited notable changes in residues 40-43 of the switch I domain [switch I: aa^{30-47}].

Ran GTPase secondary structure determination. The secondary structure of Ran GTPase in its –GDP and -GTP bound conformations were determined by using the crystal structures PDB ID: 3GJ0 and 1RRP, respectively. A table was generated to note Ran secondary structure correlated to residue number and structural domain changes as a result of nucleotide-binding (Table 3-3).

The NMR structure of Ran GTPase implicates Ran acidic tail-nucleosome interactions in RCC1 nucleotide exchange. The fully resolved NMR structure of Ran GTPase was aligned to the crystal structures of the Ran-RCC1 (PDB ID: 1I2M) and RCC1-

nucleosome (PDB ID: 3MVD) complexes. Superimposition of these structures involve direct Ran-nucleosome and Ran-RCC1 interactions in a trimeric RCC1-Ran-nucleosome complex that increase RCC1 facilitated nucleotide-exchange (Fig. 3-7). The newly resolved NMR structure of Ran GTPase can fully explain why the presence of nucleosomes increase RCC1's GEF activity on Ran GTPase (207, 216, 217).

DISCUSSION

To our knowledge, this is the first NMR as well as the first completely resolved structure of Ran GTPase. Previous attempts to solve the structure of Ran GTPase using crystallography have not been able to successfully resolve the protein's complete organization due to flexible motions in the amino and carboxyl-terminal domains. This nucleotide-free, NMR solution structure of Ran GTPase reveals an acidic tail, α-helical turn from D^{211} to L^{216} (α12). This nucleotide-free NMR structure of Ran GTPase is also more similar to the structures of Ran-GDP as solved by crystallography. A well-characterized protein core comprised of 7 β-sheets with the nucleotide-free conformation surrounded by 12 α-helices stabilizes Ran GTPase. Ran was treated with EDTA for NMR studies in order to remove bound guanine nucleotides carried over from bacterial expression, and it was noted that only a negligible amount of GDP remained present as detected using HPLC.

A comprehensive analysis of secondary structural changes revealed significant differences for switch I residues 41-44, residues 150-154, and C-terminal acidic residues 201-216 between nucleotide-free Ran and Ran-GDP (RMSD of 0.243-0.553).

Nucleotide-free Ran and Ran-GTP were extremely structurally dissimilar, with an RMSD of 0.466-0.715. Nucleotide unbound Ran is believed to be more structurally similar to Ran-GDP than Ran-GTP because GDP-bound Ran is the predominant form of Ran GTPase as purified from bacteria (218, 219). Following EDTA treatment, the low entropy, natively folded state of Ran GTPase is favored owing to NMR buffer conditions chosen to optimize Ran protein stability. The dynamic acidic tail suggested from analysis by crystallography, FRET and nucleotide analogue florescence spectroscopy, are now directly observable by NMR (30, 31, 40, 220). We observe that the ^{211}DEDDL^{216} acidic tail (α12) adopts a closed conformation that interacts with α8-helix basic patch residues ^{139}H-K^{142}, directly stabilizing GDP-bound nucleotide contacts, whereas changes in the C-terminus, induced by RCC1 binding, then disrupt these ionic interactions to stabilize Ran-GTP nucleotide association. These internal ionic contacts may also facilitate the transition of the GTP-bound state to the GDP-bound state as catalyzed by nucleotide hydrolysis.

The C-terminus (residues 176-216) of Ran-GTP adopt an open conformation that increases Ran affinity for RanBP1, Exportin 1, and Crm1 binding partners involved in Ran-export complexes (221). The NMR structure of Ran GTPase also supports the model by which RCC1 uses β-wedge residues 146-153 to induce global switch I, switch II, and C-terminal conformational changes, thereby allowing the C-terminus of Ran to interact briefly with the nucleosome for optimal nucleotide exchange activity (206) (207) (Fig. 3-7). Therefore, the NMR structural resolution of the dynamic ^{211}DEDDL^{216} acidic tail of Ran GTPase presents a mechanism of RCC1 mediated nucleotide exchange as

well as RanGAP-RanBP1 facilitated nucleotide hydrolysis, further agreeing with the models proposed by Bischoff, Görlich, and Makde (207, 222, 223).

Nucleotide-free changes in switch I residues 41-44 are involved in nucleotide binding (F35), Ran-RanBP1, and Ran-Importin β interactions (31), (206, 224). Ran-Karyopherin β and Ran-Crm1 complexes mask the switch II domain of Ran GTPase, and Ran-export complexes require RanBP1-switch I domain interactions to then allow RanGAP binding via the switch II domain to catalyze Ran-GTP hydrolysis (40). The switch I domain of the NMR structure of Ran GTPase is stabilized into an α-turn instead of random coil as observed for Ran-GDP (PDB: 3GJ0). Stabilization of Ran residues 150-154 in the NMR solution structure when compared to Ran-GDP (PDB ID: 3GJ0) comprise guanine-binding loop (GBL) NK-x-D residues 122-125 and are no longer involved in interactions with the guanine moiety. Residues 150-154 likely form more stable hydrogen bonding interactions in the absence of GDP as a result of EDTA treatment (182).

^{15}N backbone stability indicates similar switch region fluctuations between Ran-GDP (PDB ID: 3GJ0) and nucleotide-free Ran as observed for H-Ras-GDP and nucleotide-free H-Ras (225-227). Side-chain orientation differences were also observed for residues K23 and F35, which are involved in nucleotide coordination. ^{1}H, ^{15}N HSQC spectral peak splitting was not observed for EDTA treated Ran GTPase as was reported for NMR experiments involving H-Ras-GppNHp and H-RasT35S-GppNHp (227). Moreover, this lack of spectral peak splitting indicates that EDTA treated, nucleotide-free Ran GTPase does not switch between two different states (-GDP, -GTP), but is instead at equilibrium in a single conformational state.

Effector binding (RanBP1) stabilizes the highly mobile C-terminus of Ran-GTP, thereby alleviating the entropy cost associated with protein disorganization and Ran-RanBP1 complex formation. Furthermore, there is no additional entropy cost in the formation of Ran-GDP due to acidic-tail and basic patch salt-bridge interactions. Side-chain and effector protein kinetics also contribute to these favorable, negative free energy changes. Therefore, both backbone and side-chain modulations contribute to energetically favorable effector interactions, followed by a rigid, nucleotide-free conformations after effector dissociation (227).

Hydrolysis of Ran-GTP to Ran-GDP helps maintain the Ran gradient across the NPC to coordinate NCT. It is therefore imperative that regulatory factors recognize Ran in the appropriate nucleotide-bound conformation. Here, we reveal how acidic tail-basic patch Ran interactions are stabilized in Ran-GDP, where RCC1-Ran disrupts these interactions to induce C-terminal tail dynamics and nucleosome interactions that promote GDP-GTP exchange (207). We propose that the glycine brace (182) and the C-terminus of Ran GTPase switch conformation upon effector binding to not only regulate nucleotide exchange, but also regulate nucleotide hydrolysis (RCC1 or RanBP1-RanGAP). Thus, the nucleotide-free state of Ran GTPase can also be used as a model for designing dominant-negative drugs that suppress Ran GTPase coordination of cell cycle progression for potential cancer treatments (228). Future NMR studies of Ran-GDP, Ran-GTP, Ran GTPase protein mutations (T24N, G19V, Q69L, L43E), and Ran interactions with effectors (RanGAP, RanBP1, RCC1, and members of the Karyopherin protein family) could further elucidate dynamic rates of

interaction, exchange, and sequential transport pathway complex association and dissociation events (28).

The recently determined structure of nucleotide-free Ran GTPase could be used to reevaluated effector binding contacts in terms of the resolution of the Ran acidic tail, as well as suggest, in terms of evolution, why the Ran GTPase acidic tail is unique to Ran GTPase among the Ras superfamily of small GTPases. The three-dimensional NMR structure of Ran GTPase also offers residue-specific insights into Ran inter-domain cooperation and binding. These experiments also provide an important step towards understanding the mechanisms involved in GEF nucleotide exchange, dynamic GTPase conformational changes in the P-loop, switch I, switch II, basic patch, and C-terminus domains that Ran uses to orchestrate cellular NCT, RNA processing, and cell division. In conclusion, this solution structure of Ran GTPase, for the first time, resolves the amino terminus and carboxy terminal Ran GTPase acidic domain, thereby offering invaluable structure biological insight into NCT, Ran GTPase-mediated cell cycle control, and Ran-effector interactions.

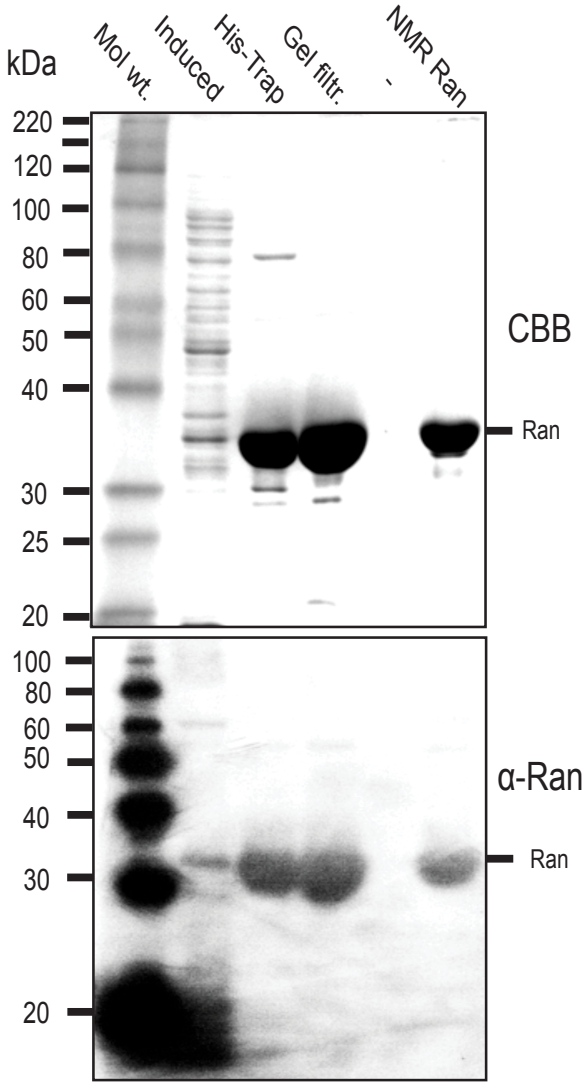

Figure 3-1. Ran GTPase protein purification. His-Xp tagged Ran GTPase was expressed in E. coli BL21 (DE3) cells. The soluble fraction (lane 2) was harvested to visualize Ran GTPase expression levels. HisTrap column bound Ran GTPase was eluted using 400mM imidazole (lane 3). Ran GTPase was then concentrated and passed over a gel filtration column in order to remove high molecular weight impurities (lane 4). Ran GTPase was EDTA treated, and dialyzed into final NMR buffer (lane 6). Proteins were visualized by coomassie brilliant blue (CBB) total protein stain and western blot.

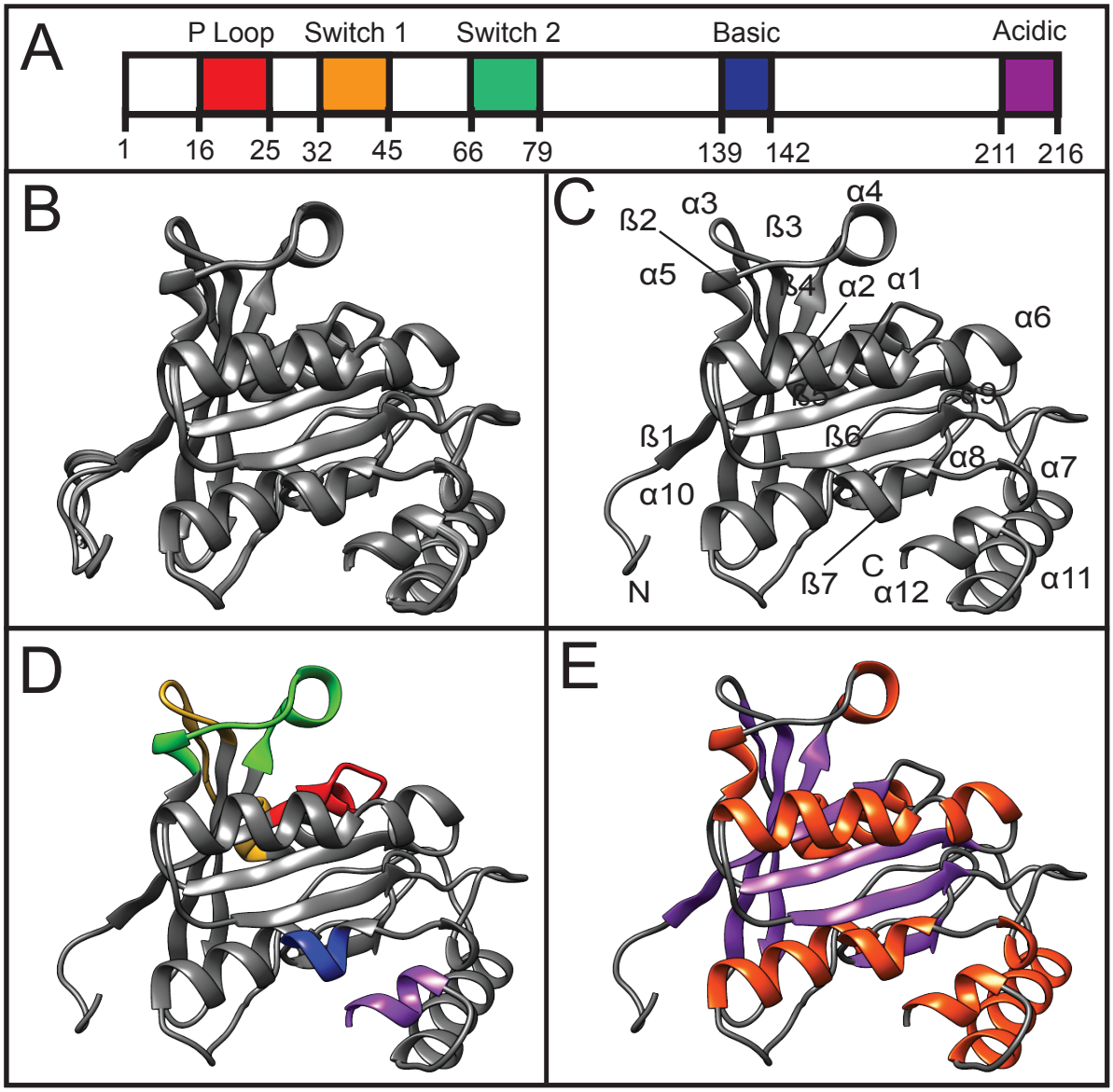

Figure 3-2. Structure of Ran GTPase. (A) Ran GTPase domain annotation. (B) Cα trace of the 10 lowest-energy Ran GTPase NMR solution structures (PDB ID: 2MMC and BMRB ID: 19852). (C) The best conformer of Ran GTPase. The N and C termini are labeled as well as the α-helices and β-strands. (D) NMR structure of nucleotide-free Ran GTPase colored in gray with structural domain colored the same as the structural schematic in panel A. (E) α-helices are colored in red, β-strands purple, and random coil gray.

TABLE 1: Ran GTPase NMR Restraints and Statistics

NMR restraints or other structural statistics	**Value for:**	**Ran**
Total distance restraints (inter-residue)		970
Number of torsion angle dynamics steps		5,000
Number of structures: Initial: 50		Final: 10
Hydrogen bonds		394
Total dihedral angle restraints		148
ϕ		74
ψ		74
Restraint violations		
Distance restraint violation > 0.2 Å		None
Distance restraint violation > 0.2 Å		2
Average rmsd (Å) among the 10 refined structures		
Residues		1-216
Backbone residues		0.155
Ramachandran statistics of 10 structures		
(% residues)		
Most favored regions		99.1
Additional allowed regions		0.9
Disallowed regions		0

.

Table 3-1. Ran GTPase NMR Restraints and Statistics. Ran GTPase CYANA structural restraints as determined using TALOS+/RAMA+ following backbone and side-chain residue chemical shift assignments.

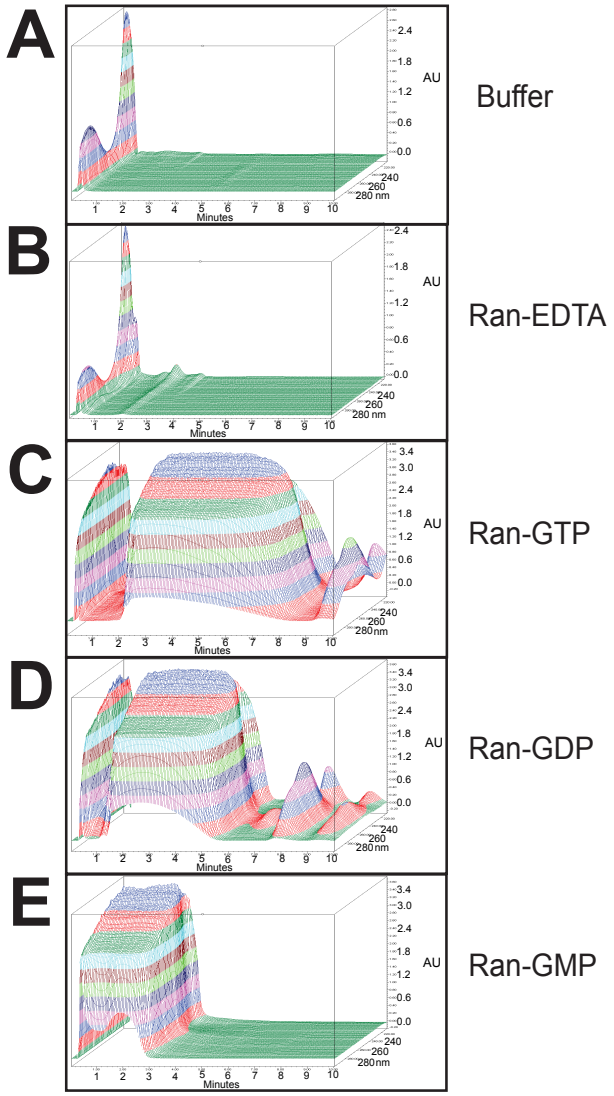

Figure 3-3. HPLC of Ran GTPase loaded with GTP, GDP, or GMP. Ran GTPase was treated with EDTA followed with buffer, 20mM GTP, GDP, or GMP and 5mM MgCl2. After 3 rounds of dialysis to remove unbound nucleotide, (B) The nucleotide-free Ran, (C) Ran-GTP, (D) Ran-GDP, and (E) Ran-GMP proteins were heated to release bound nucleotide, and samples clarified and injected onto a POROS 20 HQ column. (A) Reaction buffer was analyzed as a negative control. AU, absorbance units.

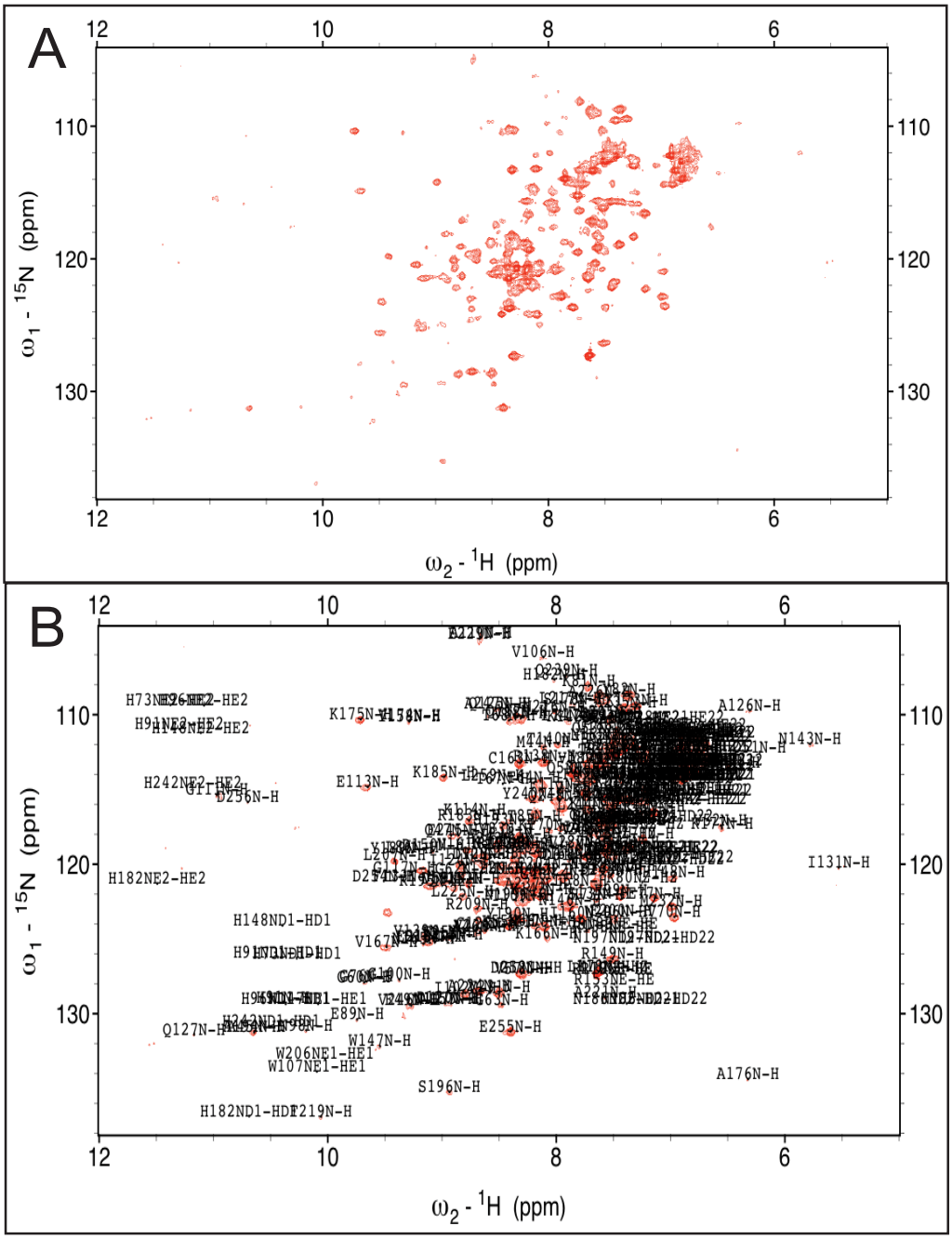

Figure 3-4. Analysis of Ran GTPase by NMR Spectroscopy. (A) Illustration of the backbone amide chemical shifts of the 2D [15N, 1H]-HSQC spectrum of Ran GTPase. (B) Residue-specific backbone assignments were illustrated on the 2D [15N, 1H]-HSQC spectrum of Ran GTPase.

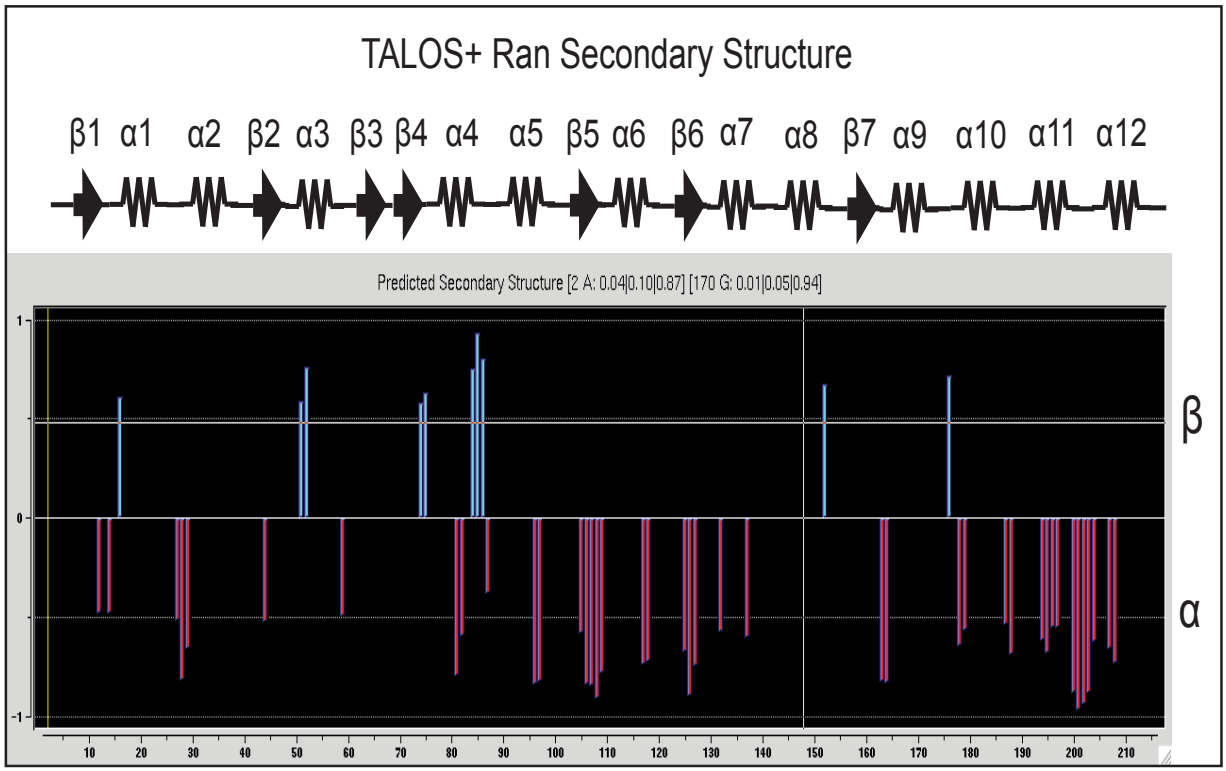

Figure 3-5. Characterization of Ran GTPase TALOS+ Refinement. TALOS+/RAMA+ used the Random coil index (RCI) method and Artificial Neural Network (ANN) to predict the secondary structures for Ran GTPase residues. Positive values (aqua) represent β-sheet structure predictions, negative values (red) represent α-helix structure predictions, and values of zero represent random coil conformations. Secondary structural elements are noted above the graph.

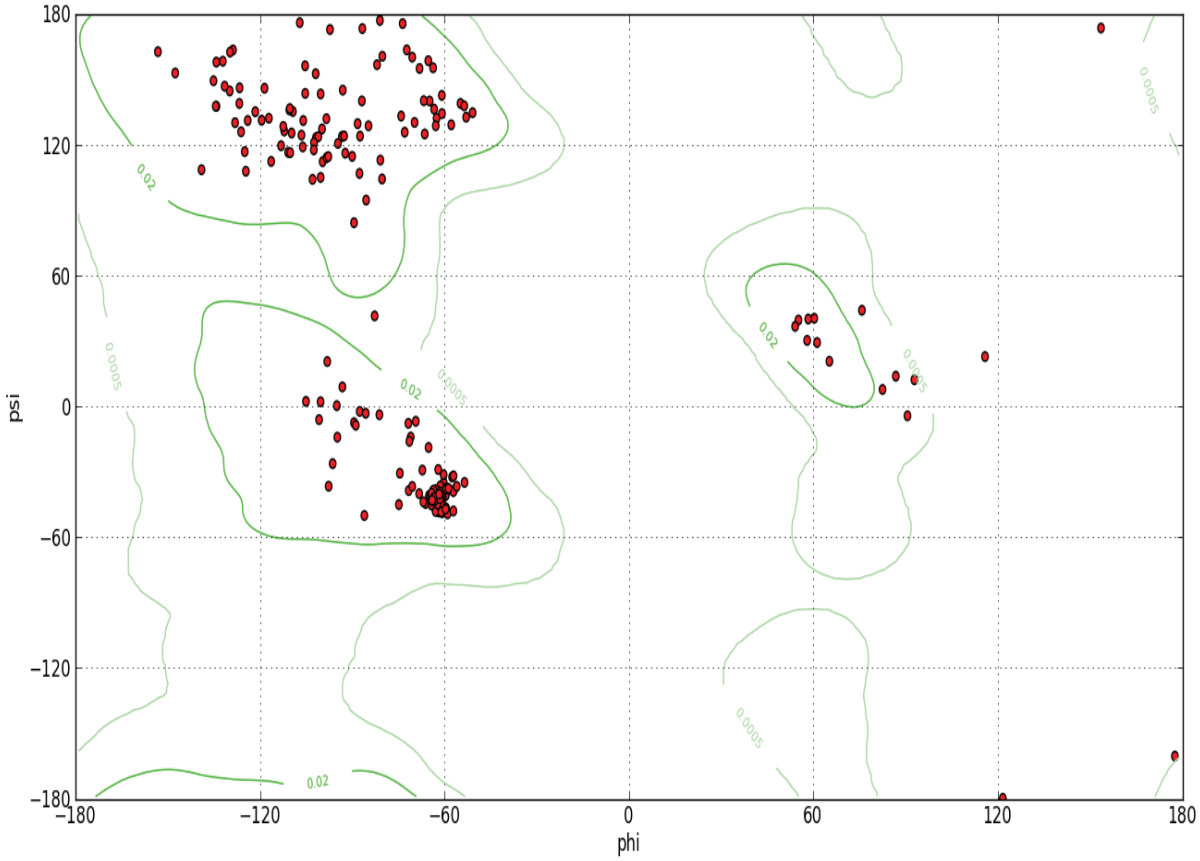

Figure 3-6. Phi-Psi torsional restrictions. The Ramachandran plot of Ran GTPase characterized 214 residues in favored regions, 2 residues in additionally allowed regions, and no residues in disallowed regions.

TABLE 2: Root Mean Square Values of Ran GTPase Alignments

			Å RMSD vs Ran (NMR)					
Ran PDB	**Bound GNP**	**Length**	**All 1-216**	**Core 8-176**	**COOH 177-216**	**P-loop 16-25**	**Switch 1 32-45**	**Switch 2 66-79**
1I2M	0	8-176	0.727	0.721	-	0.139	2.449	2.911
1BYU	GDP	9-177	0.553	0.516	-	0.211	0.491	0.243
3GJ0	GDP	1-207	0.243	0.229	0.418	0.142	0.165	0.218
3CH5	GDP	7-205	0.363	0.33	0.6	0.165	0.308	0.308
3GJ3	GDP	6-207	0.325	0.284	0.332	0.162	0.291	0.404
1A2K	GDP	8-203	0.293	0.273	0.511	0.182	0.35	0.328
1K5G	GTP	8-213	0.664	0.599	8.041	0.386	4.11	3.361
3GJX	GTP	9-179	0.466	0.463	-	0.277	4.176	3.492
3EA5	GTP	6-179	0.388	0.389	-	0.181	4.215	3.531
2BKU	GTP	9-177	0.505	0.505	3.321	0.23	4.142	3.519
1RRP	GTP	8-211	0.632	0.527	4.915	0.289	4.189	2.962
4OL0	GTP	8-179	0.471	0.462	-	0.242	4.147	3.436
1IBR	GTP	9-177	0.487	0.487	-	0.191	4.133	3.471
1QBK	GTP	8-197	0.654	0.613	4.637	0.259	4.164	3.325
4HB2	GTP	9-216	0.656	0.542	9.316	0.187	4.17	3.31
1K5D	GTP	8-213	0.715	0.592	8.266	0.26	4.2	3.359
2X19	GTP	8-179	0.535	0.535	-	0.278	4.173	3.375
3A6P	GTP	7-176	0.472	0.472	-	0.192	4.199	3.569
3NC1	GTP	8-180	0.598	0.598	1.218	0.313	4.274	3.393
3W3Z	GTP	6-176	0.485	0.477	-	0.234	4.187	3.154
3ZJY	GTP	9-177	0.498	0.494	-	0.376	4.173	3.356
1WA5	GTP	7-176	0.485	0.485	-	0.245	4.198	3.558
3NBY	GTP	9-179	0.574	0.57	-	0.246	4.238	3.346
3NBZ	GTP	8-180	0.526	0.508	1.09	0.28	4.226	3.395

Table 3-2. Root Mean Square Values of Ran GTPase Alignments. The nucleotide-free, NMR-determined structure of Ran GTPase was aligned to previously reported structures of Ran GTPase deposited in the protein data bank. Root mean square values approaching zero indicate increasing similarities of each protein structure.

TABLE 3: Ran GTPase Secondary Structural Motifs

2°	Ran-GDP (3GJ0)	2°	Ran-GTP (1RRP)	2°	Ran-empty (NMR)
β1	10-17 (P loop)	β1	10-16 (P loop)	β1	9-16 (P loop)
α1	22-28 (P loop)	α1	22-30 (P loop)	α1	22-29 (P loop)
α2	30-36 (Switch I)	β2	46-54	α2	31-36 (Switch I)
β2	38-40 (Switch I)	β3	57-65	β2	38-40 (Switch I)
β3	45-54 (Switch I)	α2	69-72 (Switch II)	α3	41-43 (Switch I)
β4	57-66 (Switch II)	β4	85-90	β3	44-53 (Switch I)
α3	68-72 (Switch II)	α3	95-111	β4	58-66 (Switch II)
α4	76-82	β5	116-121	α4	69-72 (Switch II)
β5	85-91	α4	133-135	α5	77-80 (Switch II)
α5	94-113	α5	138-141 (Basic)	β5	85-91
β6	117-122	β6	145-148	α6	94-111
α6	131-142 (Basic)	α6	159-169	β6	117-122
β7	145-148	α7	191-205	α7	132-136
α7	157-170			α8	137-143 (Basic)
α8	190-206			β7	145-149
				α9	151-153
				α10	157-170
				α11	190-206
				α12	211-216 (Acidic)

Table 3-3. Ran GTPase Secondary Structural Motifs. Ran GTPase residues associated with secondary structure and functionally characterized protein domains.

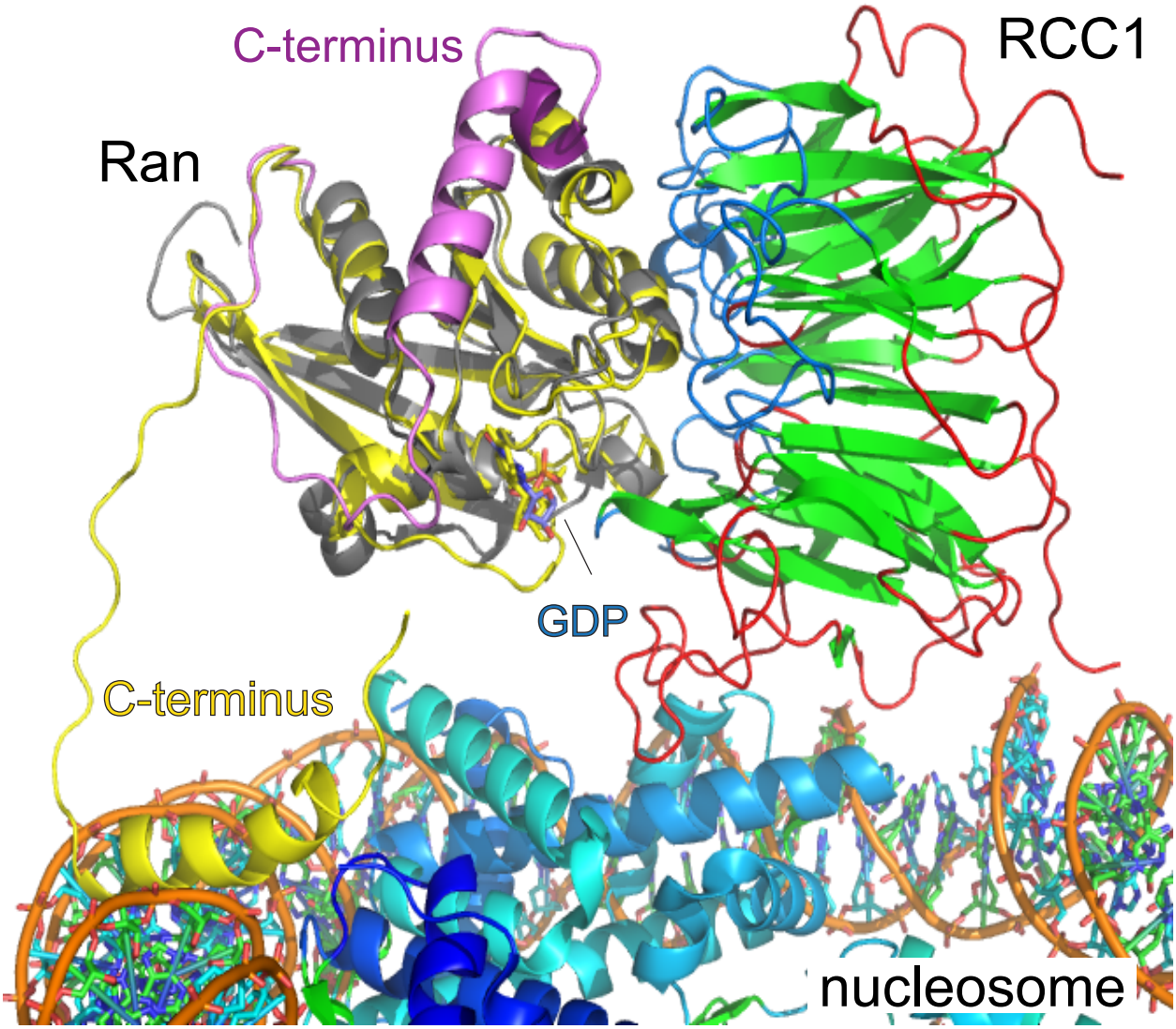

Figure 3-7. Model of Ran-RCC1-nucleosome dynamics in nucleotide exchange.

The NMR structure of Ran GTPase (gray) was aligned to the Ran-RCC1 (PDB ID: 1I2M) and RCC1-nucleosome complexes (PDB ID: 3MVD). The C-terminus of the NMR structure of Ran GTPase is shown in light purple, with the acidic tail in dark purple. GDP was also modeled by aligning the NMR structure of Ran with Ran-GDP (PDB ID: 3GJ0) and then aligned to Ran-GTP (PDB ID: 1RRP) to illustrate conformational C-terminal changes, likely induced by RCC1 to facilitate Ran nucleotide exchange. Ran-GTP is shown in yellow.

Chapter 4.

Solution Structures of Mengovirus Leader Protein, its Phosphorylated Derivatives, and in Complex with RanGTPase

Submitted to *Proceeding of the National Academy of Sciences-USA* (06-13-2014).

Claudia C. Cornilescu (NMRFAM at Madison) conducted the initial NMR studies on L_M, Holly A. Basta and Jessica J. Ciomperlik (Palmenberg Lab) performed the study described in Figure 5, and Valjean R. Bacot-Davis performed all other NMR studies.

ABSTRACT

The Cardiovirus Leader (L) protein is a viral factor that inhibits the antiviral, interferon response using a now characterized, novel mechanism. L induces potent anti-host inhibition of active cellular nucleocytoplasmic trafficking and interferon production by triggering aberrant hyper-phosphorylation of nuclear pore proteins (Nup). To achieve this, L binds RanGTPase (Ran), a key trafficking regulator, and diverts it into tertiary or quaternary complexes with required kinases. The activity of L is regulated by two phosphorylation events not required for Ran binding. Matched NMR studies on the unphosphorylated, singly-, and doubly-phosphorylated variants of Mengovirus L (L_M) show both modifications act together to partially stabilize a short internal α-helix comprising L_M residues 43 to 46. The stabilization of this motif implies that ionic and

Van der Waals forces contributed by phosphorylation help organize downstream residues 48-67 into a new interface. The full structure of L_M as bound to Ran (unlabeled) and Ran (216 aa) as bound by L_M (unlabeled), places L_M into the BP1, Ran-binding hydrolysis factor, binding site of Ran, wrapped by the conformational flexible COOH tail. The arrangement explains the tight K_D for this complex and places the L_M zinc-finger and phosphorylation interface as surface exposed and available for subsequent reactions. The core structure of Ran, outside the COOH tail, is not altered by L_M binding and remains accessible for canonical RanGTP partner interactions. Pull-down assays identify at least one putative Ran:L_M partner as an exportin, Crm1 or CAS. A model of Ran:L_M:Crm1, based on the new structures suggests L_M phosphorylation status mediate Ran's selection of exportin(s) and cargo(s), perverting these native trafficking elements into the lethal anti-host Nup phosphorylation pathways.

INTRODUCTION

The *Picornaviridae* family encompasses 26 genera and 46 species (5). Common to all isolates, the single-stranded, positive-sense RNA genome is characterized by a long open reading frame (ORF) encoding 10-14 concatenated protein-coding genes. The replication cycle initiates as soon as this ORF is translated and the resulting polyprotein is processed (co- and post-translationally) into the required active components. These include 7-8 non-structural proteins (NSP) and 3-4 capsid proteins designated according to a standard "L-4-3-4" nomenclature (229). The Leader (L) proteins when present precede the capsid proteins (1ABCD) and all the other NSPs (2ABC, 3ABCD). Most

NSPs have vital roles in viral replication, but the L and 2A proteins are key determinants for anti-host responses. The specific genes at these locales vary significantly among the genera and even among related species.

Unique to isolates in the *Cardiovirus* genus, the Leader gene encodes a small (67-76 amino acids) highly acidic protein (pI 3.2-3.6) with very unusual properties. When L is expressed in cells by viral or recombinant introduction, it binds tightly (3 nM K_D) with 1:1 stoichiometry to the nuclear transport regulator, RanGTPase (162). Ran, a member of the Ras superfamily of GTPases, normally alternates between nuclear GTP- and cytoplasmic GDP-bound conformers, acting as a molecular switch for the coordinated transport of large molecules back and forth through the nuclear pores (25). However, when L binds Ran, the perverted complex recruits and activates a specific cohort of cellular kinases responsible for the L-induced hyperphosphorylation of Phe/Gly-containing nuclear pore proteins (Nups) (73, 74, 76, 148). The consequence is rapid, potent inhibition of active nuclear-cytoplasmic trafficking. Since picornaviruses replicate in the cytoplasm and do not require many nuclear factors, nucleocytoplasmic transport inhibition is detrimental only to the cell. Among the measured effects are antagonism of interferon (IFN) transcription (70, 75, 230, 231), impediment of cellular stress granule formation (77), and retention of cellular mRNA transcripts in the nucleus (75). These cumulative activities allow cardioviruses to negate almost all host antiviral innate immune responses and enhance their pathogenicity during infection.

The best studied L proteins, representing the *Encephalomyocarditis virus* species, are from EMCV-R (L_E) and Mengovirus (L_M) isolates. The species as a whole shares ~95% identity here, but these strains differ by a single substitution ($L_{14}M$) in the 67 amino acid (aa) protein length (Fig. 1A). The change is in a conserved, amino-proximal CHCC zinc finger domain (aa 10-22), the structure of which was determined by NMR for the L_M protein (161). Technical difficulties have hampered resolution of the complete protein, but a full coordinate set was recently completed (PDB: 2M7Y). Outside of the zinc-finger, the rest of that protein configured predominantly as coiled-coil with a small β-hairpin in the COOH-proximal acidic motif (aa 37-61). The remaining interior residues, or hinge region (aa 23-36), have been mapped as the primary contact point(s) for interactions with Ran, in what is presumed to be an induced-fit binding (210). In cells or via recombinant proteins, saturation binding with L_M is best achieved when Ran is aided by catalytic amounts of its cognate guanine nucleotide exchange factor 1 (RCC1), allowing it to transform between GTP- and GDP-bound conformers (162). Complicating a resolution of the full L-dependent antiviral mechanism are observations that L_E is itself phosphorylated during EMCV infection, in sequential reactions with casein kinase 2 (CK2) and spleen tyrosine kinase (Syk) at residues T_{47} and Y_{41}, respectively (71). While not required for Ran interactions the L_E modifications are clearly important to the virus, because mutation at these same sites prevents subsequent Nup phosphorylation (148), suppresses NF-κB activation, and restricts infection-dependent IFN I stimulation (IRF-3 inhibition) (70, 75, 231).

The initial solution structure of L_M did not indicate how phosphorylation might affect the conformation of this protein, influence Ran binding, or contribute to activity of the Ran:L_M complex. Accordingly, we carried out new, matched NMR studies on the unphosphorylated (L_M0P), singly-phosphorylated (L_M1P, T_{47}), and doubly-phosphorylated (L_M2P, Y_{41}/T_{47}) variants of recombinant L_M. In addition, the solution structures of L_M (labeled) as bound to Ran (unlabeled), and of Ran (labeled) as bound to L_M (unlabeled) were resolved by NMR and docked to each other. The combined datasets clearly define the Ran:L_M interfaces available for ternary interactions. Pull down assays with GST-L_M and mutant phosphorylation derivatives, combined with previously resolved structures of Ran binding partners, predict the L_M phosphorylation interface and the L_M zinc-finger mediate Ran's selection of exportins including Crm1 or CAS, and their respective (kinase) cargos.

RESULTS

L_E phosphorylation sites. The L_E (EMCV) and L_M (Mengo) proteins differ by a single substitution (L_{14} vs M_{14}, respectively), but at the nucleotide level, convenient restriction sites make it easier to manipulate L_E rather than L_M sequences. The zinc-finger domain of L_M has been described by NMR (161), but before extending this work to the fully phosphorylated protein, we sought to confirm the kinase specificities. A panel of 12 GST-L_E proteins was prepared, with alterations at every Thr and Tyr residue. The double mutation $Y_{41}F/T_{47}A$ was also included. The experiments, summarized in Table 4-1, confirmed previous reports (71) that CK2 uniquely recognizes T_{47}. This reaction is an

obligate prerequisite to the single-site Syk phosphorylation at Y_{41}, a requirement that can be bypassed only if T_{47} position is substituted with a phosphomimetic aspartate ($T_{47}E$) or glutamate (71). The lack of phosphorylation at the Y_{41}/T_{47} mutated sites is not due to protein misfolding (210).

L_M NMR determinations. Previous attempts to determine an L_M solution structure were confounded by contaminating heavy metals with affinity for the protein acidic motif (161). The problem was solved by treating samples with EDTA after the removal of the GST tag and then refolding by gradual addition of $ZnCl_2$. Dialysis removed exogenous zinc, a requirement for subsequent co-solubility with RanGTPase. The preferred recombinant configurations extended the native L_M sequence (67 aa) by 4 aa (Gly-Ser-Thr-Ala) at the amino terminus (Fig. 4-1B). Such extensions do not affect L_E activity (74, 162). Single (CK2), or double (CK2/Syk) phosphorylation reactions preceded the EDTA step. All labeled or unlabeled materials were assayed for molecular weight (SDS-PAGE, MALDI Mass Spec), proper folding by ^{1}H spectra (210), and biological activity (72) before structural determinations.

L_M0P, L_M1P, and L_M2P samples ($^{15}N/^{13}C$) were investigated by high-field ^{1}H, ^{15}N, ^{13}C, ^{31}P NMR spectroscopy. Superimposition of 2D [^{15}N, ^{1}H]-HSQC spectra showed distinct peak changes indicating global chemical shifts upon protein phosphorylation. Residue-specific backbone assignments were obtained by cross referencing the 2D [^{15}N, ^{1}H]-HSQC of all 3 proteins, as well as 3D HNCACB, 3D CBCA(CO)NH, 3D ^{15}N-NOESY and 3D ^{13}C-NOESY spectra, using CARA analysis to verify sequential

connectivity. For all proteins, backbone resonance assignments could be obtained for 100% of the 71 residues. The buffer conditions required for solubility, elevated the ^{31}P background signals to the extent that these particular peaks had to be normalized to maximum resonance levels to obtain good resolution. No above-background ^{31}P signal was identified in L_M0P protein samples, confirming that bacterial expression did not add phosphates. After treatment with CK2 or CK2/Syk, one or two additional major ^{31}P peaks were identified for L_M1P and L_M2P, at high resolution in isolated 1D ^{31}P ppm spectral regions (data not shown). This finding confirmed the mass spectrometry results showing that >80% of L_M1P was phosphorylated, and >60% of L_M2P was doubly phosphorylated. The resolution statistics for all 3 proteins are summarized in Table 4-2. The 10 lowest energy structures for L_M0P, L_M1P and L_M2P are deposited in PDB (2MMH, 2MML, 2MMK), and their corresponding data are available from BMRB (19084, 19858, 19857). The bound zinc ion, not directly detected by these methods, was modeled into the coordinate files.

L_M0P/1P/2P comparisons. According to the residue numbering for recombinant L_M (native +4), the zinc finger (aa 14-26), hinge region (aa 35-45) and acidic motif (aa 41-65) form phenotypic landmarks defined by mutagenesis studies (210). In this nomenclature, T_{51} and Y_{45} are the phosphorylation sites (71). When L_M0P, L_M1P, and L_M2P were superimposed, the overall RMSD was 12.76 Å for all backbone atoms. The majority of L_M0P was a floppy, random coil, interspersed with 4 short helices (Fig. 4-1C, Fig. 4-2AB). As defined by TALOS+ algorithms (211), the α1 and α2 segments (aa 23-

26, 29-31) spanned the COOH-half of the zinc finger. The α3 and α4 domains, in the hinge region (aa 45-49) and near the COOH tail (aa 63-66), were less well defined.

Surprisingly, when 1 or 2 phosphates were added, the overall proteins still configured largely as random coil (Fig. 4-1DE). Superimposed L_M1P (Fig. 4-2CD) and L_M2P (Fig. 4-2EF) states, oriented by their zinc fingers, had RMSD values of 11.792 Å and 13.728 Å, respectively. The phosphates did not overtly reorganize their immediate locales and changes in the COOH halves of the proteins were statistically unexceptional. Instead, the upstream zinc finger regions now showed markedly less flexibility, to the extent that in both cases, these regions stiffened into a single contiguous helix (Fig. 4-1, Fig. 4-2GH). For L_M2P, the increased rigidity partially extended into the hinge and acidic motifs, making all of the states more compact and easier to superimpose throughout their lengths. The zinc-finger RMDS values were 0.602 Å and 1.603 Å respectively. Although compressed topology was the most noticeable structural characteristic of progressive L_M phosphorylation, in none of the states, for any of the proteins, was there evidence of direct interactions among the defined phenotypic domains. Notably though, L_M phosphorylation did affect residue H_{16} of the zinc-finger, showing solution oscillations of 5-6 Å in L_M1P and another 4-5 Å in L_M2P, relative to state-1. The H_{16} motility suggests alterations in additional zinc-finger contacts and its putative associations as a direct result of L_M phosphorylation. As a rule, the zinc-finger and acidic regions were separated in rough U-shaped conformations with independent faces, presumably available for different induced-fit binding partners.

Ran:(L_M0P) NMR determinations. The main binding partner for Cardiovirus L protein, RanGTPase, is insensitive to the phosphorylation status of L_M or L_E (71). Likewise, L_M(0P/1P/2P) is insensitive to the nucleotide status of Ran (GTP, GDP, unbound) as long as the binding mix contains catalytic amounts of RCC1, a natural nuclear auxiliary factor that helps Ran morph among its conformers (162). Simultaneous resolution of a full Ran:L_M0P complex (216 aa and 71 aa) tests the practical limits of NMR, so paired combinations of labeled ($^{15}N/^{13}C$) and unlabeled proteins were analyzed in parallel, under identical conditions to the single L_M determinations. The native (unbound) solution structure of nucleotide-free Ran will be described in detail elsewhere (PDB: 2MMC, BMRB: 19852). This dataset aided the assignment of 100% of the 216 Ran resonance peaks from the docked complex(es). The resolution statistics for Ran:(L_M0P) are summarized in Table 4-2.

The 10 lowest energy states for Ran, as bound by L_M0P (PDB: 2MMG, BMRB: 19854) showed a 6-sheet β-propeller core structure, interspersed with 9 α-helices (Fig. 4-3C), characteristic of other described crystal structures (31, 232). Relative to each other (Table 4-3), the core states (aa 8-176) were tight (RMSD of 0.260 Å), but the full protein value (RMSD: 4.551 Å) was higher because the COOH-tails (aa 177-216) in each state generally displayed as flexible, floppy arches (Fig. 4-4A). All these tails (RMSD: 4.896 Å) had the same central helix (aa 196-206), but none were similarly oriented relative to the core. Among Ran structures by crystallography, the acidic COOH-tail arrangements can vary according to nucleotide status and binding-partner induced shifts that may also involve the nucleotide-proximal phosphate binding P-loop

(aa 16-25), Switch 1 (aa 32-45), Switch 2 (aa 66-79) and basic patch (aa 139-142) internal core segments (Fig. 4-3A) (181). When L_M0P bound to Ran, the spectra recorded 36 amide ^{1}H and ^{15}N chemical shifts within a defined subset of residues. These included D_{18}, T_{21}, and K_{23} of the P-loop, E_{36} of the Switch I domain, Q_{69} and Y_{80} of the Switch II domain, H_{139} and R_{140} of the basic patch, as well as D_{211} and D_{213} of the acidic tail. Several of these locations, particularly in the COOH tail, were previously predicted by mutational mapping, as essential to L_M interactions (210)

To describe the solution structure of Ran bound by L_M0P in the context of Ran domains affected by nucleotide interactions, the state-1 coordinates were aligned pairwise with representative PDB entries (Table 4-3). Only a few such structures have resolved COOH tails so it was not unexpected that the full-length comparisons ("all"), or comparisons specific for this region ("COOH") showed variability (RMSD: ~1.5-12.5 Å). The "core" region comparisons, however, more closely aligned Ran:(L_M0P) with the known GTP-dependent conformers (RMSD: ~1.5 Å) as opposed to GDP- or nucleotide-free forms (RMSD: ~3.9 Å). Among these, the core coordinates of 1K5G fit the Ran:(L_M0P) state-1 to a remarkable degree. The overall RMSD (0.446 Å) between these structures showed very low variability in all backbone residues, including the P-loop (0.228 Å), Switch 1 (0.317 Å) and Switch 2 (0.345 Å) segments. This particular data set, and the closely related 15KD, describe Ran in complex with auxiliary factors RanBP1 and RanGAP, in a GTP-ground state and in a hydrolysis transition-state mimic (208). The NMR solution structure of Ran, as bound by L_M0P, exhibits essentially the same core coordinates.

(Ran):L_M NMR determinations. When the $^{15}N/^{13}C$ protein labels were reciprocated in Ran:L_M0P complexes, the states of L_M0P influenced by Ran showed multiple peak shifts relative to free L_M0P (Fig. 4-1G). The shifts included all residues in the hinge region, as had been anticipated from mutagenesis mapping (210). Also involved were regions from the carboxyl third of the protein (Fig. 4-1G, 4-4C). The zinc-finger region did not change, maintaining the α1 and α2 helices (Fig. 4-1F). But as with both phosphorylation datasets, the rest of (Ran):L_M0P now became more compact (Fig. 4-4B). The 10 low energy states (PDB: 2MMI, BMRB: 19855) remained predominantly coiled-coil with an average RMSD of 4.551 Å for backbone atoms. The fit with Ran was clearly induced by mutual binding, and not due to any obvious latent L_M0P rearrangements.

The state-1 coordinate sets representing Ran:(L_M0P) and (Ran):L_M0P were evaluated for fit according to GRAMM-X (190) and HADDOCK algorithms (233) without specified constraints. Previous (pseudo-) docking models (210) pairing the initial solution structure of L_M (2M7Y) with Ran (1K5G), predicted the interactions at the Ran:BP1 binding face with the Ran COOH tail wrapping around L_M0P to hold it firmly onto this surface. The real solution structures, when docked, indeed followed this pattern. For the HADDOCK outputs, the best cluster (models #1-4) had average RMSDs of 0.47-0.76 Å, with E-total of 305-343 Kcal/mole for the interface. As depicted in the optimal energy model (#1) L_M0P sits tightly on the “top” surface of Ran, without altering the Ran core, or approaching the nucleotide binding pocket (Fig. 4-4C). The L_M0P hinge and acidic motifs interact significantly with the proximal tip of the Ran

COOH tail (aa 203-210), but the remainder of this segment is free to arch without steric hindrance, transforming and encircling central interaction residues of L_M0P (Fig. 4-4D). Fundamentally, this orientation looks very similar to Ran:BP1 complexes as they are presented in determined crystal structures (e.g 1K5G). The buried Ran:L_M0P interface covers ~1700 sq Å, including about 28% of the L_M0P residues and 13% of the Ran residues (Fig 1G, Fig 3D). Extensive hydrogen bonding (>20x) and salt bridges (e.g., L_M0P K_{34} vs Ran E_{34}) readily account for the low 3 nM K_D (210). Important Ran:L_M0P contacts include T_{32}:L_{37}, A_{183}:D_{41}, P_{184}:Y_{45}, P_{185}:E_{42}, Q_{196}:Y_{36}, Y_{197}:Y_{40}; Y_{197}:W_{44}, A_{204}:G_{34}, A_{204}:L_{38}, and T_{207}:N_{33} (Fig. 4-4E). These protein placements are fully consistent with both determined Ran:(L_M0P) and (Ran):L_M0P NMR datasets and all resonance shifts relative to the unbound proteins. It explains the low RMSD for the core of bound Ran, flexibility of the Ran COOH tail, and requirements that the L_M0P zinc finger domain make no contacts with Ran that would prevent it from folding like the native L_M0P protein. In this configuration, both L_M0P phosphorylation sites are solvent exposed on the same face as the zinc finger, even though the loops which display and orient them, form key Ran contacts.

DISCUSSION

Cardiovirus L proteins are extraordinarily toxic to cells because their presence triggers massive hyperphosphorylation of Phe/Gly nuclear pore proteins (Nups). In cell-free assays with intact nuclei, within 5 minutes of the introduction of recombinant GST-L_E, there is complete inhibition of all active import and export of host proteins and RNA

through the nuclear pore complexes (NPC) (72). The discovery that L_E bound RanGTPase, the key regulator of nucleocytoplasmic trafficking (NCT), raised the initial possibility of putative stoichiometric inhibition. This idea was quickly discarded because Ran is an abundant protein (234), and only tiny amounts of L_E are required to trigger this effect. Instead, Ran:L_E binding is leveraged by consequent activation of a potent Nup phosphorylation cascade, the true cause of trafficking inhibition. This inhibition happens in infected cells even before the virus begins to replicate (73, 235). The cascade involves Erk1/2 and p38 kinases, and is absolutely dependent upon Ran:L_E interactions, and also upon the dual phosphorylation of L_E itself, an activity that is a prerequisite, not a consequence of the Nup modifications (69, 70, 74, 210). Furthermore, the L_E zinc-finger domain must remain intact and chelated to the metal for the protein to function (231). These points were clearly established with extensive activity assays, mutagenesis and biochemical studies.

Since neither L_E nor Ran is a kinase, an obvious ensuing step must involve recruitment of one or more critical ternary/quaternary partners. The identification of these elements is underway. We are focusing on plausible pathways by which Erk1/2 and p38 can be diverted from their normal activities to act upon Nups. But since native Ran has many interaction partners, and L_E must be phosphorylated for full activity, sorting out precise sequence of steps is complicated. To aid in this process, as described here, we resolved the NMR solution structures of L_M, its phosphorylated derivatives, and the Ran:L_M0P complex. The studies had three goals: (A) determine whether phosphorylation significantly altered the structure of L_M; (B) determine the

format of Ran as bound by L_M, so that germane native binding partners could be evaluated; and (C), determine the segments of L_M, not impacted by Ran, and therefore accessible to later interactions.

The L_M(0P/1P/2P) datasets showed this protein, in a free format, does not have a very organized secondary structure, except for the zinc finger domain. Phosphorylation clearly provided important constraints on the degree of coiled-coil motion, but did not by itself induce an overt, restricted format. If conformation plays a role in L_M activity, outside of the zinc finger, it must be induced by the relevant binding partners. Indeed, when bound to Ran, L_M0P condensed and made specific contacts in the central hinge and acidic motifs, via the same residues identified by mutagenesis (72, 210). Surprisingly however, the N-terminal third of the protein, including the zinc finger, and also both internal phosphorylation sites were left solvent exposed. That L_M could be phosphorylated after Ran binding had been established (71). It was not expected that these sites and the zinc finger would localize to the same exposed face.

The Ran:L_M0P complex is the first solution structure for Ran and the first to describe the intact, full-length protein. At least 45 Ran datasets have been collected and resolved by crystallography, but in almost all cases, 4-9 amino-terminal residues and >40 carboxyl-terminal residues are unresolved or were not included in the determinations. The entries differ in nucleotide-bound status and co-resolution of diverse transport-related binding partners. By NMR, it was clear that L_M0P binding induced a Ran conformer almost identical to that assumed when Ran binds normally to BP1, a

cytoplasmic auxiliary factor (e.g. 1K5G). In combination with RanGAP, which interacts on another face of Ran, BP1 helps accelerate the intrinsically slow RanGTPase function, thus recycling the protein to its GDP format. Although the Ran:(L_M0P) complex was nucleotide free, the P-loop, Switch 1 and Switch 2 regions were "set" to the typical GTP formats, as they would be naturally, whenever Ran exits the nucleus, usually bound to an exportin, and makes initial cytoplasmic contacts with BP1 and RanGAP (208). L_M and BP1 do not share sequence similarity, yet on Ran, they occupy quite similar footprints and their binding is mutually exclusive (72). Not captured by crystallography, but very apparent by NMR, was the dynamic morphing of the Ran COOH tail over the top of this binding partner face. L_M0P made important contacts with the beginning and end of this segment, but the resolved states recorded considerable movement here for both proteins.

How then does this conformation allow the Ran:L_M complex to form its next interactions? Complete phosphorylation by CK2 (T_{51}) and Syk (Y_{45}) have been demonstrated after the pair is bound (71). The observed proximity of these sites to the zinc finger, as with the solution structures of L_M1P and L_M2P, might conceivably influence the rigidity or orientation of this domain when bound to Ran. More likely, it is a combination of all these factors on this exposed L_M face, working with Ran, now locked in a GTP format, that select the next partner. Our preliminary experiments suggest exportins, like Crm1 or CAS, are likely candidates. L_E-GST can extract both native proteins from HeLa cell extracts in reactions that show a strong dependence on the L_E phosphorylation status (Fig. 4-5). Mutations in either or both of the phosphorylation sites

diminished the L_E binding. However, because these pull-downs are from extracts, it is not yet known whether similar exportin:L_E interactions are co-dependent, obligate, or independent of simultaneous Ran:L_E reactions. To work this out experimentally with recombinant proteins, will require considerable validation of step-wise protocols, including the sequential addition of phosphates, the proper nucleotide status of Ran, demonstration of an active exportin conformation, and putative cargo inclusion.

As a model to guide these parameters, we used molecular replacement algorithms testing a putative Ran:L_M0P docking, into the context of a determined Ran:Crm1:cargo structure. The selected template (PDB: 3GJX) included snurportin1 as the Crm1 cargo (236). Obviously snurportin is not relevant to the Erk1/2 and p38 Nup phosphorylation pathways, but its location helps orient the participants, especially L_M, relative to Crm1 and Ran. When native Ran binds an exportin, it must be in the GTP format (237), as it is for Ran:L_M0P, where the Ran nucleotide status is forced artificially by L_M0P interactions. Substitution of the NMR-determined Ran:L_M0P for the crystallographically determined Ran, into this structure (Fig. 4-4F) did not create steric clashes. All described Ran:Crm1 contacts were maintained (Table 4-3, 3GJX), and even each of the transforming NMR derivatives of the Ran COOH tail were without conflicts. Of importance, this enforced orientation of L_M0P, placed the phosphorylation and zinc-finger face into the immediately proximity of both Crm1 and snurportin surfaces. L_M phosphorylated residue T_{51} points towards Crm1 and L_M phosphorylated residue Y_{45} plus the zinc finger are oriented towards the Crm1 cargo. Obviously this model is only speculative, but it suggests working hypotheses that can now be tested. For example, the model predicts

the L_M phosphorylation status helps determine whether Ran:L_M:Crm1 ternary (or quarternary?) complexes can be formed. It also predicts that the L_M zinc finger domain and its nearby phosphorylated residues restrict or determine putative cargo selection, perhaps including the active Nup phosphorylation kinases themselves. These possibilities are under further investigation with binding, mutagenesis and reconstruction experiments.

MATERIALS AND METHODS

L_E mutagenesis. Recombinant GST-L_E (EMCV) and phosphorylation mutation derivatives, $Y_{41}F$, $T_{47}A$, and the double mutation $Y_{41}F/T_{47}A$ were expressed and purified as previously described (72, 73, 210). A larger mutational panel was also prepared, encoding GST-L_E with T_3A, T_4A, T_9A, $T_{15}A$, $Y_{27}F$, $Y_{32}F$, $Y_{36}F$, and $T_{47}E$ substitutions. After isolation each protein was dialyzed into buffer (25 mM HEPES (pH 7.3), 150 mM KCl, 2 mM DTT) and stored at -80°C. Concentrations were determined with BCA protein assay kits (Thermo Scientific). In phosphorylation assays, 85 pmol of GST or 85.71 pmol of GST-L_E were incubated with buffer alone, 10 units of CK2 (New England Biolabs), 10.3 units of Syk (SignalChem), or similar amounts of both enzymes, in the manufacturers' reaction buffers supplemented with 5.0 µCi [γ-^{32}P] ATP (3,000Ci/mmol, 10mCi/ml). For the combined reactions, the Syk buffer was used. After incubation at 37°C for 60 minutes, samples were loaded for SDS-PAGE fractionation. The resolved gels were silver stained then exposed to phosphorscreens for band visualization (GE Healthcare).

L_M for NMR. Unlabeled GST-L_M (Mengo) fusion protein was expressed in *E. coli* as previously described (161). Bacterial cultures contained 25 μM $ZnCl_2$ for proper protein folding. The expressed protein included a thrombin cleavage site for GST-tag removal. [$^{15}N/^{13}C$]-L_M0P was produced from BL-21 (DE3) cells transformed with pGST-L_M at 16°C in [$^{15}N/^{13}C$] M9 medium (42.3 mM Na_2HPO_4, 22.0 mM KH_2PO_4, 8.5 mM NaCl, 18.3 mM $^{15}NH_4Cl$, 2 mM $MgSO_4$, 0.1 mM $CaCl_2$, 0.2% ^{13}C -D-glucose w/v, 50 μg/ml kanamycin, pH 7.3), before induction with isopropyl-beta-D-thiogalactopyranoside (IPTG, 1 mM). Cells were collected at an OD_{600} of 2.7-3.2. Harvest was on GSTrap FF columns, where the GST tags were removed before elution, by reaction with thrombin protease as described (210). The protein was concentrated using an Amicon Ultracentrifuge device (Millipore), treated with 0.25 mM EDTA for 5 minutes at 25°C and then re-folded by dialysis (2L, 20 mM HEPES, pH 7.5, 100 mM KCl, 2 mM DTT, 0.25 mM $ZnCl_2$, 12 h, 4°C). The protein was then dialyzed twice more into NMR buffer (20 mM HEPES, pH 7.5, 150 mM KCl, 2 mM $MgCl_2$, 5 mM DTT, 0.04% NaN_3, 12 h, 4°C) before storage at -80°C. The molecular weight of [$^{15}N/^{13}C$]-L_M0P was determined by matrix assisted laser desorption ionization-mass spectrometry (MALDI-MS) using a Bruker BIFLEX III mass spectrometer. Protein purity (>95%) was determined by SDS-PAGE followed by silver stain. Care was taken at all steps to use NMR grade, metal-free reagents.

L_M phosphorylation. [$^{15}N/^{13}C$]-L_M0P was purified by gel filtration, concentrated, and then incubated with10 units of CK2 alone, or with 10 units of CK2 followed by 10.3 units of Syk in a reaction buffer supplemented with 200 μM [^{31}P] ATP. The buffers were as

provided by the manufacturers. Reactions were at 37°C for 2.5 hours. After phosphorylation, [^{15}N/^{13}C]-L_M(1P/2P) was dialyzed (10 mM Bis-Tris propane, pH 7.4, 50 mM NaCl, 2 mM DTT), and purified by anion exchange using a Mini Macro-Prep High Q cartridge (Bio-Rad) over a twenty column volume salt gradient (50 mM to 500 mM NaCl) to remove the kinases. The proteins were treated with 0.25 mM EDTA for 5 minutes at 25°C, re-folded (as above), dialyzed into NMR buffer (as above), and then stored at -80°C.

Ran for NMR. Plasmids encoding Hexa-His-Xpress tagged human Ran GTPase (His-Xp-Ran) were a gift from Mary Dasso (NIH, Bethesda, MD). Unlabeled protein was expressed in BL21 cells as previously described (210). [^{15}N/^{13}C]-preparations were similar, except the cells were grown at 30°C in M9 medium as described for [^{15}N/^{13}C]-L_M, with 50 µg/ml ampicillin. Initial protein purification steps (labeled or unlabeled) were as previously described (210), but then, if for use in NMR, the samples were treated with EDTA (5 mM, 30 min, 25°C) and dialyzed (2 hours, 25°C) into NMR buffer (2L), followed by a second dialysis into fresh NMR buffer (overnight, 4°C). Ran prepared this way (259 aa), retains the expression tag (43 aa) at the amino-terminus of the full length protein (216 aa). Recombinant GST-RCC1 (*X. laevis*) was purified as described (205), then dialyzed into NMR buffer.

NMR determinations. NMR data were collected at 25°C using 280 µl samples in a five mm Shigemi tube. The protein concentration for labeled (^{15}N/^{13}C) or unlabeled L_M(0P/1P/2P) and Ran, was 0.5 mM in the independent determinations. For Ran:L_M0P

complexes, each protein was at 0.5 mM (1 labeled, 1 unlabeled), and the samples were supplemented with (unlabeled) GST-RCC1 (1.4 nmol). The resolved spectra, including [^{1}H-^{15}N] HSQC, [^{1}H-^{13}C] HSQC, HBHA(CO)NH, CBCA(CO)NH, C(CO)NH, HC(CO)NH, HC(C)H-TOCSY, 3D ^{15}N-NOESY (t_{mix} = 150 ms), and 3D ^{13}C-NOESY (t_{mix} = 140 ms), were collected on a Bruker DRX-600 spectrometer equipped with a ^{1}H, ^{13}C, ^{15}N, ^{31}P three-axis gradient cryogenic probe. NMRPipe software was used to process the raw data (211). Backbone and side-chain residues were assigned manually using CARA (cara.nmr-software.org) (212) and SPARKY NMR analysis software (213). TALOS+/RAMA+ were used to generate dihedral angle constraint files (214) for input into CYANA (215) for CYANA structure calculations. Non-standard amino acids and refinements were finalized by using VMD-X-PLOR (238). The quality of each generated structure was analyzed for restraint and geometry violations using the Duke University MolProbity web server (239, 240). All L_M datasets (71 aa) recorded the (4 aa) amino-terminal extensions. The Ran datasets omitted tag-related peaks and numbered the protein (216 aa) according to its native sequence.

Docking and Bioinformatics. TALOS+ algorithms (211) were used to define alpha and beta domains within the determined structures. The lowest energy NMR states for L_M0P and Ran, as determined from the docked complexes, were submitted to HADDOCK via the public web portal (233). No constraints were specified. Docking interfaces for the lowest energy complex were evaluated online using PDBePISA resources (http://www.ebi.ac.uk/pdbe/pisa/) and the Protein Interactions Calculator (PIC) (241). Root mean square deviations (RMSD) for comparative states or pairwise structures

used the “align” function of PyMol, (242) specifying only the backbone c+n+ca+o atoms. Structure display was by PyMol or Chimera (243).

TABLE 1: GST-L_E Phosphorylation Sites

Substrate[a]	Kinase[b]		
	CK2	Syk	CK2+Syk
GST	-	-	-
GST-L_E	+	+	+
GST-L_E T_3A	+	+	+
GST-L_E T_4A	+	+	+
GST-L_E T_9A	+	+	+
GST-L_E $T_{15}A$	+	+	+
GST-L_E $Y_{27}F$	+	+	+
GST-L_E $Y_{32}F$	+	+	+
GST-L_E $Y_{36}F$	+	+	+
GST-L_E $Y_{41}F$	+	-	+
GST-L_E $T_{47}A$	-	-	-
GST-L_E $T_{47}E$	-	+	+
GST-L_E $Y_{41}F/T_{47}A$	-	-	-

[a] Recombinant GST-L_E and mutant derivatives were prepared as in methods.
[b] Reactions with these enzymes and ^{32}P-ATP (Methods) gave strongly labelled proteins (+) as in (71) or failed to label (-).

Table 4-1. GST-L_E Phosphorylation Sites. Various GST-L_E phosphorylation site point mutations were reacted with CK2 or SYK kinases. + indicates the ability to recognize the GST-L_E substrate.

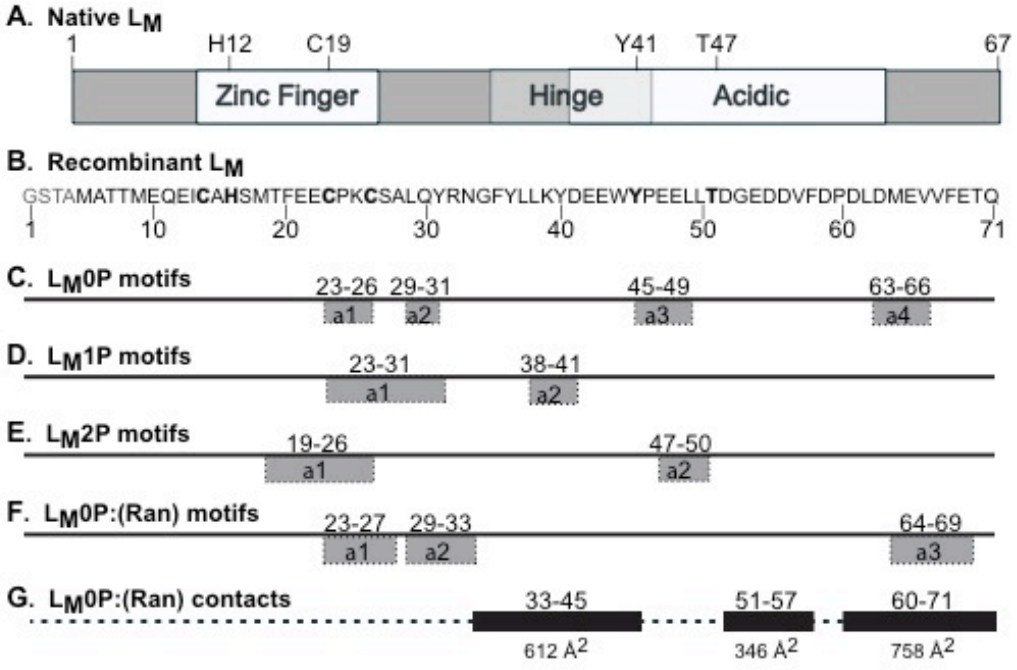

Figure 4-1. L_M schematics. (A) Protein map of native L_M shows domains and the Y_{41}, T_{47} phosphorylation sites. (B) The sequence of L_M as determined by NMR is 4 aa longer than the native protein at the NH_2 end. (C-F) NMR-determined alpha helix motifs, as defined by TALOS+ for respective structures. The remainder of each protein is coiled-coil. (G) Inclusive residue segments which shift upon binding with Ran are indicated with the extent of their contact surfaces (Å^2) in the docked (Ran):L_M0P structure.

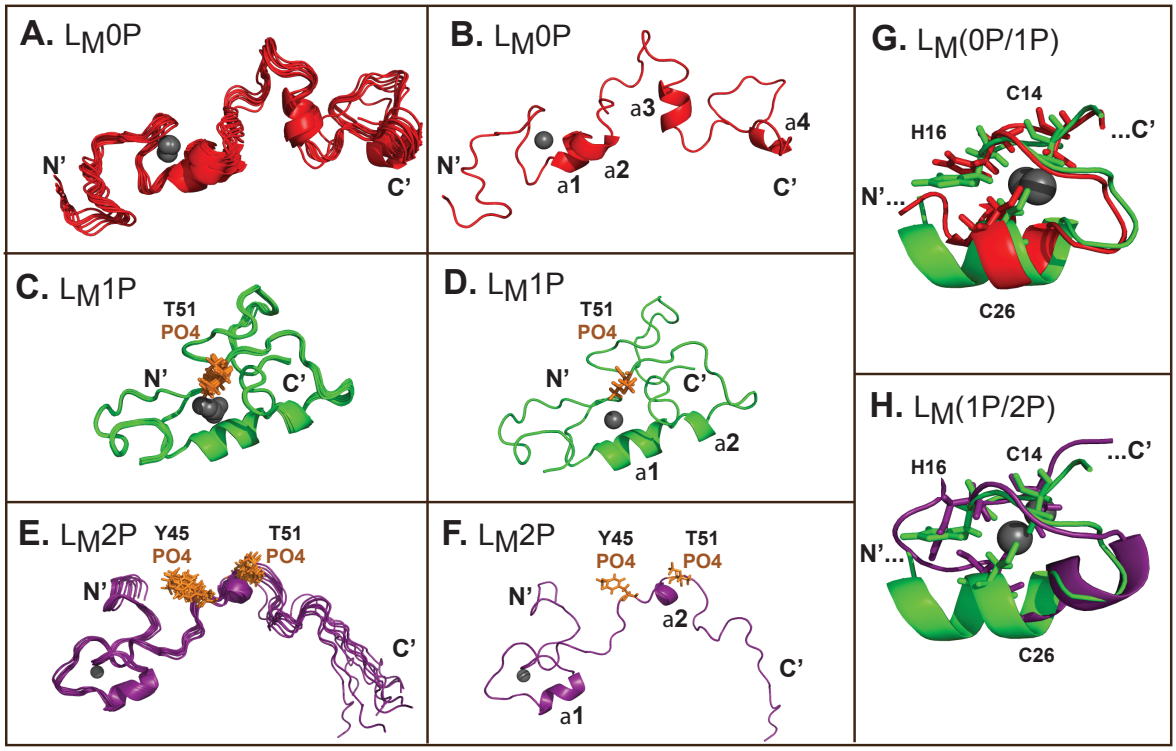

Figure 4-2. Solution structures of L_M(0P/1P/2P). (A, C, E) The 10 low-energy states for L_M0P, L_M1P and L_M2P as free solution structures are shown. (B, D, F) The state-1 structure for each protein is labeled with determined motifs. (G) Superimposition of the zinc-finger regions of L_M0P and L_M1P highlight observed rearrangements. (H) Similarly, superimposition of L_M1P and L_M2P zinc finger regions show conformational changes centering on the zinc binding domain, particularly H_{16}. In all panels, the zinc ion is a gray sphere.

TABLE 2: NMR Restraints and Structural Statistics

	L_M0P	**L_M1P**	**L_M2P**	(RAN): **L_M0P**	**Ran:** (L_M0P)
Total distance restraints (inter-residue)	104	84	186	86	746
Number of torsion angle dynamics steps	5,000	5,000	5,000	5,000	5,000
Number of structures Initial: 50	Final: 10	Final: 10	Final: 10	Final: 10	Final: 10
Hydrogen bonds	42	62	75	76	364
Total dihedral angle restraints	62	90	90	94	154
ϕ	31	45	45	47	77
ψ	31	45	45	47	77
Restraint violations					
Distance restraint violation > 0.2 Å	None	None	None	None	None
Distance restraint violation > 0.2 Å	None	1	None	None	5
Average RMSD (Å) among the 10 refined structures					
Residues	1-71	1-71	1-71	1-71	1-216
Backbone residues	8.431	11.383	10.824	9.826	0.226
Ramachandran statistics of 10 structures					
(% residues)					
Most favored regions	94.2	98.4	96.8	98.6	94.4
Additional allowed regions	5.8	1.6	3.2	0	2.8
Disallowed regions	0	0	0	1.4	2.8

Table 4-2. NMR Restraints and Structural Statistics. All values were generated by CYANA for structure determination before VMD-X-PLOR refinement.

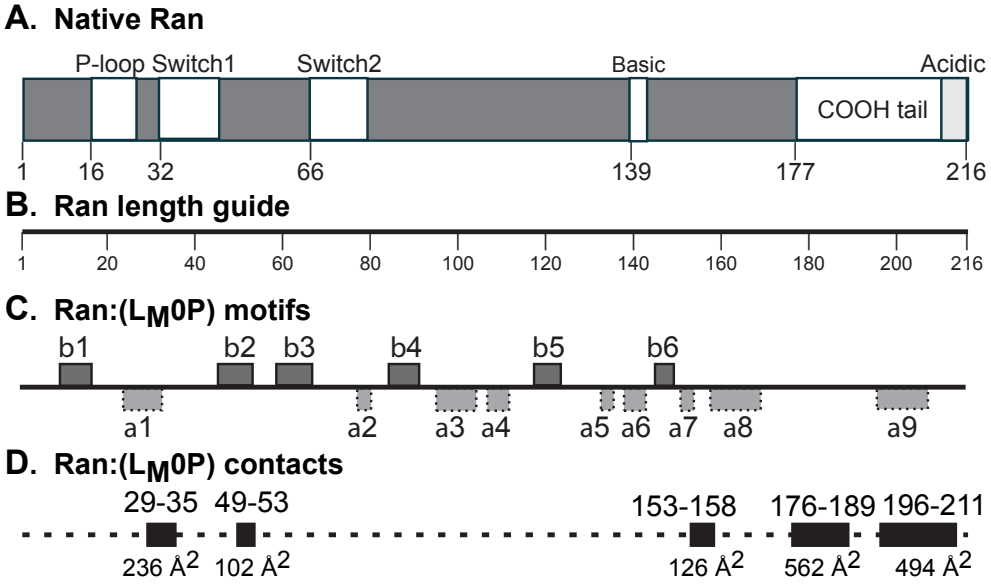

Figure 4-3. Ran schematics. (A) Native Ran protein is mapped with key activity elements. (B) Length guide for residue numbers. (C) NMR-determined alpha helix and beta sheet motifs, as defined for TALOS+, for Ran as complexed with L_M0P. (D) Inclusive residue segments which shift upon binding with L_M0P are indicated with the extent of their contact surfaces (Å^2) in the docked Ran:(L_M0P) structure.

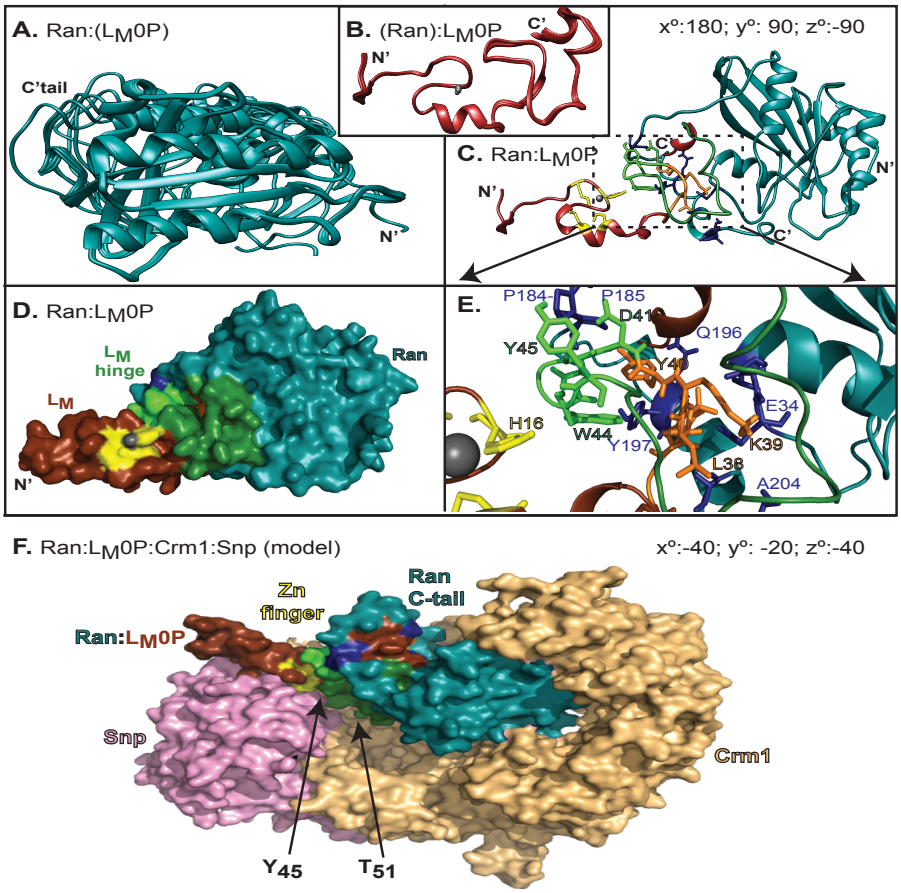

Figure 4-4. Solution structure of Ran:LM0P. (A) 10 low-energy states for (Ran):LM0P. (B) 10 low-energy states for RAN:(LM0P). (C) HADDOCK-determined model-1 of Ran:(LM0P) docked to (Ran):LM0P. Ran rotation relative to A is indicated. (D) Similar to C, Ran (blue), LM0P (brown), zinc coordination residues (yellow), hinge region contacts (green) are highlighted. (E) Similar to C and D, closeup shows orientations of key Ran:LM0P interaction regions. (F) Model-1 Ran:(LM0P) coordinates were aligned, then substituted into PDB:3GJX, a crystallographically determined complex of Ran (blue), Crm1 (tan) and snurportin1 (pink). Relative to D, the required rotation for Ran:LM0P is indicated. The loop of Ran (blue) encircling LM0P (brown, yellow, green) is the COOH tail. The LM phosphorylation sites are buried in the Crm1 (T_{51}) and Snp (Y_{45}) interfaces.

TABLE 3: Ran:(L_M0P) Relative to Crystallographic Determinations

			Å RMSD vs Ran:(L_M0P)-state 1					
Ran	**Bound**	**Length**	**All**	**Core**	**COOH**	**P-loop**	**Switch 1**	**Switch 2**
PDB	**GNP**		**1-216**	**8-176**	**177-216**	**16-25**	**32-45**	**66-79**
1I2M	0	8-176	3.939	3.947	-	0.321	3.450	3.249
1BYU	GDP	9-177	12.663	3.979	-	0.221	4.068	3.226
3GJ0	GDP	1-207	12.592	3.970	7.144	0.192	4.160	3.173
1K5G	GTP	8-213	4.577	0.446	3.572	0.288	0.317	0.345
3GJX	GTP	9-179	1.583	1.578	-	0.214	0.313	3.418
3EA5	GTP	6-179	1.902	1.827	-	0.176	0.406	3.458
2BKU	GTP	9-177	1.664	1.653		0.206	0.532	3.436
1RRP	GTP	8-211	4.930	1.137	4.261	0.324	0.594	2.317
Ran:(L_M0P) States 2-10								
average	0	1-216	4.551	0.260	4.896	0.074	0.240	0.128
variance	-	-	0.405	0.002	1.173	0.001	0.009	0.002

Table 4-3 Ran:(L_M0P) Relative to Crystallographic Determinations. RMSD values used the PyMOL align function, following VMD-X-PLOR refinement. Variance is among all pairwise Ran:(L_M0P) state 1-10 comparisons.

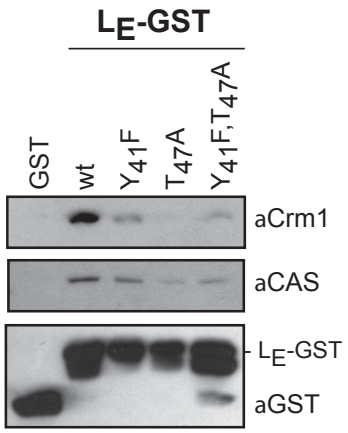

Figure 4-5. Exportin pulldown by GST-L_E. Equivalent amounts of GST-L_E proteins (or GST alone) bound to glutathione sepharose beads were reacted with HeLa cell cytosol. The extracted proteins were fractionated by SDS-PAGE and then identified by Western analyses. The antibodies included, αCrm1 (Abcam 24189 1:2000) αCAS (sc-1708 1:500, Santa Cruz Biotechnology) and αGST (GE Healthcare, 1:10000).

Chapter 5.

Ran-associated binding proteins interconnection to Leader activity

ABSTRACT

Leader (L) EMCV binds the transport protein Ran GTPase (L-Ran), the signaling factor H-Ras GTPase (L-HRas), and the Ran GTPase activating protein RanGAP (L-RanGAP). L also activates HRas-GTP, suppression of which reduces L-directed Nup hyperphosphorylation. Additionally, L impedes Ran-RanBP1 driven Ran-GTP hydrolysis. However, kinetic studies suggest that L-Ran and L-RanGAP are more significant for *in vivo* L activity than L-HRas. L-Ran and L-HRas inhibit nucleotide associations for both GTPases, and while the Ran GEF, RCC1, is known to enhance L-Ran, the secondary Ran GEF, Karyopherin β1, was not as effective at relieving L-Ran nucleotide inhibition. The NMR determined L-Ran structure in conjunction with pull-down experiments suggest L-Ran-Crm1 ternary complexes recruit activated ERK kinases to facilitate the FG-Nup hyperphosphorylation events that inhibit host immune activation to viral infection. L phosphorylation also enhances L-Ran-Crm1-ERK quaternary complexes, regulation of which is carried out by the viral 2A protein (L-2A) and not Ran (L-Ran).

INTRODUCTION

The Picornavirus Cardiovirus genus contains two representative species: Encephalomyocarditis viruses and Theiloviruses. The Encephalomyocarditis virus has one serotype (EMCV strains, including Mengovirus), while the Theiloviruses include rodent and human pathogens, such as Theiler's murine encephalomyelitis virus (TMEV) and the human Saffold virus (SAFV) (45, 66). The Cardiovirus genus encodes an L protein with a conserved amino-terminal C-H-C-C zinc-finger, linker region, and carboxy-terminal acidic motif, while the Theilovirus L protein contains additional Theilo and serine/threonine-rich C-terminal motifs after the homologous L acidic motif (67, 68). L functions include deregulation of nucleocytoplasmic transport (NCT) by inducing nucleoporin (Nup) hyperphosphorylation dependent upon ERK and p38 MAPK kinases (Nup62, 98, 153, and 214) (73, 74, 76, 148, 244) as well as interacting directly with the cellular transport factor, Ran GTPase (72). The L protein also inhibits IFN activation (70, 75, 230, 231), cellular stress granule assembly (77), and promotes nuclear retention of cellular mRNAs (75).

The L point mutations L C19A (zinc-finger domain disruption), L 4D4A (acidic motif residues $D_{48}A$, $D_{51}A$, $D_{52}A$, and $D_{55}A$), and L ΔA (acidic motif deletion of residues 37-61) result in a small plaque virus phenotype and reduced Nup hyperphosphorylation (74). The homologous L zinc-finger and acidic motif appear to be indispensable for L activity, possibly indicating why these motifs remain conserved among all Cardiovirus L proteins (152). The L protein binds Ran GTPase with a K_D of ~3nm as mediated by L hinge motif residues 31-41 and Ran GTPase C-terminal residues 176-216 (72, 162, 210).

This L-Ran interface mechanistically explains why L 4D4A and L ΔA reduce L-induced Nup hyperphosphorylation (74). The EMCV L protein also becomes phosphorylated during viral infection (pL) sequentially on residues T_{47} and Y_{41} (245) (69) (70, 231) (71). pL amplifies previously characterized L activities, such as Nup hyperphosphorylation (71), deregulating active NCT (148), suppressing NF-κB activation, and inhibiting IFN I stimulation (IRF-3 inhibition)(70, 75, 231).

In addition to the L protein, Cardioviruses encode another virulence factor: the 2A protein. The EMCV 2A protein is 143 amino acids (aa) and binds eukaryotic initiation factor 4E (eIF4E) between residues 126 and 134 (87), induces the dephosphorylation of 4E-BP1, and localizes to nucleoli due to its nuclear localization signal (NLS) to interact with ribosomal subunits and suppress host cap-dependent translation (86, 87, 89, 92, 246). When the NLS of the 2A protein is deleted, virus replication is delayed, more host apoptotic death is activated, viral particle release is suppressed, and Δ2A EMCV viruses are no longer pathogenic in mice infection (93).

The eukaryotic Ras GTPase superfamily (Ras, Rho, Rab, Ran, and Arf) cycle between active “on” (GTP-bound) or inactive “off” (GDP-bound) states in order to regulate cellular trafficking, cytoskeletal rearrangement, and kinase signaling pathways. Guanine nucleotide exchange factors (GEFs) mediate the exchange of GDP to GTP for GTPases activation, while GTPase activating proteins (GAPs) stimulate the intrinsic GTPase activity of Ras family members to hydrolyze GTP into a GDP-bound, “off” state (107, 182).

The translocation of proteins and RNAs between the nucleus and the cytoplasm is known as nucleocytoplasmic transport (NCT). NCT takes place across the selectively

permeable nuclear pore complex (NPC). The NPC is a 125 MDa structure composed of greater than 30 different proteins known as nucleoporins (Nups) that span the nuclear envelope. A family of Nups known as F-G-Nups contain disordered phenylalanine (F) and glycine (G) repeating regions that provide binding sites for transport receptors to dock and traverse the NPC. Ran GTPase provides the energy to drive NCT (234). The Ran GEF, regulator of chromosome condensation 1 (RCC1), maintains nuclear Ran-GTP levels, and the cytoplasmic RanGAP and Ran binding protein 1 (RanBP1) facilitate Ran GTPase hydrolysis of GTP into GDP, maintaining Ran-GDP-GTP spatiotemporal segregation to drive NCT.

Ran GTPase interacts with additional effectors known as karyopherins (importins, exportin, and transportins) to regulate the NCT of macromolecular cargos between the cytoplasm and the nucleus. Human members of the Karyopherin (Kpn) family include Karyopherin α [Importin α] and Karyopherin β [Importin β, Crm1 (Exportin 1), CAS] proteins. Karyopherins bind cargo molecules containing a nuclear localization signal (NLS) or nuclear export signal (NES) and interact directly with F-G-repeat Nups in order to cross the NPC and localize cargo molecules to their active locations (247, 248). In the nucleus, Ran-GTP dissociates the Importin α-Importin β-NLS complex when Ran-GTP binds directly to Kpn β (Importin β) for successful nuclear cargo delivery. Ran-GTP then associates with Crm1 (Exportin 1) or CAS carrying NES cargos, and after their export into the cytoplasm, RanGAP-RanBP1-Ran-GTP hydrolysis to -GDP dissociates the complex, releasing the NES cargo into the cytoplasm. Ran GTPase switch regions I and II recognize Kpn HEAT repeats through an induced-fit mechanism instead of using a simple and direct recognition interface (247, 248). L-Ran has been

shown to inhibit Ran-RanBP1 associations as well as interact with a higher affinity in the presence of the Ran GEF, RCC1 (L-Ran-RCC1) (72, 162).

Ras GTPase coordinates cell growth, division, and differentiation through a signaling cascade to downstream mitogen activated protein kinases (MAPK) (112). The Ras isoform HRas only binds to Raf kinases in its active form (HRas-GTP) to signal through the Raf/MEK/MAPK pathway, which leads to phosphorylation of downstream extracellular-signal-regulated kinases (ERKs), ribosomal s6 kinases (RSKs), and p38 kinases (249-251). HRas GTPase protein mutations known to affect nucleotide binding and deregulate ERK signaling incluse HRas S17N (dominant-negative HRas-GDP mutation), and HRas G12V (constitutively active HRas-GTP mutation). The importance of *in vivo* HRas GTPase activity has been widely evaluated using these characterized protein mutations (252, 253).

MATERIALS AND METHODS

Plasmids. Recombinant plasmids encoding the L_{EMCV} and L_{MENGO} proteins linked to N-terminal GST and eGFP tags have been reported (72-74, 161). Thrombin GST-tag removal for L_{MENGO} has been previously detailed(161). Hexa-His-Xpress tagged human Ran GTPase (His-Xp-Ran) was a gift from Mary Dasso (National Institutes of Health, Bethesda, MD). Wild-type His-HRas was acquired from Dr. Michael A. White (Southwestern Medical Center) and has been previously characterized (254). His-Importin β was received from Dr. Stephen A. Adam (Northwestern University) and has been previously characterized (255). His-RanGAP 1 was acquired from Dr. Mary Dasso

(NIH) and has been previously described (256). GST-Ran BP1 was obtained from Dr. Christiane Weise (New Mexico State University). FLAG-H-Ras WT was obtained from Dr. Douglas A. Andres (University of Kentucky: College of Medicine). FLAG-H-Ras S17N was a gift by Dr. Takaya Satoh (Kobe University Graduate School of Medicine) and has been previously defined (257). pAL8-H-Ras G12V was acquired from Dr. Xosé Bustelo (Universidad del Salamanca-CSIC) and has been previously detailed (258). GST-Raf1-RBD was provided by Dr. Xianjun Fang (Virginia Commonwealth University), and has been previously characterized (259, 260). pTriex 1.1 His-GB1 and His-GB1-EMCV 2A plasmids were provided by Dr. Bradley A. Brown (UW-Madison). All plasmid insert sequences were verified by Sanger techniques.

GST Pull-down Assays. GST-fusion proteins [GST, GST-L_{EMCV}, GST-pL_{EMCV} [pL treated with CK2 (L1P) or CK2 and SYK (L2P)], GST-L_{MENGO}, GST-Ran] were added to 50 µl of glutathione sepharose 4B beads and gently rotated for 1 hour at 25°C. Purified target proteins [His-Xp-Ran, His-HRas, His-RanGAP1, His-Kpnβ1, RanBP1, L_{MENGO}] or HeLa whole cell extract were incubated under gentle rotation (1 hour, 25°C) with pre-bound GST-fusion bead complexes to facilitate protein interactions. Protein complexes were washed thrice in pull-down wash buffer A (PBS + 500mM NaCl + 0.02 % Triton X-100) by centrifugation (5 min, 500 x g), and samples were analyzed by SDS-PAGE gel electrophoresis followed by coomassie brilliant blue stain, silver stain, or western blot. Pull down concentrations were as follows: 2.2µg GST [73 pmol], 3.2 µg GST-Raf1 RBD [76.19], 3.0µg GST-L [75 pmol], 10.4µg His-Xp-Ran [347 pmol, 2.1µg GB1-2A [78 pmol], 7.5 µg His-Ran GAP [75 pmol], 10.4µg His-Xp-HRas [347 pmol], 19 µg GST-Ran

WT [350 pmol], 7.5 µg His-Kpnβ1 [75 pmol], 2.0 µg Ran BP1 [360 pmol], 1.0 µg L_{MENGO} [100 pmol], 20mM GTP, 20mM GDP.

Transfections. Transfection was carried out using Lipofectamine 2000 according to the manufacturer's protocol (Invitrogen). HeLa cells (1.5×10^6) were seeded onto 35 mm (6-well) plates at 70-90% confluence and transfected using 10µl of Lipofectamine 2000 with 5µg of the corresponding plasmid (eGFP, eGFP-L WT, eGFP-L C19A, pFlag-HRas WT, pFlag-HRas S17N, pAl8-HRas G12V), mock transfected with H_20 or DMSO, or treated with 20nM Okadaic Acid (OA). At 18 h post-transfection, cells were collected for analysis. Expression was verified by western blot using α-GFP, α-HRas, or α-Flag antibodies. WT, wild type.

Nup Phosphorylation. L-induced nucleoporin (Nup62 and Nup98) hyperphosphorylation levels were determined as previously reported (73, 210).

***In vivo* HRas activation during L transfection.** HeLa cells were transfected with eGFP, eGFP-L WT, or eGFP-L C19A as previously described. 18 hours post transfection, the cells were lysed by scraping into 500 µl of non-denaturing lysis buffer (20mM Tris, 137mM NaCl, 10% glycerol, 1% NP-40, 2mM EDTA, pH 8.0, 2mM PMSF, 1 µM leupeptin, 1µM pepstatin). 30 µl of whole-cell lysates were removed for separate analysis. GST [2.2 µg] or GST-Raf1 RBD (Ras-binding domain) [3.2 µg] were incubated with the remainder of the transfected cell lysates (3 hours, 4 °C). 50 µl of glutathione sepharose 4b beads were incubated with the cellular lysate (3 hours, 4 °C).

Bead complexes were washed 3 times in PBS, collected by centrifugation (5 minutes, 500 rpm, 4 °C), and resuspended in 50 µl of loading dye buffer. Samples were boiled for 5 minutes and analyzed by western blot analysis following SDS-PAGE gel electrophoresis. eGFP and total HRas were detected from whole cell lysate, and activate HRas was detected from GST-Raf1 RBD pull-down, bead samples.

Isothermal Titration Calorimetry. Isothermal titration calorimetry (ITC) was carried out using a VP-ITC system (MicroCal Inc.). L_{MENGO}, Ran GAP, and HRas were dialyzed into ITC buffer [100mM NaH_2PO_4 (pH 8.0), 1mM BME, 25µM $ZnCl_2$] and degassed under vacuum pressure before titration analysis. Titrations were executed at 37°C by 20 x 20µl injections of L_{MENGO} or buffer into an ITC cell (1.4ml) containing Ran GAP, HRas, or buffer alone. The standard reference power was set to 10µCal with a 500s injection delay and 200s delay before the start of titration. Heats of protein dilution were determined using buffer controls. Protein concentrations used for titration were as follows: L_{MENGO} [76µM], Ran GAP [8.75µM], HRas [20µM]. Binding stoichiometries, enthalpy, and equilibrium K_D values were calculated by fitting the titration data to a one-site binding interaction model using Origin 7 software (MicroCal Inc.).

Guanine Nucleotide Analysis by HLPC. Recombinant His-Xp-Ran GTPase [2.3 mg] or His-HRas GTPase [2.4 mg] in 1 ml exchange buffer (50 mM Tris, pH 8, 100 mM KCl, 5 mM EDTA, 1 mM DTT) were incubated (1 hr, 25°C) with buffer, GMP, GDP, and/or GTP (20 mM), then transferred to ice after the addition of $MgCl_2$ (5 mM). The samples were dialyzed (3x, 20 mM HEPES, pH 7.5, 150 mM KCl, 5 mM $MgCl_2$, 2 mM DTT) using

Amicon Ultracentrifuge devices (Millipore). Nucleotide-loaded Ran and HRas were either analyzed directly, or incubated with GST [225 µg], GST-L_{EMCV} (WT, C19A, 4D4A, ΔA) [300 µg], L_{MENGO} [61.5 µg], Ran BP1 [225 µg], and/or Ran GAP 1 [750 µg] for 0-90 minutes in reaction buffer (20 mM HEPES, pH 7.5, 150 mM KCl, 2 mM $MgCl_2$, 2 mM DTT). Reactions were terminated by incubating each sample at 95°C for 3 minutes. The sample lysates were clarified by centrifugation at 16,100x g for 5 min and stored at -20°C before HPLC analysis. HPLC was performed using a Waters (Milford, MA) system equipped with two 515 pumps, a 717 plus autosampler, a 996 photodiode array detector, and a POROS 20 HQ column, 1.7 ml bed volume (PerSeptive Biosystems). Nucleotide bound Ran and HRas were confirmed by HPLC chromatography using nucleotide standards as previously described (191). Chromatogram peaks were processed and quantified using Empower 2 software, then graphed and analyzed using Prism GraphPad software.

Phosphorylated L EMCV Purification. The generation of phosphorylated L using CK2 and SYK kinases (L1P and L2P) and Y_{41}, T_{47} point mutations have been previously characterized (71, 210).

EMCV L Phosphorylation Competition Assay. Purified GST [2.2µg] and GST-L_{EMCV} [3.2µg] fusion proteins were incubated (1 hour, 25 °C) with 50µl glutathione sepharose 4b beads. GB1 [1.4 µg], GB1-2A [2.1µg] (EMCV 2A), or His-Xp-Ran [10.4µg] (Ran) were incubated (1 hour, 25 °C) with pre-bound bead complexes. Manufacturer reaction buffers containing 5.0 µCi [γ-^{32}P] ATP (3,000Ci/mmol, 10mCi/ml), 10.0 units of CK2

(New England Biolabs), 10.3 units of SYK (SignalChem), or 10.0 units of both CK2 and SYK, were added to protein-bead complexes and incubated at 37°C for 1 hour. Protein complexes were washed thrice with PBS buffer containing 500mM NaCl and 0.02% Triton X-100, then subjected to SDS-PAGE gel anaylsis. The gels were either exposed to a phosphorscreen and visualized with a typhoon scanner (GE Healthcare), or silver-stained for total protein analysis.

Antibodies for Western blot Analyses. Protein samples were separated by SDS-PAGE gel electrophoresis (187), transblotted onto membranes (Immobilon-P, Millipore), and probed with primary antibodies against the carboxyl-terminus of human Ran (goat polyclonal IgG, C-20; Santa Cruz Biotech, 1:5,000), GST (mouse monoclonal IgG; Novagen, 1:10,000), 1:2,500), Phe-Gly containing Nups (mouse monoclonal IgG mAb414; Covance,1:5,000), GFP (rabbit polyclonal, ChIP grade, 1:2,500), HRas (mouse monoclonal, Abcam, 1:5,000), Tubulin (mouse monoclonal, Sigma-Aldrich, 1:5,000), FLAG tag (mouse monoclonal OctA-Probe, F-tag-01, Santa Cruz Biotech, 1:2,500), Karyopherin β1 (goat polyclonal, C-19, Santa Cruz Biotech, 1:5,000), Ran GAP1 (goat polyclonal, N-19, Santa Cruz Biotech, 1:5,000), Ran BP1 (goat polyclonal, C-19, Santa Cruz Biotech, 1:5,000), Phospho-ERK (rabbit monoclonal, T202/Y204, Cell Signaling, 1:2,500), Phospho-p90RSK (rabbit monoclonal, T573, Cell Signaling, 1:2,500), Phospho-c-Raf (rabbit polyclonal, S259, Cell Signaling, 1:2,500), and Phospho-p38 MAPK (mouse monoclonal, T180/Y182, Cell Signaling, 1:2,500). After membrane washing, either rabbit anti-goat horseradish peroxidase (HRP) (Sigma-Aldrich, #A5420, 1:5,000), goat anti-mouse HRP (Sigma-Aldrich, #A2554, 1:5,000), or

goat anti-rabbit HRP (Promega, #W4011, 1:5,000) was added as the secondary antibody. Reagents for chemiluminescence were added (GE Healthcare, Amersham ECL Prime; or Thermo Scientific, Pierce ECL) as per manufacturer's instructions and signals were detected with a CCD camera (Fotodyne, Inc) or X-ray film (Fujifilm).

RESULTS

L EMCV and L Mengo bind Ran and HRas. To investigate whether $L_{EMCV/MENGO}$ directly bound Ran GTPase and HRas GTPase, we conducted GST pull-down reactions. GST (2.2 µg) or GST-L (3 µg) fusion proteins were incubated with Ran GTPase or HRas GTPase (0, 2.3, 4.6, 10.2 µg) under 1:0, 1:1, 1:2, and 1:4 reaction condition ratios. L-Ran and L-HRas complexes were observed for both L_{EMCV} and L_{MENGO}, indicating that L interacts directly with both Ran GTPase and HRas GTPase in a 1:1 ratio (Fig. 5-1A&B).

L directly interacts with RanGAP. To examine associations between L and RanGAP, we conducted GST pull-down assays. Various fusion proteins of GST- L_{EMCV} (WT, C19A, 4D4A, ΔA) were immobilized on glutathione-sepharose agarose beads and incubated with an equimolar amount of recombinant RanGAP. Analysis of protein complexes by western blot and total protein stain revealed stable L-RanGAP complexes that did not form in the presence of GST alone. (Fig. 5-1C). L zinc-finger and acidic motif mutations retained the ability to interact with RanGAP, although LΔA bound more weakly to RanGAP than L still in possession of its C-terminal acidic motif.

***In vivo* immunoprecipitation of L-Ran and L-HRas.** To confirm *in vitro* L-Ran and L-HRas observations, *in vivo* co-immunoprecipitation experiments were performed. HeLa cells were transfected with eGFP, eGFP-L WT, or eGFP-L C19A. 18 hours post transfection, cells were lysed in non-denaturing buffer, and eGFP fusion proteins were efficiently immunoprecipitated using anti-GFP antibodies conjugated to protein G beads. GFP bead complexes were washed, separated by SDS-PAGE, and the appropriate antibodies were used to detect the co-precipitation of Ran GTPase or HRas GTPase by western blot. L-induced Nup hyperphosphorylation was also observed for L_{EMCV} WT using anti-FG-Nup antibodies on total lysates (Fig. 5-2A). Immunoprecipitation results further confirmed direct L-Ran and L-HRas interactions.

L activates HRas when overexpressed in HeLa cells. HeLa cells were transfected with eGFP, eGFP-L WT, or eGFP-L C19A. 18 hours post-transfection, HeLa cell lysates were collected and incubated with glutathione sepharose 4b beads pre-bound to GST or GST-Raf1 Ras-binding domain (RBD). Total HeLa cellular lysate and washed bead complexes were analyzed by SDS-PAGE followed by western blot analysis. Immunoblot using an anti-GFP antibody confirmed *in vivo* expression of eGFP, eGFP-L WT, and eGFP-L C19A. The HRas immunoblot against GST and GST-Raf1 RBD complexes specifically detected HRas-GTP in cells expressing active L_{EMCV} (eGFP-L WT). HRas-GTP was not activated to detectible levels for other samples (Fig. 5-2B).

Kinase activation rescues HRas dominant-negative inhibition of L-induced Nup62 phosphorylation. HeLa cells were transfected with eGFP, eGFP-L WT, or eGFP-L C19A (inactive zinc-finger mutation) and then co-transfected with pFlag-HRas WT, pFlag-HRas S17N (dominant-negative), or pAl8-HRas G12V (constitutively active). Cells co-transfected with HRas S17N-eGFP-L WT were also incubated with 20nM of okadaic acid or DMSO alone. 18 hours post-transfection, *in vivo* GFP, Flag-tagged fusion proteins, endogenous Nup62 hyperphosphorylation, HRas, phospho p38, phospho p90RSK, and tubulin were detected using appropriate antibodies. L-directed Nup62 hyperphosphorylation was inhibited by the expression of dominant-negative HRas S17N (HRas-GDP). However, the broad-spectrum kinase activator, okadaic acid, was able to rescue wild-type, levels of L-induced Nup62 hyperphosphorylation (Fig. 5-3). This suppression and rescue correlated with the activation of downstream p38 and ERK (p90RSK) kinases, implicating ERK and p38 as playing a direct role in L-mediated Nup hyperphosphorylation, while HRas activation is a pleiotropic effect of downstream kinase activation.

L directly inhibits Ran-RanBP1 complex formation. In order to determine if L directly competes with RanBP1 for Ran binding, GST pull-down assays were conducted. GST or GST-Ran were incubated with RanGAP, RanBP1, Karyopherin β1, L_{MENGO}, or HRas. Ran formed complexes with known Ran-binding proteins RanGAP1 and Karyopherin β1 as expected, but did not interact with HRas, suggesting that Ran-RanGAP and Ran-Karyopherin β1 interactions were specific. The Ran-RanGAP-RanBP1 complex was only able to form in the absence of L_{MENGO}, with HRas having no

effect on the formation of the Ran-RanGAP-RanBP1 Triplex (Fig. 5-4). This experiment confirmed previous *in vitro* observations that the Ran-RanGAP-L complex excludes RanBP1 (72). L inhibition of Ran-RanGAP-RanBP1 can be explained by the steric hindrance of L-Ran and the weaker affinity of Ran-RanGAP-RanBP1 to the more favorable L-Ran-RanGAP complex.

ITC measurements of L-RanGAP and L-HRas. L binding to RanGAP and HRas GTPase were studied by ITC. 20 injections of L into buffer showed miniscule exothermic heat changes indicative of no binding interaction, with a fitted K_D of 755M. Similarly, Buffer-RanGAP (K_D of 1.2mM) and Buffer-HRas (K_D of -27μM) demonstrated no buffer binding interactions (Fig. 5-5A-C). A similar titration experiment using L injection into a cell containing RanGAP1 resulted in considerable exothermic heat changes in the first few rounds of injection, indicative of L-RanGAP binding. A one-site binding model that gave a K_D of 12nM could fit the L-RanGAP heat changes (Fig. 5-5D). Furthermore, L-RanGAP binding is predominantly enthalpically driven as well as an exothermic process. Another titration experiment using L injection into a cell containing HRas GTPase resulted in large endothermic heat changes after the first few injections indicative of L-HRas interactions. A one-site binding model that gave a K_D of 1.4 μM could fit the L-HRas heat changes (Fig. 5-5E). L-HRas binding is predominantly enthalpically driven, but endothermic. Lastly, L-RanGAP was 10-fold more favorable than L-HRas interactions.

L inhibits RanGTPase nucleotide association. Ran GTPase was incubated with an equimolar (20mM) mixture of GTP, GDP, and GMP followed by L_{MENGO}. Ran-bound nucleotide was detected by HPLC (Fig. 5-6A). L-Ran interactions result in a Ran-bound nucleotide population of 38% Ran-GTP, 31% Ran-GDP, and 31%Ran-GMP compared to 96% Ran-GTP, 4% Ran-GDP, and undetectable levels of Ran-GMP for Ran untreated with L_{MENGO} (Fig. 5-6A). Ran GTPase was subsequently incubated with 20mM GTP or 20mM GDP followed by GST or various GST-L_{EMCV} proteins (C19A, 4D4A, and ΔA). L WT, C19A, and 4D4A reduced the ability of Ran to associate with GTP (~20%) and GDP (~30%) from 100%. However, LΔA restored Ran nucleotide-associations (Fig. 5-6B). Ran was also treated with a 20mM nucleotide mixture of GTP, GDP, and GMP preceding or proceeding incubation with GST or various GST-L_{EMCV} proteins (C19A, 4D4A, and ΔA). Untreated Ran was 80% Ran-GTP, 19% Ran-GDP, and 1% Ran-GMP. Ran treated with L WT, C19A, and 4D4A had a greatly reduced ability to bind GTP and GDP along with an increased ability to bind GMP (~18% Ran-GTP, ~29% Ran-GDP, ~53% Ran-GMP). LΔA restored the ability of Ran to preferentially associate with GTP (80% Ran-GTP, 19% Ran-GDP, and 1% Ran-GMP) (Fig. 5-6B-C).

L-Ran and L-HRas interactions inhibit GTPase nucleotide association. Ran GTPase and HRas GTPase were treated with 20mM GTP (1), GDP (2), GMP (3), or equimolar GTP, GDP, and GMP in the absence of (4), preceding (5), or proceeding (6) L Mengo. > 80% of GTPases were observed to be GTP, GDP, or GMP bound when treated alone with 20mM GTP, GDP, or GMP respectively. L-Ran interactions promoted

Ran-GMP > Ran-GDP > Ran-GTP whether L was added before or after nucleotide incubation. It was therefore concluded that L-Ran sterically destabilizes Ran nucleotide affinity (empty/GMP >GDP > GTP) (Fig. 5-7A). A similar phenotype was observed for L-HRas interactions (Fig. 5-7B).

Karyopherin β only slightly relieves L-Ran nucleotide inhibition. L-Ran binding is limited by the presence of exogenous GDP and GTP (162, 210). Karyopherin β1 was reported to have Ran GEF activity and was therefore evaluated for its ability to relieve L-Ran nucleotide interference (201). While the Ran GEF, RCC1 was able to drive L-Ran to 100% binding completion in the presence of GTP after 60 minutes (162), Karyopherin β1 was only able to drive L-Ran to 25% completion in the presence of GTP after 60 minutes (Figure 5-8A). It was therefore concluded that the RanGEF, RCC1, preferably induces L-Ran interactions *in vivo* in the presence of GTP-GDP nucleotides than does Karyopherin β1.

L phosphorylation does not affect L-Ran. GST pull-down assays were conducted using previously characterized GST-L_{EMCV} phosphorylation protein mutations (WT, Y41F, T47A, T7E, Y41F/T47A, L1P, L2P) to investigate their interactions with Ran GTPase (71, 210). It was observed that L phosphorylation had no effect on L-Ran interactions (Figure 5-8B).

L-Ran-Crm1-ERK form quaternary complexes. GST-L_{EMCV} protein mutations (WT, 1P, 2P, W40V, D37A, K35Q, T47A, Y41F, T47E, Y41F/T47A, C19A, 4D4A, ΔA) were

incubated with glutathione beads and total HeLa cellular extracts (71, 210). L protein phosphorylation (L1P and L2P) increased L-Ran-Crm1-ERK interactions while unphosphorylated L formed more stabilized interactions with importin Karyopherin β1 than exportin Crm1. The L acidic motif was also found to facilitate L-RanGAP interactions (Fig. 5-9A). L-Ran complexes were quantified and plotted for comparison (Fig. 5-9B).

L-Ran-CRM1-ERK docking model. The L-Ran protein structure was determined by NMR and aligned with the Ran-Crm1-Snurportin (cargo) protein complex (PDB: 3GJX) (Fig. 5-9C). Phosphorylated L T_{47} (T_{51} in the L protein structure) was aligned and found to interact directly with Crm1 (3-4Å) in the L-Ran complex, while the L zinc finger remained free to associate with the Crm1 protein cargo molecule (2.2-3Å). Interactions distances between L-Ran-Crm1-ERK are noted from aligned protein structures (Fig. 5-9D).

2A-L blocks L Y_{41} phosphorylation while Ran-L has no effect on L phosphorylation events. GST-L_{EMCV} (WT, Y41F, T47A, Y41F/T47A, T47E) was incubated with the EMCV 2A protein or Ran GTPase in the presence or absence of CK2 (L T_{47}) or SYK (L Y_{41}). 2A-L and Ran-L did not inhibit CK2 phosphorylation of L_{EMCV} T_{47} (Fig. 5-10A). However, 2A was able to inhibit L_{EMCV} Y_{41} phosphorylation, as indicated by the absence of L WT and L T47E phosphorylation in the presence of 2A and SYK (Fig. 5-10B). Furthermore, L-Ran had no effect on L_{EMCV} Y_{41} phosphorylation (Fig. 5-

10B-C). It was concluded that L-2A interactions either sterically mask Y_{41}, or allosterically alter L conformation such that it is no longer recognizable to SYK.

DISCUSSION

For these studies, we investigated the specificity of L-Ran protein interactions in comparison to other possible L binding partners. Our data suggest that L can form interfaces with the following proteins: Ran GTPase, HRas GTPase, RanGAP, and members of the Karyopherin α/β family. These protein-protein interactions have diverse enhancer effects on L-directed nucleoporin (Nup) hyperphosphorylation in the interference of nucleocytoplasmic transport (NCT). We found that L interacts directly with Ran GTPase, HRas GTPase, RanGAP, EMCV 2A, karyopherin Crm1 (Ciomperlik, J.J. and Basta, H.A. Unpublished observations.) and indirectly with Karyopherin β (importin β). Our data suggest that Ran-L interactions (K_D ~3nM) (162) are both pivotal as well as energetically favored over RanGAP-L (K_D ~12nM), HRas-L (K_D ~1.4 μM) and 2A-L (K_D ~ 3.6 μM) (Petty, R.V. Unpublished observations.).

Our first observation was that $L_{EMCV/MENGO}$ proteins interact directly with Ran GTPase and HRas GTPase to form L-Ran and L-HRas complexes both *in vitro* (GST pull downs) as well as *in vivo* (IP) (Fig. 5-1A&B. Fig. 5-2A). This was consistent with the fact that Mengovirus is a strain of EMCV, and $L_{EMCV/MENGO}$ differ by only 4 amino acids. The L acidic motif was also found to help facilitate L-RanGAP complex formation (Fig. 5-1C). The next observation was that L over-expression activates HRas-GTP *in vivo* (Fig. 5-2B). Although inhibition of HRas GTPase (HRas S17N) could suppress L-induced Nup hyperphosphorylation, the broad-spectrum kinase activator, okadaic acid, revealed this

to be dependent upon p38 and ERK (p90RSK) kinase activation rather than HRas-GTP itself (Fig. 5-3) (74). Furthermore, kinetic studies determined that L-Ran complexes (K_D ~3 nM) and L-RanGAP complexes (K_D ~12 nM) are stoichiometrically favored over L-HRas complexes (K_D 1.4 μM), and therefore more likely to be biologically relevant during EMCV infection where L protein concentrations are minute (Fig. 5-5).

Ran GTPase is 96% GTP-bound and 4% GDP-bound when incubated with 20mM GTP/GDP/GMP. L interactions with Ran GTPase alter these nucleotide stoichiometric proportions, such than Ran-L is 53% GMP-bound (nucleotide-free), 29% GDP-bound, and 18% GTP-bound (Fig. 5-6, Fig. 5-7A). Based on structural, spectroscopy, and pull-down studies, it is proposed that L inhibits nucleotide binding to Ran GTPase, with -GDP being less inhibitory than -GTP, and Ran GEF, RCC1, enhances conformational changes in Ran GTPase under *in vivo* nucleotide conditions to induce L hinge and acidic motifs onto the Ran C-terminal binding interface (Fig. 5-6B-C). This induced fit model is also supported by gel-filtration complex studies of Ran-L and RCC1-Ran-L (Bacot-Davis, V.R. Unpublished observations). It had also been recently suggested that Karyopherin β acts as an alternate Ran GEF (201), but we found that Karyopherin β is 4-fold less effective than RCC1 at inducing L-Ran complex formation (Fig. 5-8A).

L interactions with HRas GTPase also inhibit HRas nucleotide association, changing stoichiometries from 95% HRas-GTP, 4.8% HRas-GDP, 0.2% HRas-GMP into 13% HRas-GTP, 22% HRas-GDP, 65% HRas-GMP (Fig. 5-7B). Because both HRas GTPase and Ran GTPase are both members of the small Ras GTPase protein super family, it is reasonable to assume that their shared structural domains allow L to inhibit

HRas GTPase and Ran GTPases nucleotide associations using a similar mechanism of binding inhibition.

At the same time, RanGAP-Ran-L was able to inhibit RanGAP-Ran-RanBP1 trimer formation and consequently suppress Ran-GTP hydrolysis to Ran-GDP (determined using HPLC). The exclusion of RanBP1 was specific to L activity, as HRas had no effect on RanGAP-Ran-RanBP1 (Fig. 5-4). L exclusion of RanBP1 from the RanGAP-Ran-RanBP1 trimer likely traps RanGAP-Ran-L complexes at the NPCs due to the reduced activity of Ran-GTP hydrolysis.

The EMCV 2A protein also interacts directly with L (Brown, B.A., and Petty, R.V. Unpublished observations). The nuclear localization signal (NLS) of the 2A protein (87) is hypothesized to initially escort L to the NPC where L induces Nup hyperphosphorylation. The L protein, itself, becomes phosphorylated on residues T_{47} and Y_{41} (245) (69) (70, 231) (71). L phosphorylation has no effect on L-Ran interactions (Fig. 5-8B), whereas L-2A sterically interferes with the phosphorylation of L Y_{41} (Fig. 5-10). One mechanism that explains these observations is that L protein phosphorylation alters additional L binding partners. Indeed, it has been recently characterized that phosphorylated L has a higher affinity for the exportin, Crm1, as well as a lower affinity for the importin Karyopherin β1 (Fig. 5-9A&B). L-2A could shuttle L to the nucleus where it regulates L binding partners until L-Ran-Crm1-ERK and L-Ran-RanGAP-kinase complexes complete L-directed hyperphosphorylation of FG-Nups in order to hinder NCT (Fig. 5-9).

Given this cascade of L-binding partners, the currently model for L NCT deregulation is as follows: L-2A translocates L to the nucleus where L preferentially

interacts with Ran GTPase, facilitated by the Ran GEF, RCC1. 2A then preferentially interacts with RNA of the nucleoli (87, 89, 90). The L-Ran-Crm1 complex selectively binds cargo with activated ERK and RSK kinases translocating through the NPC. Alone, *in vivo* L expression is enough to activate ERK/RSK and p38 kinases (73, 74, 261) (262, 263). Here, these L-Ran-Karyopherin-Kinase complexes hyperphosphorylate the NPC, and RanGAP-Ran-L-Kinase interactions concentrate L-Kinase complexes along the nuclear rim. Nup hyperphosphorylation reduces receptor-cargo interactions with the NPC, effectively halting NCT (244) to hinder upregulation of the host immune response to viral infection. Additionally, the direct exclusion of RanBP1 from the RanGAP-Ran complex limits cellular Ran-GTP hydrolysis, further disrupting the Ran GTPase gradient to suppress NCT (228, 264).

In conclusion, L-Ran interactions likely trap RanGAP-Ran-L at the NPCs due to reduced Ran-GTP hydrolysis where Ran-L-Crm1 complexes recruit translocating, activated ERK/RSK kinases to carry out L-induced Nup hyperphosphorylation (73, 74, 76, 148, 244). Future studies using FRET of L-2A as well as Crm1/ERK/p90^{RSK} micro-RNA knock-downs of L-Ran-Crm1-ERK would verify the *in vivo* formation of these L-Ran-Crm1-ERK/RSK protein complexes in NPC hyperphosphorylation. High-resolution electron microscopy of L localization could also contribute to better characterizations for this model of L cellular activity during EMCV infection as well as development of L-derived NCT inhibitors for potential cancer therapeutics.

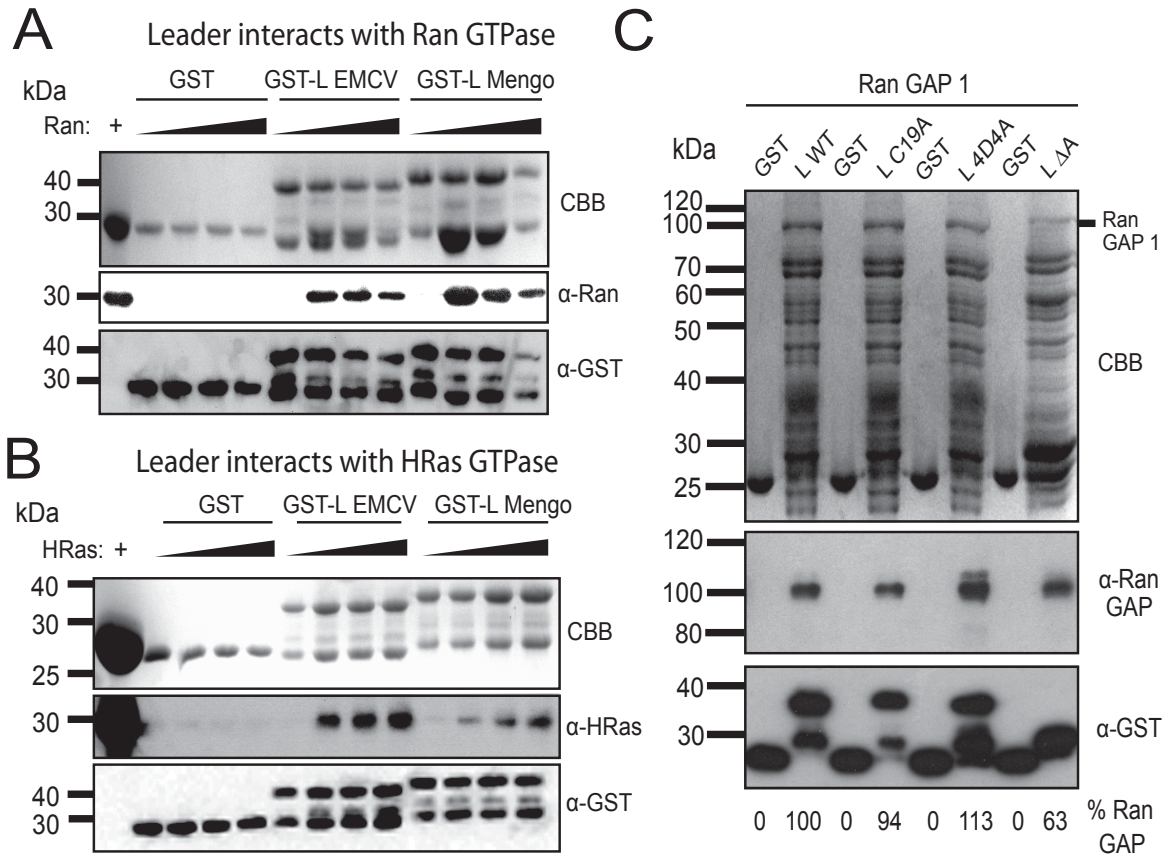

Figure 5-1. L interacts directly with Ran, HRas, and RanGAP. Pulldown experiments using glutathione beads directed against GST-tagged L incubated with recombinant (A) Ran GTPase [L-Ran 1:0, 1:1, 1:2, 1:4], (B) HRas GTPase [L-HRas 1:0, 1:1, 1:2, 1:4], and (C) RanGAP [L-RanGAP 1:1]. Binding was determined by immunoblot using anti-Ran, anti-HRas, and anti-RanGAP antibodies. L input was confirmed by anti-GST immunoblotting.

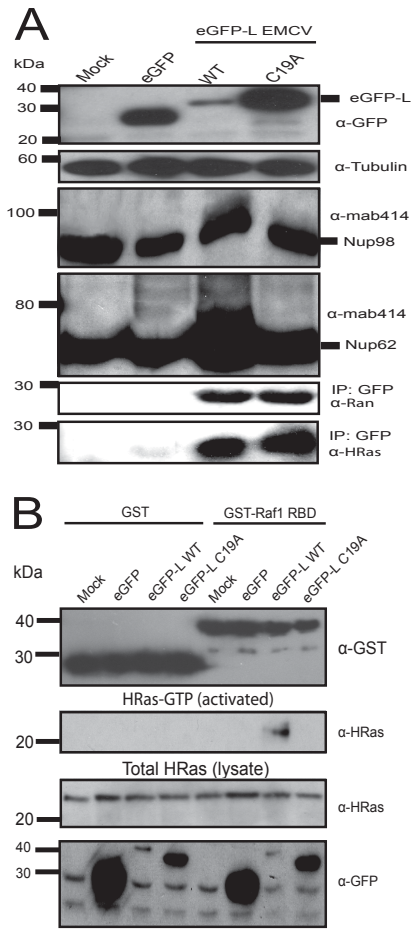

Figure 5-2. L induces HRas activation. (A) Co-immunoprecipitation assay on lysates from HeLa cells were transfected with wild-type eGFP-L (WT), eGFP-L zinc-finger mutation (C19A), or empty vector control (eGFP) as indicated. L expression (α-GFP) and L-induced Nup hyperphosphorylation (α-mab414), were confirmed by immunoblotting total cell lysates. Ran GTPase and HRas GTPase were only detectable in samples expressing L by immunoprecipitation (IP). (B) Pulldown experiment directed against GST-tagged Raf1 Ras binding domain (RBD). Raf1 RBD binding affinity determined activated levels of HRas-GTP as a result of L expression. Total HRas GTPase (α-HRas), and eGFP-L (α-GFP), were confirmed by immunoblotting crude cell lysates.

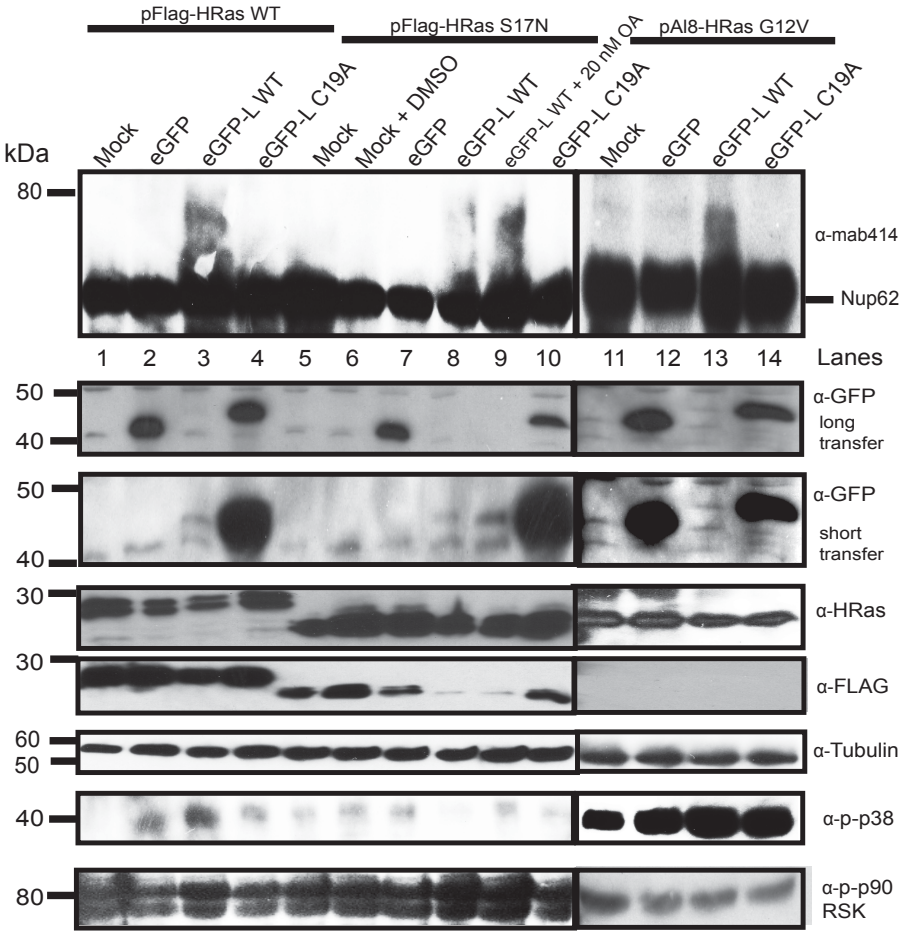

Figure 5-3. L-induced Nup hyperphosphorylation is enhanced by HRas signaling. HeLa cells were transfected with wild-type eGFP-L (WT), eGFP-L zinc-finger mutation (C19A), or empty vector control (eGFP) and then co-transfected with Flag-tagged, wild-type HRas (HRas WT), Flag-tagged dominant-negative HRas (HRas S17N), or untagged, constitutively activated HRas (HRas G12V). L (α-GFP) and HRas (α-HRas and α-Flag) expression were confirmed by immunoblotting. MAPK activation and Nup phosphorylation were determined using α-p38, α-p90RSK, and α-Nup (mab414) antibodies. L was treated with okadaic acid (18hr) to complement dominant-negative HRas inhibition.

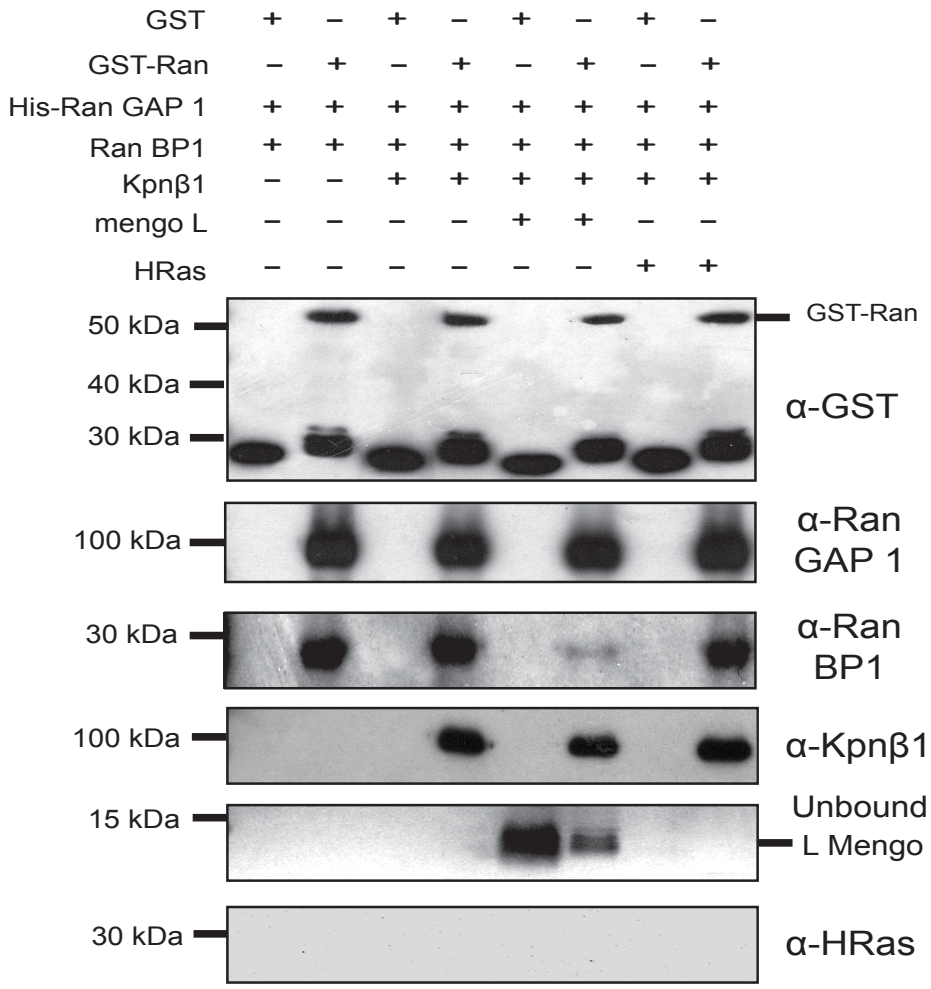

Figure 5-4. L inhibits Ran-RanGAP-RanBP1 formation. Pulldown experiments directed against GST-tagged Ran. Binding of recombinant proteins was determined by immunoblot: RanGAP (α-RanGAP), RanBP1 (α-RanBP1), Karyopherin β1 (α-Tubulin) and HRas (α-HRas). Unbound L_{MENGO} was visualized by acetone-TCA precipitation of the glutathione bead wash fractions followed by silver stain. Trichloroacetic acid (TCA).

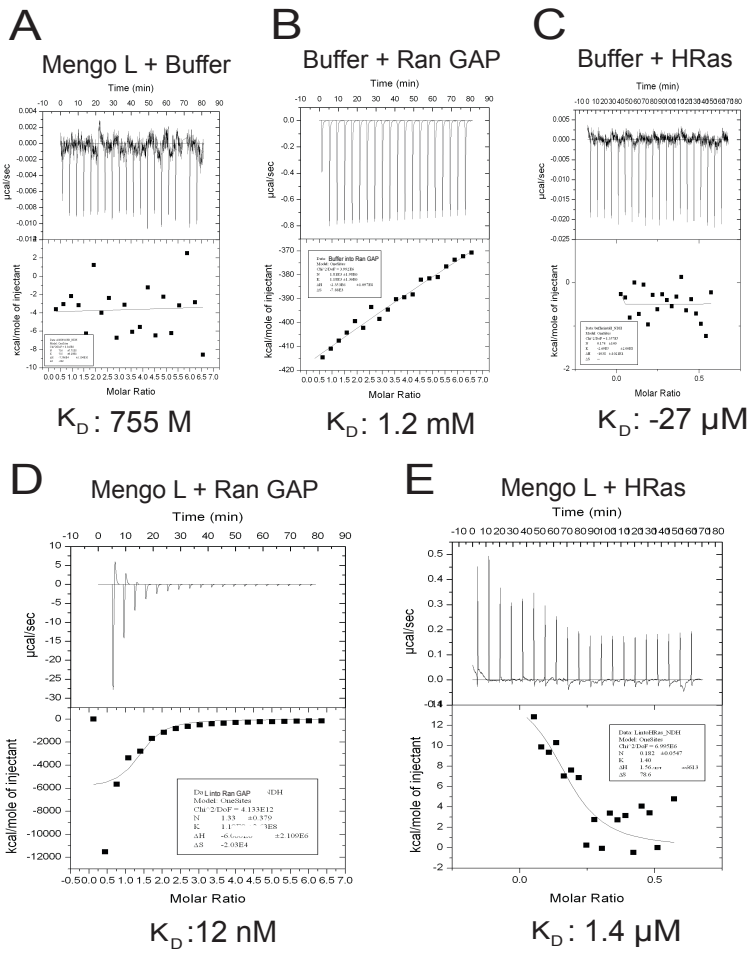

Figure 5-5. Isothermal titration calorimetry profiles of L-HRas and L-RanGAP. Binding isotherms were obtained as characterized in Materials and Methods. Isotherms were fitted to a one-site binding model in order to obtain the best dissociation constant (K_D), enthalpy (ΔH), and entropy (ΔS) values. K_D values were corrected for protein heats of dilution (buffer controls) and are indicated below.

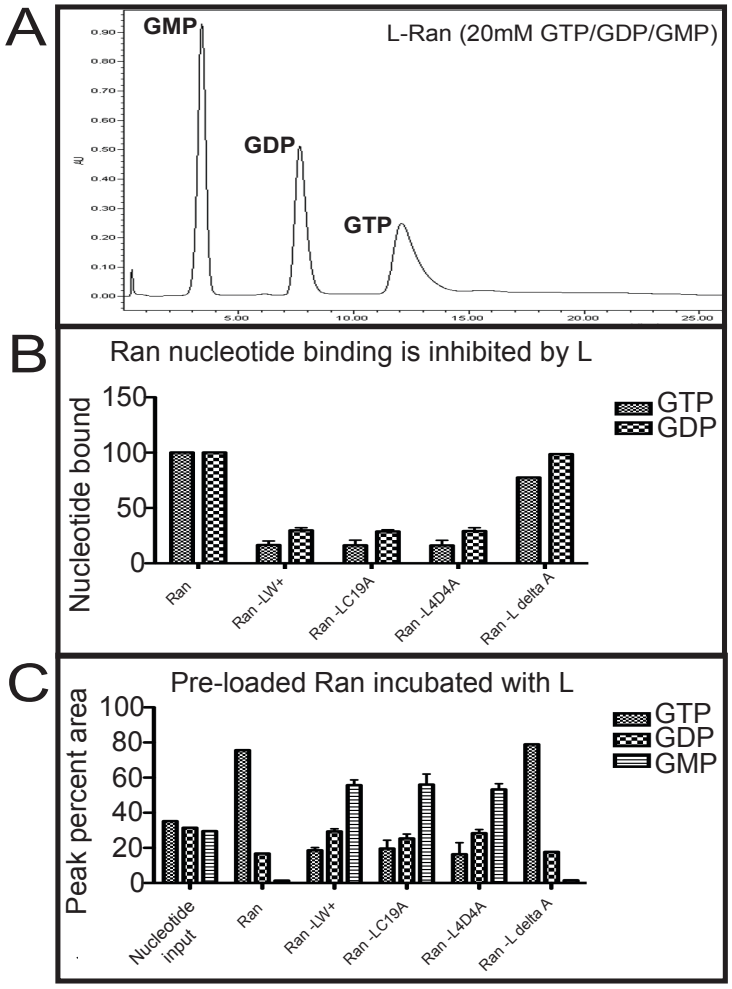

Figure 5-6. L-Ran constrains Ran nucleotide interactions. (A) HPLC chromatogram of Ran-bound nucleotides in the L-Ran complex favor GMP > GDP > GTP. (B) Ran-GTP or Ran-GDP nucleotide binding in the presence of various L protein mutations was determined using HPLC. With the exception of acidic domain deletion LΔA, > 50% of complexes were nucleotide-free, ~29% GDP-bound, and ~18% GTP-bound. (C) Ran was pre-incubated with an equimolar mixture of GMP, GDP, and GTP followed by various L protein mutations. L-Ran complexes favored GMP > GDP > GTP except for the L acidic domain deletion mutation.

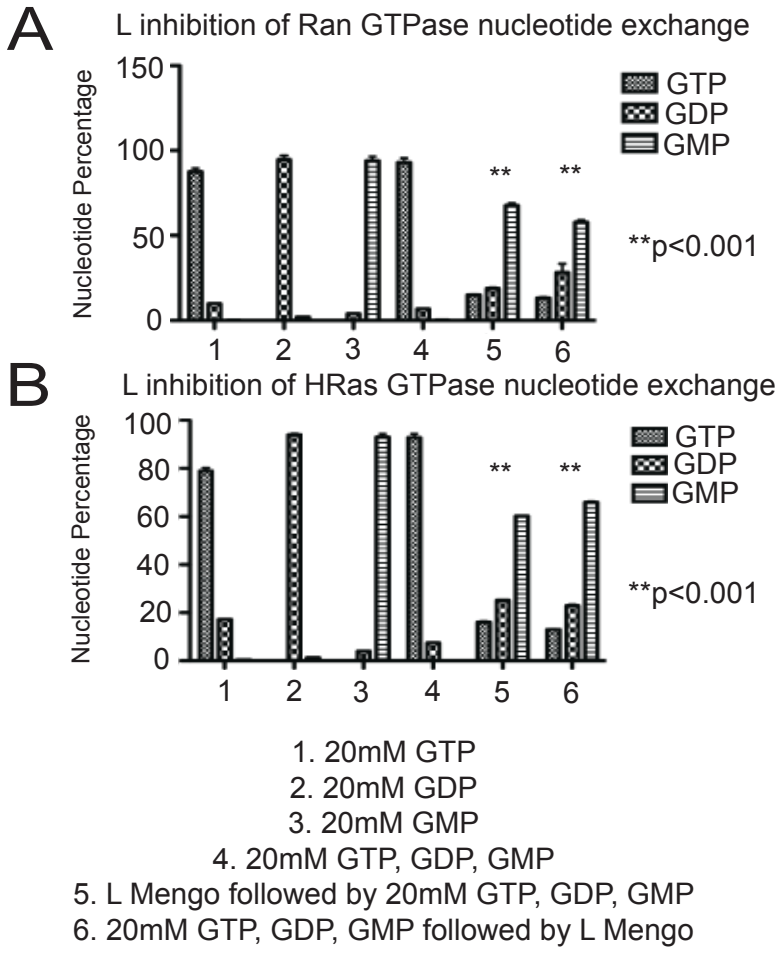

Figure 5-7. L inhibits Ran and HRas nucleotide binding. (A) Ran GTPase or (B) HRas GTPase were incubated with (1) GTP, (2) GDP, or (3) GMP to verify GTPase nucleotide binding by HPLC. Recombinant L_{MENGO} was reacted with (A) Ran GTPase or (B) HRas GTPase (5) following or (6) preceding GTPase incubation with an equimolar mixture of GTP, GDP, and GMP. Both L-Ran and L-HRas complexes favored the binding of GMP > GDP > GTP with > 50% of the complexes GMP-bound.

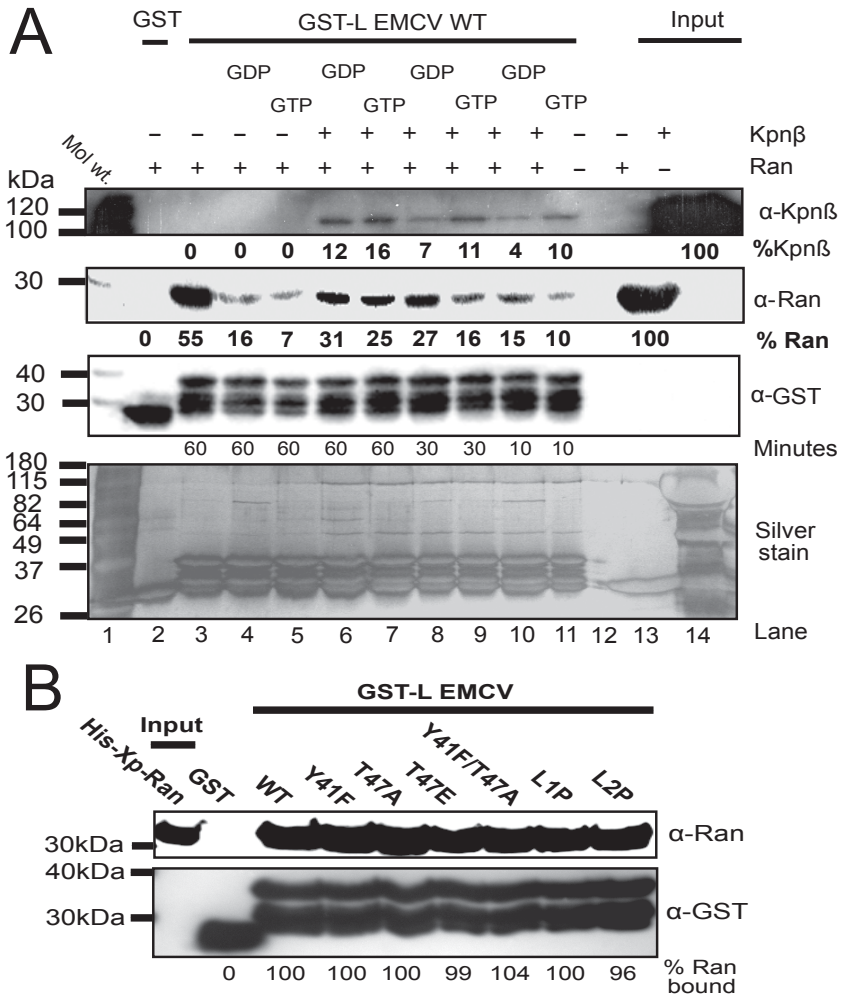

Figure 5-8. The role of nucleotide exchange and L phosphorylation on L-Ran.

(A) Glutathione beads pre-bound to GST-L_{EMCV} were incubated with Ran GTPase in the presence or absence of GDP, GTP, and Karyopherin β1 for 10, 30, or 60 minutes. The percent of Ran GTPase and Karyopherin β1 bound to L-Ran complexes were calculated by densitometry and normalized to input. (B) Glutathione beads pre-bound with GST-L_{EMCV} WT, Y41F, T47A, T47E, Y41/T47A, 1P (CK2), 2P (CK2 and SYK) were incubated with Ran GTPase. The percent of Ran bound to L-Ran complexes was normalized to WT L-Ran. Wild-type (WT).

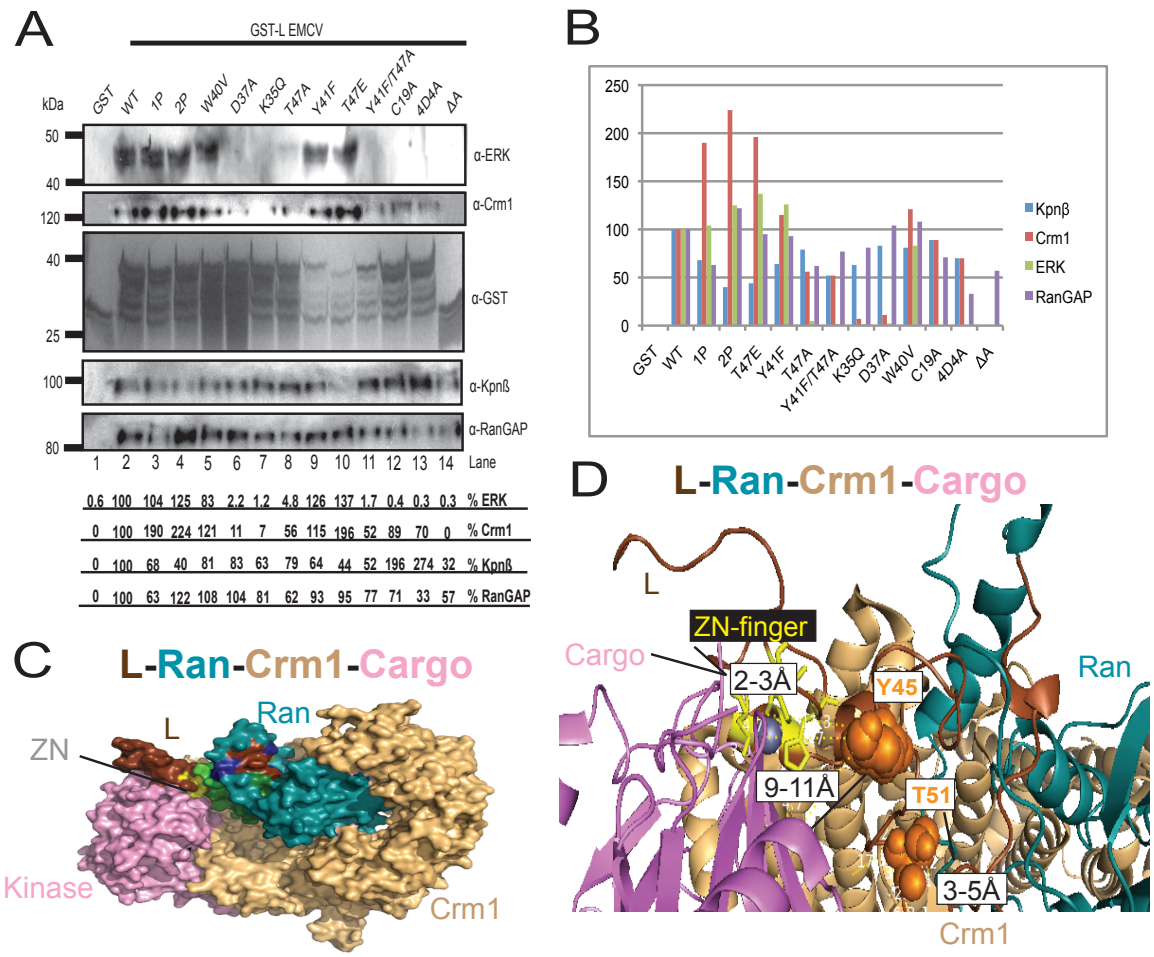

Figure 5-9. L-Ran-Crm1 interacts with ERK. (A) Pulldown experiment using glutathione bound GST-L$_{EMCV}$ mutations directed against total HeLa lysates. Binding of ERK, Crm1, Karyopherin β1, and RanGAP were determined by immunoblot using α-ERK, α-Crm1, α- Kpnβ, α-RanGAP antibodies. (B) L binding partner interactions were quantified by densitometry and graphed as normalized to WT binding. (C) The L-Ran complex was determined by NMR and aligned to the Ran-Crm1-Snurportin cargo complex [PDB: 3GJX]. Crm1-Kinase (ERK) cargo complexes are postulated to make contacts with the L zinc-finger domain. (D) The distances of L zinc-finger-cargo contacts and L TPO51-Crm1 contacts are denoted. Wild-type (WT). Karyopherin β1 (Kpnβ). O3-Phosphothreonine (TPO).

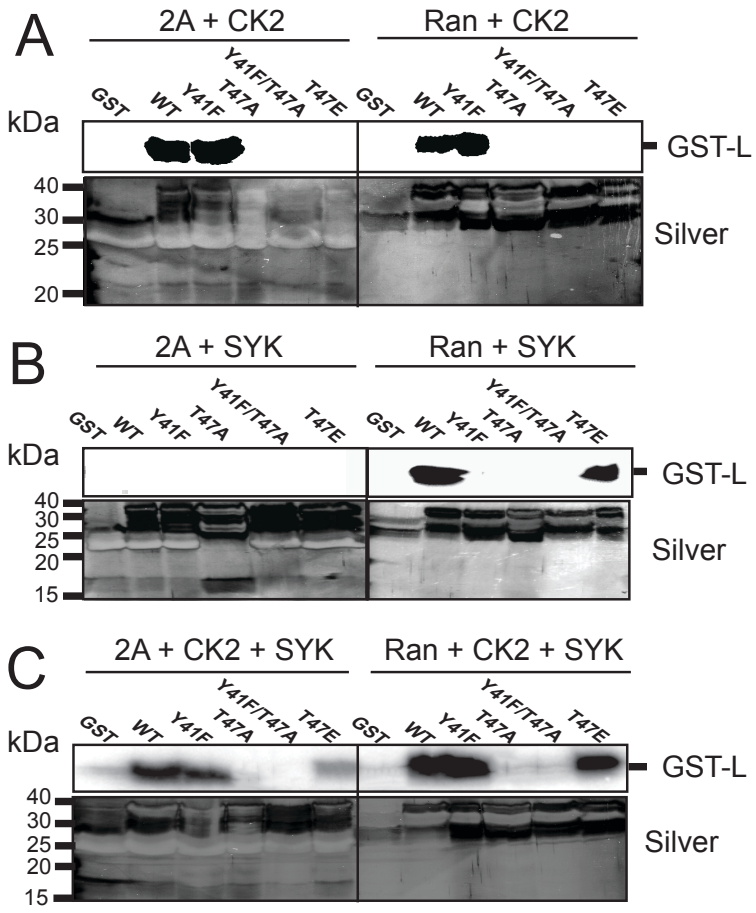

Figure 5-10. L-2A but not L-Ran affects L phosphorylation. GST-L_{EMCV} (WT, Y41F, T47A, Y41F/T47A, T47E) was treated with CK2 and/or SYK in the presence of 2A or Ran GTPase. (A) Pre-formed L-2A and L-Ran complexes were treated with CK2 in order to quantify L T_{47} phosphorylation using γ-32P-ATP. (B) Pre-formed L-2A and L-Ran complexes were treated with SYK following CK2 treatment with 31P-ATP in order to quantify L Y_{41} phosphorylation using γ-32P-ATP. (C) Pre-formed L-2A and L-Ran complexes were treated with CK2 and SYK in order to quantify L Y_{41} and T_{47} phosphorylation using γ-32P-ATP. Phosphor-screen imaging and total protein silver stain was used to detect L-2A and L-Ran phospho-protein complexes. Wild-type (WT).

Chapter 6.

Conclusions and Future Directions.

Chapter Highlights:

Chapter 2: Encephalomyocarditis virus Leader protein hinge domain is responsible for interactions with Ran GTPase.

- Deletion of the L acidic domain (aa. 37-61) inhibits L-Ran binding.
- Mutagenesis identified L aa. 35-40 as indispensable for L-Ran interactions.
- L-Ran interactions increase L-induced FG-nucleoporin hyperphosphorylation.
- Ran acidic tail (aa. 211-216) residues are involved in the L-Ran interface.

Chapter 3: Nuclear magnetic resonance structure of Ran GTPase determines C-terminal tail conformational dynamics.

- The Ran acidic-tail forms an α-helix that interfaces with the Ran GTPase basic patch.
- Low conformational dynamics suggest that the GDP-bound conformation of nucleotide-free Ran GTPase is enthalpically favored.
- These structures are the first to completely resolve as well as determine the structure of Ran GTPase using NMR.
- Ran GTPase C-terminal flexibility suggests involvement in RCC1-nucleosome catalyzed nucleotide exchange.

Chapter 4: Solution structures of Mengovirus Leader protein, its phosphorylated derivatives, and in complex with RanGTPase.

- L interacts with a GTP-core conformation of Ran GTPase.
- L hinge interactions stabilize Ran C-terminus interactions for L-Ran complex formation.
- L phosphorylation enhances L-Ran-Crm1 complexes.
- L-Ran-Crm1 could recruit kinases using the L zinc-finger to direct NPC hyperphosphorylation.

Chapter 5: Ran-associated binding proteins interconnection to Leader activity.

- L favors interactions with Ran and RanGAP to interactions with HRas, with K_Ds of 3nM (L-Ran), 12nM (L-RanGAP), and 1.4μM (L-HRas) respectively.
- L-Ran-Crm1-ERK complexes likely mediate L-induced Nup hyperphosphorylation for host immune inactivation and are enhanced by L T_{47} and Y_{41} phosphorylation.
- L Y_{41} phosphorylation is regulated by the viral 2A protein.
- L T_{47} phosphorylation favors L-Ran-Crm1 export complexes over L-Ran-Kpnβ import complexes

The Cardiovirus Leader (L) protein disrupts nucleocytoplasmic transport (NCT) by inducing nucleoporin (Nup) hyperphosphorylation as well as through interactions with the energy-gradient protein of NCT, Ran GTPase (71-73, 75, 76, 210, 231, 244). Other picornaviruses, such as members of the *Enterovirus* genera, disrupt proteins of the nuclear pore complex (NPC) by proteolysis using the viral encoded $2A^{pro}$ and $3C^{pro}$ proteins (140, 141, 146). Cardioviruses do not appear to use a proteolytic mechanism to disrupt NCT, depending instead on the activities of L. It is interesting that many viruses other than members of *Picornaviridae* target the same F-G Nups (Nup358, Nup214, Nup153, Nup98, and Nup62) using their own viral encoded proteins (VSV M protein, SARS ORF6, Enterovirus $2A^{pro}$, EBV BGLF4) in order to modulate the host immune response (265, 266). L-induced hyperphosphorylation of Nups 214, 152, 98, and 62 are dependent on host factors and perhaps on other viral proteins, such as 2A, when L is not over-expressed or early in infection (3-4hr) when L expression is low (73, 148, 151). Furthermore, the ERK and p38 MAPK kinase effector proteins, or their activated downstream kinases substrates, such as RSK, were implicated in coordinating L-induced Nup hyperphosphorylation (74). Although L is the only viral protein required in order to observe the atypical hyperphosphorylation levels of Nups 214, 152, 98, and 62, these additional host-factors needed to facilitate those events had remained unclear.

In this thesis, we set out to determine the structure of the L-Ran complex, changes in the L structure as a consequence of L phosphorylation, and identify potential cellular factors involved in L disruption of NCT. Early in structure determination process, finding a compatible buffer where both L and Ran were stable was exhaustive. L requires Zn^{2+}

for the proper folding of its zinc-finger domain, while Zn^{2+} buffer conditions cause the precipitation of Ran GTPase. Inversely, phosphate buffer is optimal of Ran GTPase stability, while L becomes misfolded. Therefore chemical amino acid modification and protein mutagenesis studies were carried out on L and Ran GTPase to determine residues involved in forming the L-Ran interface while buffer optimizations continued (Chapter 2). Next, the structure of nucleotide-free Ran GTPase was solved in the absence of L as a step in the determination of the L-Ran complex structure, and is the first completely resolved structure of Ran GTPase as well as the first structure of Ran GTPase determined using NMR (Chapter 3). The NMR structures of L-Ran and phosphorylated L implicate L-Ran-Crm1-Kinase quaternary complexes as the interface that carries out L-induced Nup hyperphosphorylation and L suppression of host immune activation (69-71, 75, 267). Therefore, changes in the structure of L as a result of L protein phosphorylation enhance L-Ran-Crm1 kinase recruitment for L-directed Nup phosphorylation (Chapter 4). Finally, the role of additional cellular binding partners on L activity was scrutinized (Chapter 5).

The L protein had been previously shown to interact with the eukaryotic regulator of nucleocytoplasmic translocation, Ran GTPase (72). Chemical modifications, protein mutagenesis, and NMR structural studies have since been used to determine that L residues 29-42 (including hinge-motif residues 31-41) interact with residues 176-215 of Ran GTPase (including C-terminal and acidic motif residues 211-216) to form the biological interface for L-Ran. L-induced Nup62 hyperphosphorylation was also inhibited by point mutations disruptive to the L-Ran complex, indicating a role for L-Ran in L docking around the NPC during EMCV infection (73, 210).

As expected, we found that L was able to out-compete RanBP1 for Ran binding, and that the stimulation of Ran-GTP hydrolysis by RanGAP-RanBP1 was suppressed in the presence of the L protein. We postulate that L exclusion of RanBP1 from RanGAP-Ran-RanBP1 complexes further disrupts the Ran gradient necessary for NCT (72)(Bacot-Davis. V.R. Unpublished observations).

Due to the observations that L preferentially interacts with nucleotide-free Ran GTPase, we solved the solution structure of nucleotide-free Ran GTPase. Although Ran GTPase is most stable in a high ionic phosphate buffer, the structure was determined in HEPES buffer to remain compatible with L protein structure determination. We showed that EDTA-treated Ran GTPase is nucleotide-free using ^{31}P NMR as well as HPLC. Nucleotide-free Ran GTPase adopts a GDP-bound conformation. The only minor difference between nucleotide-free and GDP-bound Ran GTPase were stabilizations in the switch I domain and increased hydrogen binding of several loop domains into α-helices. The crystal structure of GDP-bound Ran GTPase also has an unresolved acidic-tail domain ^{211}D-^{216}L, but NMR was able to determine that the acidic tail domain forms a short α-helix (α12) that interacts directly with the Ran GTPase basic patch (α8) by salt-bridge contacts. These results support the model suggesting that GDP stabilizes the Ran GTPase C-terminus through acidic tail and basic patch interacts, whereas the GTP-bound conformation of Ran GTPase is stabilized after GEF facilitated nucleotide exchanged by additional Ran-binding partners.

The L zinc-finger is crucial for proper L protein folding as well as L-induced Nup hyperphosphorylation (72-75, 161, 210). The conservation of the L zinc-finger and

acidic motifs among the *Cardiovirus* genus suggest that all Cardiovirus L proteins adopt similar conformations, with the two additional motifs of the *Theiloviruses* (Theilo-domain and S/T-rich region) having unique folds separate from the core L zinc-finger and acidic motifs. The acidic motif was found to be a secondary participant in L-Ran interactions, perhaps allowing conserved acidic motif residues (L 4D4A residues D48, D51, D52, D55) to interact with Ran and additional Ran-binding partners (Crm1 or RanGAP) to participate in L-induced Nup hyperphosphorylation.

L phosphorylation complements L activity by enhancing the rate at which L inhibits NCT, suppresses host immune activation, and induces Nup hyperphosphorylation (71, 148). L phosphorylation also alters the three-dimensional structure of the L protein by stabilizing the zinc-finger domain (α1 residues) from residues 23-26 (L0P) to residues 23-31 (L1P) and residues 19-26 (L2P). Interestingly, L phosphorylation is not necessary for L disruption of NCT, but instead, serves to enhance this activity (148). This kinetic delay (V_{max}) suggests that an ordered ternary- or quaternary-complex mechanism is involved in L-induced Nup hyperphosphorylation, where an EAB/EABC complex (L-Ran-Crm1/L-Ran-Crm1-ERK) still forms in the absence of L phosphorylation, but has a higher dissociation constant that is slowly overcome when L protein concentrations reach more favorable levels for the reactions to finally proceed.

In vitro as well as in vivo experiments have demonstrated that L not only interacts directly with Ran GTPase, but L also forms complexes with the viral 2A protein and the host factors RanGAP, Karyopherin β (importin β), Crm1, and HRas GTPase (72). The K_Ds for many of these protein interactions were determined by surface plasmon resonance and isothermal titration calorimetry. L-2A interactions are in the μM range

(Petty, R.V. Unpublished observations), but are believed to be favorable due to their covalent proximity during viral polyprotein translation. After the NLS of the 2A protein delivers L to the NPC through scaffolding, the higher concentration of Ran GTPase around the nuclear envelope leads to the formation of the L-Ran complex (K_D 3nM) facilitated by RCC1. Here, L-Ran interacts with various karyopherins, such as Crm1, and the L zinc-finger is able to differentiate Crm1-ERK/RSK cargoes using an induced-fit mechanism.

Mitogen activated protein kinases p38 and ERK/$p90^{RSK}$ were previously determined to be involved in L-induced hyperphosphorylation of Nups 214, 153, 98, and 62 (74). Recently, additional pull-down experiments have show that the $p90^{RSK}$ and ERK kinases form a complex with L from HeLa cell lysates to carry out L-directed Nup hyperphosphorylation (Ciomperlik, J.J, unpublished results)(244, 268). While the L hinge and acidic motifs are involved in forming the L-Ran complex, the zinc-finger of the L protein remains accessible to contact karyopherin cargos in an L-Ran-Karyopherin-cargo quaternary complex. The zinc-finger of the L protein could recognize and preferentially stabilize activated ERK/RSK either being imported or exported from the nucleus (L-Ran structure docked with PDB: 3GJX). This quaternary L-Ran-Crm1-ERK/RSK complex could then become tethered around the NPC due to L interactions with RanGAP, which is covalently bound to Nup358 by myristoylation (269-271). Furthermore, L phosphorylation enhances these L-Crm1 interactions. L-RanGAP (K_D 12nM) interactions could displace the karyopherin adaptor, leaving a final ERK/RSK-L-Ran-RanGAP quaternary complex localized to the NPC, where ERK and RSK kinases direct the hyperphosphorylation events of Nups 214, 153, 98, and 62. **This proposed**

ping-pong model of L-induced Nup hyperphosphorylation as mediated by Ran and various Ran-binding partners is outlined in Fig. 6-1.

Continued research is needed to determine the formation of the L-2A complex *in vivo.* The cloning of recombinant fluorescent L and 2A proteins using YFP (yellow fluorescent protein) and CFP (cyan fluorescent protein) would enable direct *in vivo* detection of L-2A interactions as well as their sub-cellular localizations by FRET-based assays (272, 273). Furthermore, electron microscopy of HeLa cells infected with EMCV encoding Flag-tagged L would also be helpful in determining the exact cellular localization of the EMCV L protein, with clear resolution of the nuclear and cytoplasmic faces of the NPC.

Moreover, the determination of ERK1/2/5 subcellular localization (mCherry-ERK) and activation re-localization as a result of EMCV infection would provide additional evidence for the proposed model of L activity. Determination of the structure of the *Theilovirus* L protein (Saffold or TMEV BeAn strain) would also aid in evaluating whether or not the *Theilovirus* L proteins have additional binding partners that interact with their Theilo or S/T-rich motifs. Above all, micro-batch buffer optimizations to determine the structure of L-Ran-Karyopherin (Crm1)-ERK/RSK quaternary complex by crystallography would offer the most definitive evidence supporting our model for L activity. Lastly, siRNA knockdowns of Crm1 and Karyopherin β7 during EMCV infection would offer direct evidence for Crm1/ERK *in vivo* L complex interactions as well as reinforce their importance in facilitating L-induced Nup hyperphosphorylation and NCT inhibition.

Suggested Future Directions

- FRET: L-2A (L-2A *in vivo* interactions)

YFP-L

CFP-2A

- siRNA: Crm1 and Kpnβ7 (ERK)
- Alanine mutagenesis scanning of L

Separate various L-binding partners from Nup phosphorylation

- Electron microscopy (L localization)
- ERK5 phosphorylation
- ERK/RSK localization during EMCV infection

YFP-ERK/mCherry-ERK/RSK

CFP-MEK

The most intriguing of these experiments would be fluorescent kinase expression in order to visualize relocalization during EMCV infection. The dynamics of this experiment would verify the proposed model of L activity and capture unique viral alterations of host signaling pathways. The next most interesting experiment would be to knock down Crm1 expression to determine how Crm1 directly affects L-induced nucleoporin hyper-phosphorylation. This experiment would provide significant evidence for L-Ran-Crm1-kinase complexes that mediate L-induced nucleoporin phosphorylation to inhibit the host innate immune response.

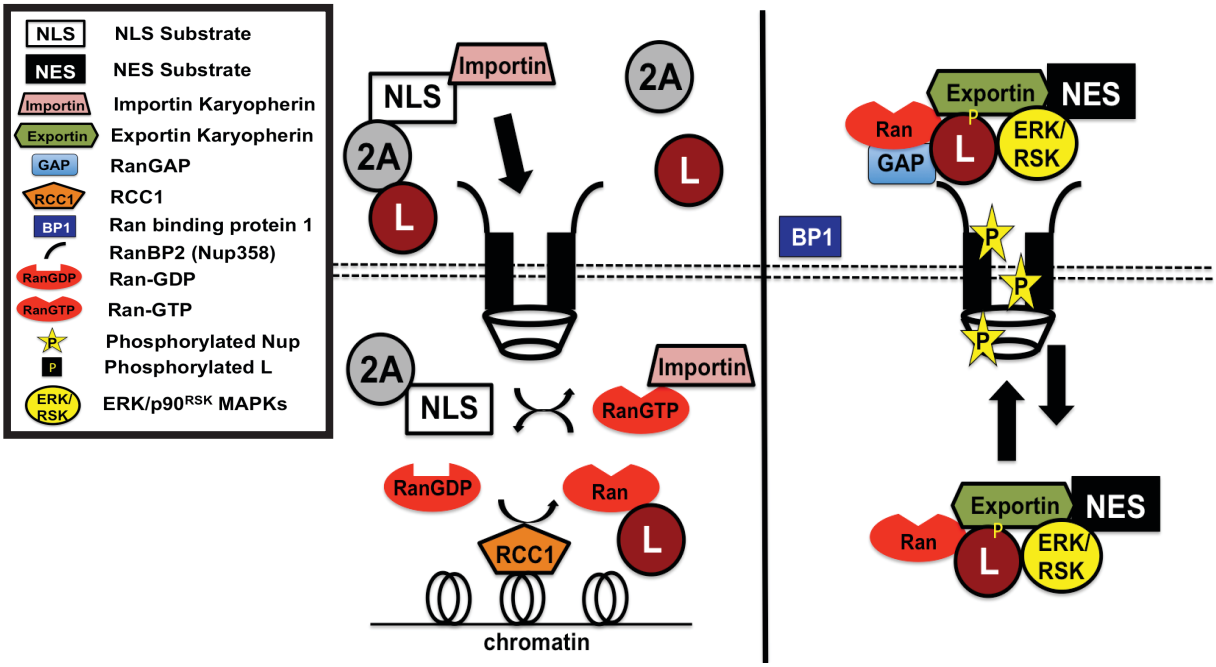

Figure 6-1. Proposed mechanism for L activity. L-2A scaffolding carries L to the nuclear rim where L-Ran-Crm1-ERK/RSK interactions direct L-induced hyperphosphorylation of nucloporins (Nups). L-RanGAP interactions maintain L concentrations along the nuclear rim to enhance L kinase recruitment that drives Nup phosphorylaiton events.

Appendix.

Appendix Chapter 1

Encephalomyocarditis Virus Leader is Sequentially Phosphorylated by CK2 and Syk as a Requirement for Subsequent Phosphorylation of Cellular Nucleoporins

Published in: *Journal of Virology*, Volume 88, pages 2219-26 (2014)

The studies described in figure 2 and figure 3 were performed by Valjean R. Bacot-Davis; those show in figure 1 and figure 5 were performed by Holly A. Basta (Palmenberg Lab); and those shown in figure 4 and figure 6 were performed by Jessica J. Ciomperlik (Palmenberg Lab).

ABSTRACT

Encephalomyocarditis virus and *Theilovirus* are species in the C*ardiovirus* genus of the *Picornaviridae* family. For all cardioviruses, the viral polyprotein is initiated with a short Leader (L) protein unique to this genus. The NMR structure of L_E from encephalomyocarditis virus (EMCV) has been determined. The protein has an NH_2-proximal CHCC zinc-finger, central linker and a contiguous, highly acidic motif. The *Theiloviruses* encode the same domains, with one or two additional, COOH-proximal domains, characteristic of the human Saffold viruses (SafV), and Theiler's murine encephalomyelitis viruses (TMEV), respectively. The expression of a cardiovirus L, in

recombinant form, or during infection/transfection, triggers an extensive, cell-dependent, anti-host phosphorylation cascade, targeting nucleoporins (Nups) that form the hydrophobic core of nuclear pore complexes (NPC). The consequent inhibition of active nucleocytoplasmic trafficking is potent, and prevents the host from mounting an effective anti-viral response. For this inhibition, the L proteins themselves must be phosphorylated. In cells, extracts or recombinant form, L_E was shown to be phosphorylated at Thr_{47} and $Tyr_{41.}$ The first reaction (Thr_{47}), by casein kinase 2 (CK2) is an obligatory, sequential precedent to the second event (Tyr_{41}), catalyzed by spleen tyrosine kinase (Syk). Site mutations in L_E, or kinase-specific inhibitors, prevented L_E phosphorylation and subsequent Nup phosphorylation. Parallel experiments with L_S (SafV-2) and L_T (TMEV BeAn) proteins confirmed the general cardiovirus requirement for L phosphorylation, but CK2 was not the culpable kinase. It is likely L_S and L_T are both activated by alternative kinases in different cell types, probably reactive within the Theilo-specific domains.

INTRODUCTION

Cardioviruses in the *Picornaviridae* family are subdivided into two species, the *Encephalomyocarditis viruses* (EMCV) and *Theiloviruses* (TMEV). EMCV-R is the prototype isolate for this genus. Although various EMCV have been isolated from diverse mammalian hosts, predominantly these are rodent viruses. Most are fairly homogeneous in sequence, host-range and pathogenicity (for review see (62)), in that they cause myocarditis, encephalitis or diabetes-like symptoms (274). The TMEV in

contrast, include variants like Vilyuisk human encephalomyelitis virus, Theiler's-like rat virus, Theiler's murine encephalitis virus (TMEV) and the Saffold viruses (SafV) 1-8. Strains of TMEV are subdivided into those which are neurovirulent (e.g. GDVII and FA) and those that cause persistent demyelination (e.g. DA and BeAn). The demyelinating strains are frequently used to model multiple sclerosis etiologies in mice (for review, see (275)). The SafV are human viruses, first isolated from a stool sample of a feverish child (276). They are yet to be linked to any particular human disease, although recent work suggests they can stubbornly persist in their hosts (50) and SafV-2 has the potential to become neurotropic when inoculated intracerebrally into mice (277).

A hallmark of all cardioviruses is the short Leader (L) protein translated at the NH_2-terminus of the viral polyprotein (Supplemental Fig. 1). While other picornaviruses can encode alternative proteins at this location (e.g. *Aphtho*- and *Erbovirus* L^{pro}), the cardiovirus Ls always display an unusual CHCC zinc-binding domain, a central linker, a short, concentrated acidic region, and additional Ser/Thr-rich motifs, characteristic of their species (67-69, 161, 278). After translation, these highly charged (pI of ~ 3.7) proteins are released from an L-P1-2A precursor by the activities of the downstream 3C protease. Post-release from the polyprotein during infection, or as a recombinant protein, the L from EMCV-R (L_E, 67 amino acids), triggers a lethal cellular phosphorylation cascade, aimed at the nucleoporins (Nups), which form the hydrophobic core of nuclear pore complexes (NPC). The degree of Nup hyper-phosphorylation is so extensive, and so unlike anything that happens during the normal cell cycle, that it completely disrupts all tested active host nucleocytoplasmic trafficking pathways (73, 76, 148) (J. Ciomperlik unpublished results). The altered NPC become

open to widespread passive diffusion, allowing essential components to leak from the nucleus and become available for cytoplasmic viral replication. At the same time, active trafficking of signaling proteins (e.g. for interferon induction) or transport of transcribed cellular mRNAs, ceases abruptly. This potent, unique anti-host response presumably prevents the cell from mounting an effective retaliation against the virus, and is probably the reason most EMCV, and certainly EMCV-R, are highly pathogenic to mice (LD_{50} = <100 pfu) (279).

The L_E-dependent Nup phosphorylation cascade requires an early obligate binding between L_E and the NPC transport regulatory protein, Ran-GTPase (72, 210). Stoichiometric interaction requires catalytic facilitation by RCC1, a nuclear-localized guanidine-nucleotide exchange factor, which helps Ran morph into the appropriate (GDP or empty) conformer (38). Once bound however, L_E:Ran complexes are virtually non-dissociable. They have a K_D of ~3 nM and cannot be disrupted by exogeneous nucleotides, implying that Ran becomes locked into some virus-preferred format (162). L_E:Ran is the foundation complex through which host kinases are subsequently recruited in poorly understood secondary steps, to carry out the actual Nup hyper-phosphorylation events within the NPC. Inhibition of ERK1/2 or p38 pathways prevents L_E activities during EMCV-R infection, identifying these kinases as participants, if not the actual phosphate contributors (74).

Complicating this picture are observations (69, 70), or in some cases predictions (68, 280), that L_E as well as L_T (from TMEV), are themselves phosphorylated during infection. L_E (recombinant or during infection) exposed to eukaryotic cells or cytosol, reacts with antibodies specific to phospho-tyrosine, predicted as Tyr_{41} (69), but other

studies have suggested Thr_{47} as the target site (70). Mutation here (Thr_{47}Ala) disrupts L_E functions during infection, such that active NPC trafficking inhibition is delayed (148), Nup phosphorylation is abrogated (76) and IFN-α/β transcription is no longer blocked (231). The L_E functions can be restored by substituting a phosphomimetic glutamate (Thr_{47}Glu) at this key position (76, 148, 231). However, *in vitro* Nup phosphorylation assays with digitonin-treated cells and recombinant L_E, are not responsive to mutation at Tyr_{41} or Thr_{47} (69, 73). Casein kinase II (CK2) can phosphorylate recombinant L_E at Thr_{47} in cell-free assays (70), but there is no evidence this is the kinase that acts upon L_E *in vivo*. Nor is there evidence in cells, or any recombinant reconstructions, that currently discriminate L_E, L_T, or L_S (SafV) phosphorylation as a consequence or antecedent to the Nup phosphorylation cascades.

The L_T and L_S proteins share many properties with L_E, including the NH_2 zinc-binding domain, central linker, acidic domain and COOH terminal eight amino acid domain leading to the $3C^{pro}$ cleavage site (see Sup Fig. 1). They are shorter by 7 residues at the immediate NH_2 terminus, but instead have insertions of 10 (Saf) or 15 (TMEV) extra residues just upstream of the conserved COOH motif. The extra common residues (“Theilo domain”), and the extra TMEV-specific residues (“Ser/Thr domain”), make the L_S (71 aa) and L_T (76 aa) a bit longer than the L_E although they all are expected to have reasonably similar biological functions (67). The L_T (DA strain) has been linked to disruption in active NPC trafficking (151), induction of Nup phosphorylation (specifically Nup98) (75) and inhibition of interferon responses (230). The L_E from EMCV-R can actually replace L_T (DA) in infectious virus, albeit with somewhat reduced viral replication efficiency (67). Neither L_T nor L_S from any strain has

ever been tested directly as a phosphorylation substrate. Thr_{63} of L_T (DA) was suggested as such, because Thr_{63}Ala substitution reduced Nup98 phosphorylation in L929 cells. Virus with this mutation had reduced toxicity to BALB/3T3 cells, while an analogous phosphomimetic, Thr_{63}Asp, retained the wild-type phenotype (68). The L_T Ser_{57} (DA, BeAn) locale, was also proposed as a putative phosphorylation site, because as one of the few known sequence discontinuities in the Ser/Thr rich domain, this amino acid (Pro_{57}, GDVII), correlates with virus growth kinetics in BHK cells (280).

Now, with recombinant proteins, infections, transfections and cell-free assays, we have identified 2 obligate, sequential L_E phosphorylation steps. Neither influences the initial L_E binding to Ran (210), and yet both are both required for subsequent activation of the L-dependent Nup hyper-phosphorylation pathways. The primary event at Thr_{47} is catalyzed to completion by cellular CK2. The secondary event at Tyr_{41} is by cellular spleen tyrosine kinase (Syk). In parallel, recombinant L_T (BeAn) and L_S (SafV-2) are shown to be directly phosphorylated by various cell extracts, including HeLa, but CK2 is not the primary agent, and the sites are not orthologous to L_E.

MATERIALS AND METHODS

Plasmids. Bacterial plasmids encoding active N-terminal GST-tagged EMCV-R L protein (GST-L_E), (pGEX-2P vector with EMCV-R L from pEC_9 (279)) have been described (72, 161). The full sequence of EMCV-R is available at GenBank accession number M81861. Pilot studies indicated analogous GST-fusions were not active for L_T and L_S proteins (not shown), so a new panel was engineered to place equivalent GST

tags at the COOH termini, using multi-step PCR and a common backbone vector (pTriEx1.1, Novagen). A GST amplicon from pDEST24 (Invitrogen) converted the normal initiation AUG into a Leu codon (Sup Table 1, primers 1437 and 1390). Ligation into the backbone vector (pTriEx1.1) preceded ligation with a second amplicon (primers 1426 and 1345) encoding L_E from pFluc/L (72). Then, the vector sequence upstream of the L_E AUG codon was altered to provide stronger translation activity during eukaryotic transfection (primers 1433 and 1434). Plasmids pL_T-GST and pL_S-GST were constructed in parallel. A SafV-2 L amplicon was generously provided by Dr. Howard Lipton, after PCR from a full-length cDNA, (primers 1238 and 1239). After subcloning, the L_S gene was reamplified (primers 1393 and 1394) then ligated into the backbone vector (pL_S-GST). Plasmid pL_T-GST was similar, except the starting cDNA was from TMEV (BeAn), using primers 1120 and 1121 (into pGEX-6p-2, Amersham Biosciences). Two more steps into pT1.1 (primers 1244 and 1245) and then into pT1.1-GST (primers 1391 and 1392) completed the process. The final plasmid set (pL_E-GST, pL_S-GST, pL_T-GST) differ only in the sequence of the L genes. Site-directed mutagenesis used 2-step PCR on these templates (281) with the indicated inside (mutagenic) and flanking primers (Supp. Table 1) to create single or double-mutant sequences. Sequencing and restriction digests confirmed all constructs. The panel encodes T7 and CMV promoters and readily expressed the respective L_X-GST proteins as COOH-terminal GST fusions in *E.coli* (after IPTG induction) or HeLa cells (after plasmid transfection).

Protein Expression and Isolation. Protein samples for GST-L_E, L_E-GST, L_T-GST, L_S-GST and mutated derivatives were prepared as described (161, 210). Briefly, after IPTG induction of plasmid-transformed *E.coli* (Rosetta Competent Cells, Novagen), the

lysates were fractionated with Glutathione Sepharose High Performance columns (GE Healthcare Life Sciences). Retained protein was exchanged into buffer (10 mM Bis Tris propane, 50 mM NaCl, 2mM DTT, pH 7.4) via spin column concentration (Millipore), and then subjected to anion exchange chromatography using a Bio-Scale Mini Ion Exchange cartridge (Bio-Rad). The L_X-GST peaks were concentrated (into 25 mM HEPES, 150 mM KCl, 2 mM DTT, pH 7.3) and stored at -80^{o}C. Protein samples prepared this way typically contain 10-20% GST truncation products from premature termination within ORF, in addition to the full-length Lx-GST. In contrast, GST-L_E preparations, especially those which undergo an additional Sephacryl S-100 fractionation (210) don't have such fragments. His-Ran was expressed and purified as described (210). Recombinant kinases CK2 (New England Biolabs), Syk (SignalChem) and Src (Cell Sciences) were obtained commercially.

Cell Procedures. HeLa cells (ATCC CRL-1958) were grown in suspension (37°C, 10% calf serum, 5% CO_2) in modified Eagle's medium. At 24 h pre-infection or transfection, they were plated into dishes. Infection (MOI=30) with vEC_9 (279) used an attachment period (30 min, 20^o) before the cells were transferred to 37^{o}C (4-5 h). In kinase inhibition studies, the cells were pretreated with (E)-3-(2,3,4,5-tetrabromophenyl) acrylic acid (TBCA, 10μM, Calbiochem) or 4,5,6,7-tetrabromo-2-azabenzimidazole (TBB, 50μM, Calbiochem) for 1 h pre-infection. The samples were maintained in the dark before, during and after (4-5 h) infection. Transfections with pL_X-GST cDNAs (1μg) used lipofectamine (1μM, Invitrogen) techniques (37°C, 5% CO_2, overnight) in 24-well plates with OptiMem media (Invitrogen). BHK-21 cells were a generous gift from Dr. John Yin.

At harvest, all cells were washed with PBS, lysed in gel loading buffer (SDS), boiled and then fractionated by Laemmli SDS-PAGE.

Western Analyses. Proteins fractionated by SDS-PAGE were electro-transferred onto polyvinylidene difluororide membranes (Immobilon-P, Millipore), then blocked (10% nonfat dry milk) in Tris-buffer saline (TBST: 20 mM Tris, pH 7.6, 150 mM NaCl, 0.5% Tween-20, 20^{o}C, 1 h). The membranes were washed (3x) with TBST before incubation (4^{o}C, overnight) with an appropriate primary antibody (1% milk, TBST). These included αNup (mAb414, Covance) against Phe/Gly-containing Nups, αGST (mAb, 71087, Novagen) and αtubulin (mAb, T4026, Sigma-Aldrich). After further washes (3x, TBST), a secondary antibody (αmouse A2554, Sigma-Aldrich) was added (1% milk, TBST), incubated (20^{o}C, 1 h) then removed (3x, TBST) before the membranes were reacted with enhanced chemiluminescence substrate (GE Healthcare) and exposed to film.

Phosphorylation Reactions. HeLa or BHK-21 cytosol from uninfected cells was prepared via dounce homogenization (142). Rabbit reticulocytes lysates were commercial (Promega). For inhibitor testing, TBCA (10μM) or TBB (50μM) in DMSO pretreated the HeLa cytosol (30 min, 37°C, in the dark) before use, and then were maintained in the reactions at the same concentrations. Phosphoryation reactions (80 μl, with 30 μl cytosol, 2 μl 10 mM ATP, 2 μg Lx-GST, 0.75 μl [γ-^{32}P]-ATP, ~12μCi/μl) were in GST binding buffer (50 mM HEPES, 150 mM NaCl, 0.5% NP40, pH 7.4) for 45 min (37^{o}C). Glutathione Sepharose 4B beads (10 μl per sample, GE Healthcare Life Sciences) were then added, followed by agitation (room temp, 2 h). The beads were collected by centrifugation (500xg), washed with GST buffer (4x) then boiled with SDS gel loading buffer. Protein fractionation was by SDS-PAGE (8-10%), with band

visualization by phosphoimaging (Typhoon 9200 Variable Mode Imager, GE Healthcare), silver stain or Western analysis.

Reactions with recombinant kinases were similar, except CK2 (10 units, New England Biolabs), Syk (10.3 units, SignalChem) and/or Src (10 units Cell Sciences) replaced the cytosol, and the commercial buffers recommended for these enzymes were used. Phosphorylation reactions with GST-L_E:Ran complexes were initiated with GST or GST-L_E bound-Ran complexes on Glutathione Sepharose 4B beads, as described (210). The beads were collected by centrifugation (500xg) and then resuspended in reaction buffer (commercial for each kinase, 25 μl), containing 0.5 μl [γ-^{32}P] ATP (12.16μCi/μl), CK2 (10 U), Syk (10.3 U), or both enzymes (10 U each). Incubation was at 37^{o}C for up to 60 min. For Syk reactions, L_E-GST was pre-incubated with CK2 and cold ATP before addition of Syk and γ-^{32}P] ATP. The bead-bound complexes were washed, boiled with SDS and fractionated by SDS-PAGE.

Phosphorylation Quantitation. After Western assays or phosphoimigaging the gel-fractionated proteins bands were scanned by densitometry (Total Lab-TL 100, Sigma-Aldrich). Observed pixels were normalized to GST or tubulin loading controls in the wild type (L_E) or untreated (inhibitor) control samples. Stoichiometry measurements required the excision of (^{32}P) gel bands after autoradiography (4 independent lanes per sample type), followed by scintillation counting, using a method similar to S. Hollinger and J.R. Hepler 2004 (282). Controls and calibrated standards measured the degree of quench (4-8%). The dpm of recovered ionizing radiation was divided by the [γ-^{32}P]-ATP specific activity (304 μCi/μM) to determine the recovered phosphate. The protein content of analogous samples was assayed with BCA protein assay reagent kits (Thermo

Scientific). Typically, this averaged ~78 pM of GST or GST-L_E per isolated gel slice. Stoichiometry, expressed as percent, recorded recovered phosphate (pM) per recovered protein (pM). Values >100% indicate multiple phosphorylation events (282).

Sequence Analysis. A dataset of unique Cardiovirus L sequences (Sup. Fig. 1) was compiled from GenBank and aligned by ClustalX (283). Post-translational modification predictions were performed with NetPhos2.0 (284), Phosphomotif Finder (285) and Phosida (286). Alignments were displayed with Weblogo (287).

RESULTS

L_E Mutagenesis. Recombinant EMCV (Mengo strain) Leader protein (L_M) can be phosphorylated *in vitro* with CK2 at Thr_{47} (70). Deletion analysis and ^{32}P-labeling experiments by C.M.T. Dvorak et al 2001 (69) showed the closely-related EMCV-R L protein (L_E) is phosphorylated during infection at a Tyr residue, presumed to be Tyr_{41}. Motif identification alogrithms, NetPhos 2.0 (284), Phosida (286) and PhosphoMotif Finder (285) concurred that both sites could be kinase targets (Sup. Fig. 1), but it was unknown whether these sites were alternatives, or additive. Accordingly, single and double substitution mutations (Tyr_{41}Phe, Thr_{47}Ala) were engineered into recombinant L_E-GST cDNA and the isolated proteins were tested for ^{32}P-incorporation (γ-ATP) after incubation with HeLa cell extracts (Fig. A-1A). GST tags were included because the small, highly charged L_E proteins by themselves are captured inefficiently by membranes during blotting steps (69, 72, 73). Relative to the wild-type protein, Thr_{47}Ala and Tyr_{41}Phe reduced label incorporation by 82% and 40% respectively. It required both

mutations to eliminate all detectable phosphorylation. Parallel, single-proton NMR determinations confirmed these L_E sequences were properly folded (210). Therefore, both sites are phosphorylation targets and they contribute additively.

Phosphorylation by CK2 and Syk. Kinase identification by motif prediction is an uncertain process because many enzymes accept numerous related substrates and there is often functional redundancy. Of the multiple algorithms queried in this study, all concurred that L_E Thr_{47} fit the general consensus, [S/T]XX[D,E], for CK2. The Tyr_{41} site was anticipated less frequently, but when identified, spleen tyrosine kinase (Syk), and the related Src tyrosine kinase (Src) were the most commonly suggested enzymes. Syk and Src both phosphorylate a family of overlapping substrates, but neither has a precisely-defined target consensus with which they are guaranteed to react. Generically, both will accept Tyr in a regional acidic environment (+3, -3), with a preference for nearby aliphatics (288, 289).

When (commercial) recombinant CK2 was added to GST-L_E the reactions reached completion within 10-15 min (Fig. A-2B). Samples (4x) from each time-point were measured for both protein content and ^{32}P incorporation allowing an approximation of the stoichiometry. Although there is always variation in such measurements (Sup Table 2), in this case, the values fluctuated around a median of ~96% (StDev ±37%), or close to saturation. Surprisingly, parallel reactions with Syk had virtually undetectable incorporation when the enzyme was tested alone (Fig. A-2A). But when both enzymes were added together (Fig. A-2C), the ^{32}P counts more than doubled over that of CK2 alone, to a median of ~195% (StDev ±57%). In this case, completion required 15-30 min of reaction. These results are consistent with a secondary, Syk-dependent

phosphorylation of GST-L_E at Tyr_{41}, sequential to that of CK2 at Thr_{47}. Reactions with Src, instead of Syk were not equivalent (Fig. A-2D). This enzyme did not react with GST-L_E even when added in combination with CK2.

During infection, L_E undergoes a tight 1:1 binding interaction with Ran-GTPase as an obligate step in active NPC trafficking inhibition (72, 162). The complexes form between GST-L_E and Ran recombinant proteins (210) in the complete absence of L_E phosphorylation. The primary hinge-linker contact points for L_E (Lys_{35}-Trp_{40}) lie immediately adjacent to the Tyr_{41} and Thr_{47} phosphorylation sites, and although neither mutation inhibits complex formation (210), it was unknown whether Ran binding subsequently masked these sites, or if L_E phosphorylation needed to occur before Ran binding. Pre-formed recombinant GST-L_E:Ran complexes for the panel of L_E phosphorylation mutants were reacted with CK2, Syk or a combination of these kinases. The phosphomimetic (Thr_{47}Asp) was included as a structural mimic for pseudo-phosphorylation at this site. As with the isolated GST-L_E samples, CK2 readily labeled the wild-type protein as well as the Tyr_{41}Phe mutant, the only other sequence with an intact Thr_{47} (Fig. A-3A). When similar complexes were pre-reacted with CK2 (cold ATP) and then labeled in the presence of Syk, the wild-type and the phosphomimetic were the only active substrates (Fig. A-3B). Simultaneous addition of CK2 and Syk again allowed Tyr_{41}Phe, to be actively labeled (Fig. A-3C). Clearly, neither kinase was inhibited by the Ran binding status of GST-L_E. With or without Ran, CK2 reactions at Thr_{47}, or a phosphomimetic at this position, were obligatory precursors to subsequent Syk reactions at Tyr_{41}.

CK2 Inhibition. HeLa cell extracts contain endogeneous CK2, and presumably this enzyme is responsible for initial L_E-GST reactions in that context (e.g. Fig. A-1A). The addition of CK2 inhibitors, TBCA and TBB, reduced HeLa cytosol-mediated incorporation significantly (Fig. A-4A). However, neither drug was completely effective, with 57% and 61% inhibition respectively. Parallel reactions with recombinant CK2 in buffer gave similar results (Fig. A-4B), indicating these particular inhibitors do not prevent all activity by this enzyme. The experimental "normalized" values in cytosol, were determined by relative densitometry and cannot distinguish L_E-GST samples with 1 or 2 added phosphates. Even partial phosphorylation by the primary kinase could (putatively) have still allowed reactions with the secondary enzyme. Collectively, though, the data demonstrate that CK2 is present in HeLa extracts, and logically it acts as the natural, dominant phosphorylation agent for the first L_E event (at Thr_{47}), just like the purified enzyme.

L_E-GST and Nup Phosphorylation. Digitonin-treated HeLa cells in the presence of *Xenopus* or HeLa extracts undergo GST-L_E dependent hyper-phosphorylation of Nups (73). The activity can be assayed by upward mobility shifts, particularly for Nup_{62}, when samples are labeled with ^{32}P or reacted with Nup-specific antibodies. GST-L_E with large deletions (e.g. removal of the acidic domain), or gross structural rearrangements (e.g. $C_{19}A$), do not induce this activity. Surprisingly, recombinant L_E with single point mutations at Tyr_{41} and Thr_{47} are functional in this assay, although mutation to Thr_{47} in Mengovirus is debilitating to virus growth (69, 70, 73). The primary difference in these approaches is the dose of Leader protein. Digitonin assays expose nuclei to high levels of GST-L_E. Infections provide significantly lower concentrations of translated L_E. To test

the Leader phosphorylation mutations independent of infection, the panel of matched L_X-GST cDNAs was transfected into HeLa cells. As expected, the conformational mutation, $C_{19}A$, prevented Nup_{62} phosphorylation (Fig. A-5A). The $Thr_{47}Ala$ mutation and the phosphomimetic, $Thr_{47}Asp$, both reduced the Nup_{62} phosphorylation signal to 33-34%. The observed values at this primary site were lower than for the secondary $Tyr_{41}Phe$ mutation (by itself). However, when both GST-L_E phosphorylation sites were changed ($Tyr_{41}Phe$ + $Thr_{47}Ala$), there was no observable shift in the Nup_{62} band. Therefore, at least one and preferably both L_E phosphorylation events must be prerequisites for this activity.

The Leader phosphorylation requirement is also manifest during virus infection. When vEC_9 is infected into HeLa cells, Nups become phosphorylated in a L_E-dependent manner (73). But, exposure of the cells with TBCA or TBB reduced the Nup_{62} phosphor-shifts to 62% and 16% respectively (Fig. A-6). For intact cells, TBCA is specific for CK2 at this concentration (Calbiochem screen of 28 common kinases) as is TBB (Calbiochem screen of 33 common kinases, *www.emdmillipore.com*). CK2 itself is not responsible for Nup phosphorylation (data not shown and (74)). The process only occurs when there is properly folded L_E that can act as a phosphorylation-competent substrate for CK2 and Syk.

Other Cardioviruses. The TMEV and SafV Leader proteins are orthologs and presumed functional analogs to L_E with regard to Nup phosphorylation triggers. Well-characterized cDNAs for SafV-2 and TMEV (BeAn) were chosen to represent this species. Ls and L_T share 43% and 39% amino acid identity relative to L_E, respectively (Sup. Fig. 1). Matched L_S-GST and L_T-GST genes were cloned into the same

eukaryotic/prokaryotic expression vector as L_E-GST. Upon transfection of HeLa cells, both Theilovirus proteins induced Nup_{62} phosphorylation, but neither was as effective as GST-L_E, where the band shift was nearly twice as pronounced (Fig. A-5B). All the shifts were L_X-dependent activities though, because disruption of each Leader conformation with a debilitating zinc-finger mutation (i.e. $Cys_{11}Ala$) significantly reduced Nup_{62} phosphorylation.

Among the known set of SafV and TMEV viruses, none conserve the identical context of Thr_{47} required for primary kinase recognition of L_E (Sup. Fig. 1). That Theilovirus Leader proteins are themselves phosphorylated *in vitro* or *in vivo*, or whether such activity is dependent on cell type, has never been demonstrated. Transfections (e.g. L_X-GST) and infections rarely produce enough Leader from any cardiovirus for a thorough study of native phosphorylation status. Instead, as a first test of such activity, the matched set of recombinant L_X-GST proteins were reacted with cytosol from HeLa cells, BHK cells or rabbit reticulocytes (Fig. A-1B). All 3 extracts labeled L_E-GST and L_T-GST with ^{32}P, albeit with quite different efficiencies. For L_E-GST, the preferred efficiency, normalized to the amount of protein, was reticylocytes> BHK > HeLa, with a nearly 4-fold difference over spectrum of cell types. For L_T-GST, it was reticulocytes > HeLa> BHK. Equivalent amounts of L_S-GST were only weakly labeled in HeLa and BHK by comparison, and not phosphorylated at all in reticulocyte extracts.

The varied reactivity of these proteins in multiple cell types is expected if each Leader sequence relied on different kinases for self-phosphorylation. Indeed, when recombinant CK2 was added directly to these proteins, it was unable to label L_S-GST or L_T-GST (Fig. A-2E). Therefore, while phosphorylation is obviously part of the Leader

activity profile for all cardioviruses, each species (or clade?) seems to take advantage of its unique sequences to present preferred sites to different endogeneous kinases, perhaps in a cell-specific manner.

DISCUSSION

Many viral proteins are phosphorylated by cellular kinases for a variety of functional reasons. The dengue virus NS5 RNA-dependent-RNA-polymerase, for example, has a bipartite nuclear localization signal (NLS) that is turned on and off by phosphorylation with CK2 (290). In fact, CK2 is one of the most commonly identified kinases utilized by viruses to phosphorylate their proteins (291). Before the current report, it was known that the EMCV Leader protein was phosphorylated during infection, presumably by CK2 at Thr_{47}. The significance of that modification, or of dual modification at Thr_{47} and Tyr_{41}, was unclear.

The data presented here show that L_E phosphorylation, first at Thr_{47} and then at Tyr_{41}, are both required to optimize the ability of EMCV to trigger Nup phosphorylation and the consequent inhibition of active cellular nucleocytoplasmic trafficking. Logically, such an important, initial reactive step should be performed by a constitutively active, ubiquitous kinase like CK2 (292). L_E mutations and CK2 inhibitors identified this enzyme in cells or recombinant form, as reactive with Thr_{47}. This event was an obligate precursor to subsequent phosphorylation with Syk at Tyr_{41}. Although several other kinases are known to require CK2 activity before they can act, for example, glycogen synthase kinase (293, 294), to our knowledge this is the first example of CK2 priming a

Syk event. Syk, another ubiquitous kinase, usually selects tyrosine sites surrounded by negative charges (295). Yet Tyr_{41} within the highly acidic domain of L_E (pI 3.7) was completely unreactive, unless CK2 was added beforehand. Cooperation between Syk and CK2 has been reported before. S. Luz et al 2011 found that CK2 and Syk will co-phosphorylate CFTR, the protein responsible for cystic fibrosis. Those data attributed the primary phosphorylation event to Syk, with the consequence as altered CFTR trafficking (296).

The exact cellular mechanistic steps enabled by L_E phosphorylation, remain to be determined, although intracellular localization, active trans-nuclear trafficking, or changes in binding partner preference are certainly possibilities. Syk reactions at Tyr_{41} were able to bypass the requirement for prior phosphorylation by CK2 at Thr_{47} when a phosphomimetic aspartate was encoded at this position (Fig. A-3). However, both sites needed to be wild-type and properly phosphorylated for maximum Nup phosphorylation (Fig. A-5). Surprisingly, the L_E phosphorylation status does not inhibit tight Ran binding (162) and the protein could be readily phosphorylated after complex formation (Fig. A-3). If simple L_E trafficking were affected by phosphorylation, one might not expect this result. Rather, we favor the idea these L_E modifications play a role subsequent to Ran binding, perhaps in the selection, tethering or retention of the actual Nup phosphorylation agents, like ERK1/2 and p38 ((74), J. Ciomperlik unpublished results). Now that sequential, defined self-phosphorylation by CK2 and Syk are acknowledged precursors to L_E-directed active trafficking inhibition, the next steps in reconstruction the full reaction cascade can be approached.

The Theilovirus Leaders, L_T and L_S are presumed to have analogous functions to L_E, and yet they differ in their display of 1-2 added short peptide insertions that are exceptionally rich in putative cellular phosphorylation motifs. Neither the L_T with $[C_{40}]$XDLD, or the L_S with $[T_{40}]$XXL[D,E], from any described virus in this species has the required CK2 consensus sequence (Sup. Fig. 1). Furthermore, only the L_S but not the L_T sequences maintain the potential secondary site (Tyr_{34}) equivalent to L_E Tyr_{41}. CK2 does not react with either protein in recombinant form, although both proteins do become phosphorylated when treated with extracts from HeLa or BHK cells (Fig. A-1). It will require extensive mutagenesis, NMR folding studies, and kinase "guesses" to establish where and how L_T and L_S encode their alternative sites. That they behave different from each other in reticulocyte extracts, suggests the individual Theilo-domains may be targeted independently. It is clear however, that each of these Leader proteins participates directly in the pathways causing Nup phosphorylation. Transfection of L_X-GST cDNA into cells directly triggered this activity. Parallel L_X zinc-finger mutations were inhibitory in all cases (Fig. A-5). These functional differences are conceivably clade-specific adaptations to particular cell types, and most probably, the respective differential phosphorylation patterns are the key to these proteins' variability.

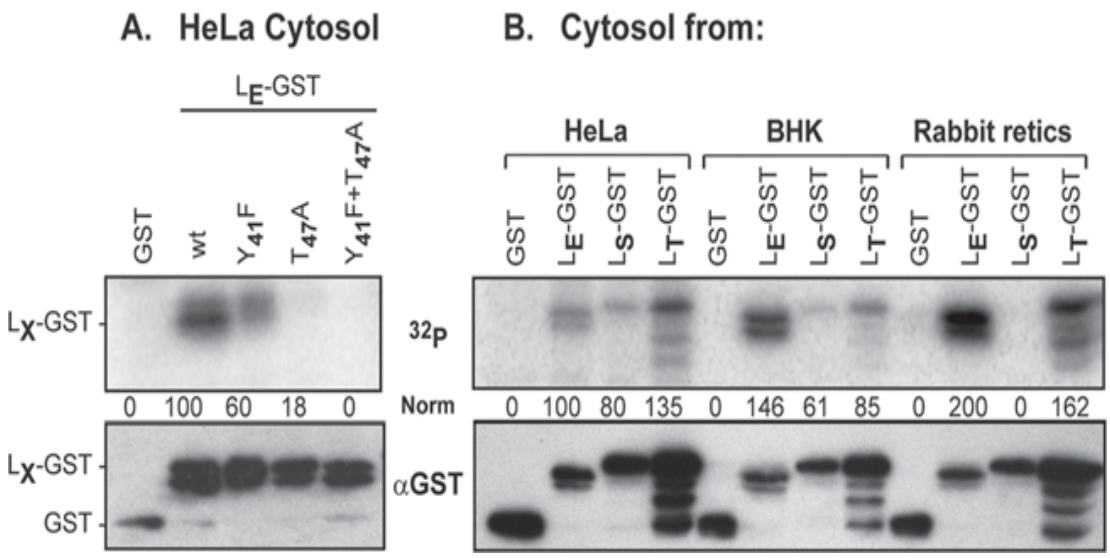

Figure A-1. 1 Lx-GST phosphorylation in cytosol. (A) Recombinant LE-GST and its phosphorylation site mutants were reacted with HeLa cytosol and [γ-32P]ATP. After SDS-PAGE, bands were detected by phosphor imaging (32P) or Western analyses (αGST). Captured pixels were normalized relative to the wild type (wt) for 32P and GST signals (Norm). (B) As described for panel A, the proteins in the recombinant Lx-GST panel were eacted with cytosol from HeLa cells, BHK cells, or rabbit reticulocytes (Rabbit retics). Normalization was to LE-GST.

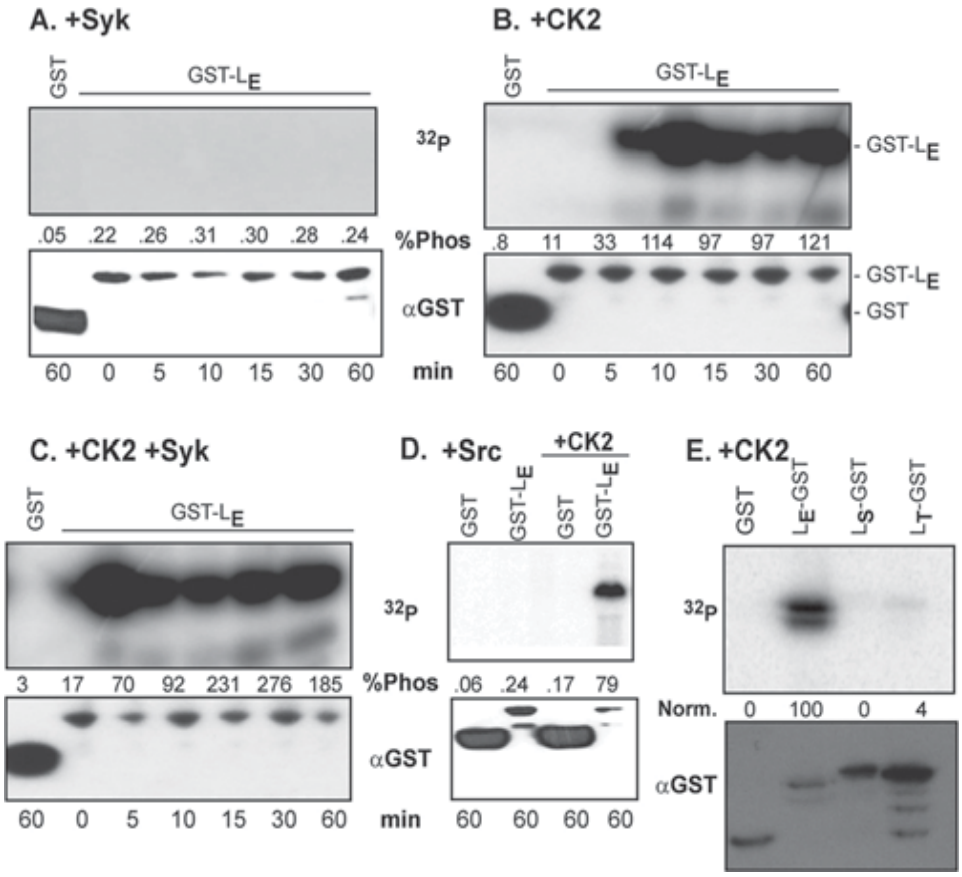

Figure A-2. Phosphorylation quantitation. (A, B, and C) GST-L_E was reacted with recombinant Syk (A), CK2 (B), or Syk plus CK2 (C) for the indicated times (min). After SDS-PAGE, samples were cut from the gel(s) and analyzed for protein and 32P content (see Materials and Methods). Averaged values for 4 replicates (see Table S2 in the supplemental material) are shown as "%Phos." (D) As described for panel B and C, GST-L_E was reacted with recombinant Src or with Src plus CK2. (E) As described for panel B, the panel of L_X-GST proteins was reacted with CK2. In this case, captured pixels were normalized to L_E-GST for 32P and GST signals (Norm).

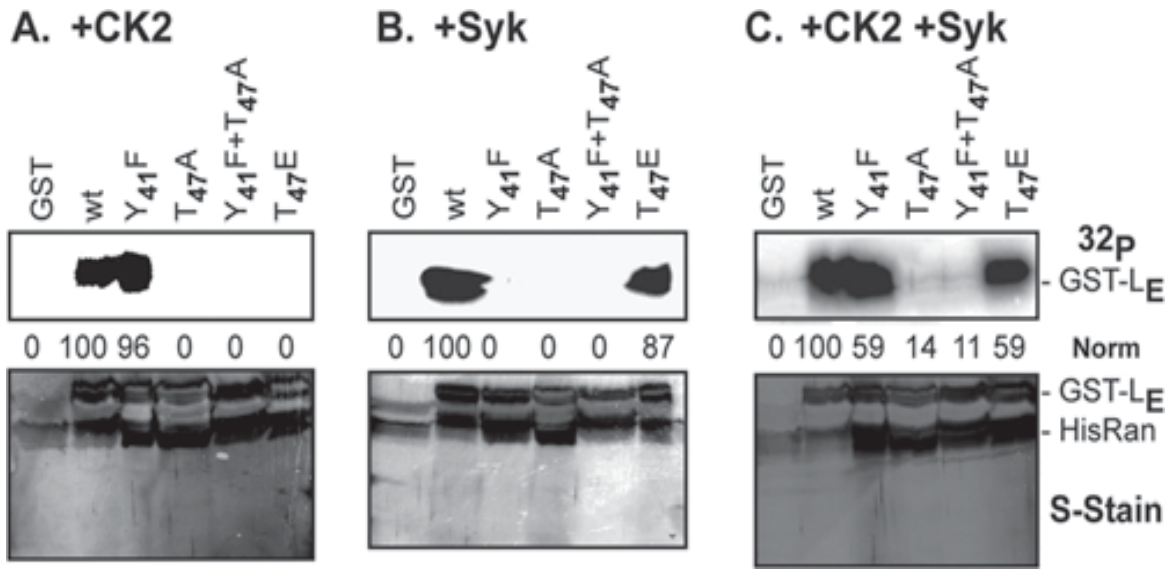

Figure A-3. Phosphorylation of GST-LE:Ran complexes. GST-LE and the indicated mutant derivatives were reacted with recombinant His-Ran. The stoichiometric (1:1) complexes were isolated as described previously (17). Equivalent fractions were reacted with [γ-32P]ATP and CK2 (A), CK2 plus Syk (C), or Syk (B) as described for Fig. A-2 (60 min). The Syk-only reactions were preceded with a prior incubation with CK2 and cold ATP. After SDS-PAGE, bands were detected by phosphorimaging (32P) or silver stain ("S-stain"). Captured pixels were averaged (n =4) and normalized relative to the wild type (wt) for 32P signals (Norm). For panels A and B, "100" denotes the maximum signal for one phosphorylation event. For panel C, "100" denotes the maximum signal for up to two events.

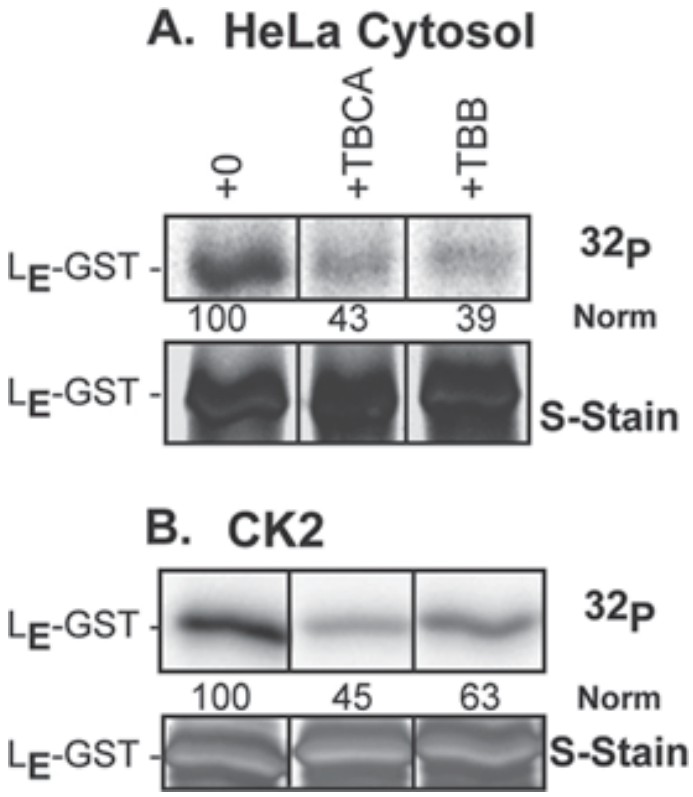

Figure A-4. CK2 inhibitors. (A) HeLa cytosol was pretreated with TBCA or TBB before LE-GST was added with [γ-32P]ATP as described for Fig. A-1A. (B) GST-LE was reacted with recombinant CK2 in the presence of TBCA or TBB and [γ-32P]ATP as described for Fig. A-2B (45 min). After SDS-PAGE, bands were detected by phosphorimaging (32P) or silver staining (S-stain). Captured pixels were normalized relative to the wild type (wt) for 32P signals (Norm).

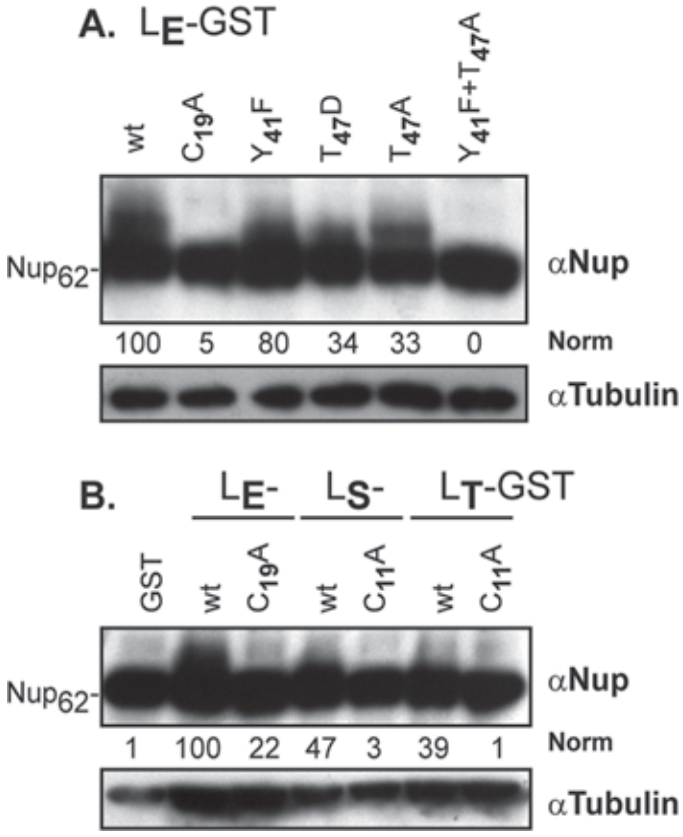

Figure A-5. Nup phosphorylation after transfection. HeLa cells were transfected with the panel of L_E-GST cDNAs (see Materials and Methods). After 24 h, the cells were collected, lysed, and then fractionated by SDS-PAGE. Western analyses were performed with αNup and αtubulin. Phosphoshift was quantified using TotalLab Quant. Normalization was relative to tubulin and the wild-type (wt) signal. Upward mobility shift values were quantified as described by Porter et al. (20). (B) As described for panel A, cDNAs for L_X-GST and inactive (C_XA) mutant derivatives were transfected into HeLa cells and then monitored for Nup_{62} phosphorylation activity.

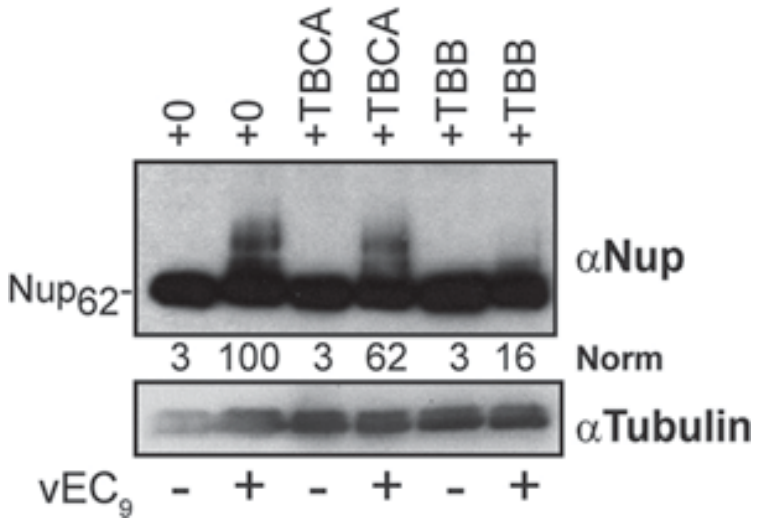

Figure A-6. Nup phosphorylation during infection. HeLa cells were pretreated with TBCA or TBB and then infected with vEC_9 (MOI=30). The inhibitors were maintained during infection. Harvested cells (5 h) were fractionated by SDS-PAGE and subjected to Western analyses as described for Fig. A-5.

References

1. Li L*, et al.* (2011) The Fecal Viral Flora of California Sea Lions. *J Virol.* 85(19):9909-9917.
2. Semler BL & Wimmer E (2002) *Molecular Biology of Picornaviruses.* (ASM Press, Washington, D.C.).
3. Honkavuori KS*, et al.* (2011) Novel picornavirus in turkey poults with hepatitis, California, USA. *Emerg Infect Dis.* 17(3):480-487.
4. Boros A*, et al.* (2014) Comparative complete genome analysis of chicken and turkey megriviruses (family Picornaviridae): long 3' untranslated regions with a potential second open reading frame and evidence for possible recombination. *J Virol* 88(11):6434-6443.
5. Adams MJ & Carstens EB (2013) Ratification vote on taxonomic proposals to the International Committee on Taxonomy of Viruses. *Arch Virology* 157:2023-2030.
6. Donnelly ML*, et al.* (2001) Analysis of the aphthovirus 2A/2B polyprotein 'cleavage' mechanism indicates not a proteolytic reaction, but a novel translational effect: a putative ribosomal 'skip'. *J Gen Virol* 82:1013-1025.
7. Hales L*, et al.* (2008) Complete genome sequence analysis of Seneca Valley virus-001, a novel oncolytic picornavirus. *J Gen Virol* 89:1265-1275.
8. Whitton JL, Cornell CT, & Feuer R (2005) Host and virus determinants of picornavirus pathogenesis and tropism. *Nature Reviews Microbiology* 3:765-776.
9. Wessels E*, et al.* (2006) Effects of picornavirus 3A proteins on protein transport and GBF1-dependent COP-I recruitment. (Translated from eng) *J Virol* 80:11852-11860 (in eng).
10. Greninger AL, Knudsen GM, Betegon M, Burlingame AL, & Derisi JL (2012) The 3A protein from multiple picornaviruses utilizes the golgi adaptor protein ACBD3 to recruit PI4KIIIβ. *J Virol.* 86(7):3605-3616.
11. Shingler KL*, et al.* (2013) The Enterovirus 71 A-particle forms a gateway to allow genome release: a CryoEM study of picornavirus uncoating. *PLoS Pathog.* 9(3):e1003240.
12. Agol VI & Gmyl AP (2010) Viral security proteins: counteracting host defences. *Nat Rev Microbiol.* 8(12):867-878.
13. Thompson D*, et al.* (2003) Economic costs of the foot-and-mouth disease outbreak in the United Kingdom in 2001. *A report prepared for Department of Environment, Food and Rural Affairs.*
14. Reddy PS*, et al.* (2007) Seneca Valley virus, a systemically deliverable oncolytic picornavirus, and the treatment of neuroendocrine cancers. *J. Natl. Cancer Inst.* 99(21):1623-1633.
15. Grünwald D & Singer RH (2012) Multiscale dynamics in nucleocytoplasmic transport. *Curr Opin Cell Biol.* 24(1):100-106.
16. Terry LJ & Wente SR (2009) Flexible gates: dynamic topologies and functions for FG nucleoporins in nucleocytoplasmic transport. *Eukaryotic Cell* 8:1814-1827.
17. Dingwall C & Laskey RA (1991) Nuclear targeting sequences--a consensus? *Trends Biochem. Sci.* 16(12):478-481.

18. Gorlich D, Vogel F, Mills AD, Hartmann E, & Laskey RA (1995) Distinct functions for the two importin subunits in nuclear protein import. *Nature* 377(6546):246-248.
19. Michaud N & Goldfarb DS (1991) Multiple pathways in nuclear transport: the import of U2 snRNP occurs by a novel kinetic pathway. *J Cell Biol.* 112(2):215-223.
20. Xu D, Farmer A, Collett G, Grishin NV, & Chook YM (2012) Sequence and structural analyses of nuclear export signals in the NESdb database. *Mol Biol Cell.* 23(18):3677-3693.
21. Nigg EA (1997) Nucleocytoplasmic transport: signals, mechanisms and regulation. *Nature* 386(6627):779-787.
22. Gorlich D (1998) Transport into and out of the cell nucleus. *EMBO J.* 17(10):2721-2727.
23. Vetter IR & Wittinghofer A (2001) The guanine nucleotide-binding switch in three dimensions. *Science* 294(5545):1299-1304.
24. Bourne HR, Sanders DA, & McCormick F (1991) The GTPase superfamily: conserved structure and molecular mechanism. *Nature* 349(6305):117-127.
25. Wennerberg K, Rossman KL, & Der CJ (2005) The Ras superfamily at a glance. *J Cell Sci.* 118(Pt 5):843-846.
26. Colicelli J (2004) Human RAS superfamily proteins and related GTPases. *Sci STKE* 2004(250):RE13.
27. Weis K (2003) Regulating access to the genome: nucleocytoplasmic transport throughout the cell cycle. *Cell* 112(4):441-451.
28. Sun C, Fu G, Ciziene D, Stewart M, & Musser SM (2013) Choreography of importin-α/CAS complex assembly and disassembly at nuclear pores. *PNAS* 110(17):E1584-1593.
29. Bischoff FR, Klebe C, Kretschmer J, Wittinghofer A, & Ponstingl H (1994) RanGAP1 induces GTPase activity of nuclear Ras-related Ran. *Proc Natl Acad Sci U S A* 91(7):2587-2591.
30. Richards SA, Lounsbury KM, & Macara IG (1995) The C Terminus of the nuclear RAN/TC4 GTPase stabilizes the GDP-bound state and mediates interactions with RCC1, Ran-GAP, and HTF9A/RanBP1. *Journal of Biological Chemistry* 270(1):14405-14411.
31. Neuwald AF, Kannan N, Poleksic A, Hata N, & Liu JS (2003) Ran's C-terminal, basic patch, and nucleotide exchange mechanisms in light of a canonical structure for Rab, Rho, Ras, and Ran GTPases. *Genome Res.* 13:673-692.
32. Wozniak RW, Rout MP, & Aitchison JD (1998) Karyopherins and kissing cousins. *Trends Cell Biol.* 8(5):184-188.
33. Strambio-De-Castillia C, Niepel M, & Rout MP (2010) The nuclear pore complex: bridging nuclear transport and gene regulation. *Nat Rev Mol Cell Biol.* 11(7):490-501.
34. Pemberton LF & Paschal BM (2005) Mechanisms of receptor-mediated nuclear import and nuclear export. *Traffic* 6(3):187-198.
35. Kohler M*, et al.* (1999) Evidence for distinct substrate specificities of importin alpha family members in nuclear protein import. *Mol Cell Biol.* 19(11):7782-7791.

36. Kalab P, Pralle A, Isacoff EY, Heald R, & Weis K (2006) Analysis of RanGTP-regulated gradient in mitotic somatic cells. *Nature* 440(7084):697-701.
37. Hahn S & Schlenstedt G (2011) Importin β-type nuclear transport receptors have distinct binding affinities for Ran-GTP. *Biochem Biophys Res Commun.* 406(3):383-388.
38. Klebe C, Prinz H, Wittinghofer A, & Goody RS (1995) The kinetic mechanism of Ran-nucleotide exchange catalyzed by RCC1. *Biochemistry* 34:12543-12552.
39. Kuhlmann J, Macara I, & Wittinghofer A (1997) Dynamic and Equilibrium studies on the interaction of Ran with its effector, RanBP1. . *Biochemistry.* 36(40):12027-12035.
40. Seewald MJ*, et al.* (2003) Biochemical characterization of the Ran-RanBP1-RanGAP system: Are RanBP proteins and the acidic tail of RanGAP required for the Ran-RanGAP GTPase reaction? *Molecular and Cellular Biology* 23:8124-8136.
41. Philipps A*, et al.* (2012) Isolation and molecular characterization of a second serotype of the Encephalomyocarditis virus. *Vet Microbiol.* 161(1-2):49-57.
42. Himeda T & Ohara Y (2012) Saffold virus, a novel human cardiovirus with unknown pathogenicity. *J Virol.* 86(3):1292-1296.
43. Stanway G*, et al.* (2005) *Family Picornaviridae.* (Elsevier Academic Press, London, United Kingdom).
44. Chiu CY*, et al.* (2008) Identification of cardioviruses related to Theiler's murine encephalomyelitis virus in human infections. *PNAS* 105(37):14124-14129.
45. Liang Z, Kumar ASM, Jones MS, Knowles NJ, & Lipton HL (2008) Phylogenetic Analysis of the species Theilovirus: Emerging Murine and Human Pathogens. *J Virol* 82:11545-11554.
46. Lin JY*, et al.* (2009) Viral and host proteins involved in picornavirus life cycle. *J Biomed Sci.* 16(103).
47. Huber SA (1994) VCAM-1 is a receptor for encephalomyocarditis virus on a murine vascular endothelial cells. *J.Virol.* 68:3453-3458.
48. Reddi HV & Lipton HL (2002) Heparan sulfate mediates infection of high-neurovirulence Theiler's viruses. . *J Virol.* 76(16):8400-8407.
49. Zhou L, Luo Y, Wu Y, Tsao J, & Luo M (2000) Sialylation of the host receptor may modulate entry of demyelinating persistent Theiler's virus. *J Virol.* 74(3):1477-1485.
50. Himeda T, Hosomi T, Okuwa T, Muraki Y, & Ohara Y (2013) Saffold Virus Type 3 (SAFV-3) Persists in HeLa Cells. *PloS one* 8(1):e53194.
51. Rueckert RR (1996) *Picornaviridae: the viruses and their replication.* (Lippincott Williams & Wilkins, Philadelphia, US) 3 Ed p 45.
52. Hughes PJ & Stanway G (2000) The 2A proteins of three diverse picornaviruses are related to each other and to the H-rev107 family of proteins involved in the control of cell proliferation. *J.Gen.Virol.* 81:201-207.
53. Takata H*, et al.* (1998) L* protein of the DA strain of Theiler's murine encephalomyelitis virus is important for virus growth in a murine macrophage-like cell line. *J Virol.* 72(6):4950-4955.

54. Loughran G, Firth AE, & Atkins JF (2011) Ribosomal frameshifting into an overlapping gene in the 2B-encoding region of the cardiovirus genome. *PNAS* 108(46):E1111-1119.
55. Chen H-H, King W-P, Zhang L, Ward BP, & Roos RP (1995) A picornaviral protein synthesized out of frame with the polyprotein plays a key role in a virus-induced immune-mediated demyelinating diease. *Nat Med.* 1:927-931.
56. Ghadge GD, Ma L, Sato S, Kim J, & Roos RP (1998) A protein critical for a Theiler's virus-induced immune system-mediate demyelinating disease has a cell type-specific antiapoptotic effect and a key role in virus persistence. *J Virol.* 72:8608-8612.
57. Asakura K, Murayama H, Himeda T, & Ohara Y (2007) Expression of L* protein of Theiler's murine encephalomyelitis virus in the chronic phase of infection. *J Gen Virol.* 88(8):2268-2274.
58. Roos RP (2002) Pathogenesis of Theiler's Murine Encehalomyelitis virus-induced disease. . *Molecular biology of Picornaviruses.*, eds Semler BL & Wimmer E (ASM Press, Washington, D.C.), 1 Ed Vol 1, pp 427-435.
59. Brahic M, Stroop WG, & Baringer JR (1981) Theiler's virus persists in glial cells during demyelinating disease. *Cell* 26(1):123-128.
60. Lin X, Thiemann NR, Pease LR, & Rodriguez M (1995) VP1 and VP2 capsid proteins of Theiler's virus are targets of H-2D-restricted cytotoxic lymphocytes in the central nervous system of B10 mice. *Virology* 214(1):91-99.
61. Lipton HL, Twaddle G, & Jelachich ML (1995) The predominant virus antigen burden is present in macrophages in Theiler's murine encephalomyelitis virus-induced demyelinating disease. *J Virol.* 69(4):2525-2533.
62. Carocci M & Bakkali-Kassimi L (2012) The encephalomyocarditic virus. *Virulence* 3(4):351-367.
63. Duke GM, Osorio JE, & Palmenberg AC (1990) Attenuation of Mengo virus through genetic engineering of the 5' noncoding poly(C) tract. *Nature* 343:474-476.
64. Nielsen AC, Bottiger B, Banner J, Hoffmann T, & Nielsen LP (2012) Serious invasive Saffold virus infections in children, 2009. *Emerg Infect Dis.* 18(1):7-12.
65. Drexler JF*, et al.* (2008) Circulation of 3 lineages of a novel Saffod cardiovirus in humans. *Emerg Infect Dis* 14(9):1398-1405.
66. Zoll J*, et al.* (2009) Saffold virus, a human Theiler's-like cardiovirus, is ubiquitous and causes infection early in life. *PLoS Pathogens* 5(5):1-10.
67. Paul S & Michiels T (2006) Cardiovirus leader proteins are functionally interchangeable and have evolved to adapt to virus replication fitness. *J. Gen. Virol* 87:1237-1246.
68. Ricour C*, et al.* (2009) Random mutagenesis defines a domain of Theiler's virus leader protein that is essential for antagonism of nucleocytoplasmic trafficking and cytokine gene expression. *J Virol* 83:11223-11232.
69. Dvorak CMT*, et al.* (2001) Leader protein of encephalomyocarditis virus binds zinc, is phosphorylated during viral infection and affects the efficiency of genome translation. *Virology* 290:261-271.

70. Zoll J, Melchers WJ, Galama JM, & van Kuppeveld FJ (2002) The mengovirus leader protein suppresses alpha/beta interferon production by inhibition of the iron/ferritin-mediated activation of NF-kappa B. *J Virol* 76(19):9664-9672.
71. Basta HA, Bacot-Davis VR, Ciomperlik JJ, & Palmenberg AC (2014) Encephalomyocarditis virus Leader is phosphorylated by CK2 and syk as a requirement for subsequent phosphorylation of cellular nucleoporins. *J Virol* 88:2219-2226.
72. Porter FW, Bochkov YA, Albee AJ, Wiese C, & Palmenberg AC (2006) A picornavirus protein interacts with Ran-GTPase and disrupts nucleocytoplasmic transport. *PNAS* 103:12417-12422
73. Porter FW & Palmenberg AC (2009) Leader-induced phosphorylation of nucleoporins correlates with nuclear trafficking inhibition of cardioviruses. *J Virol* 83:1941-1951.
74. Porter FW, Brown B, & Palmenberg A (2010) Nucleoporin phosphorylation triggered by the encephalomyocarditis virus leader protein is mediated by mitogen-activated protein kinases. *J Virol* 84:12538-12548.
75. Ricour C*, et al.* (2009) Inhibition of mRNA export and dimerization of interferon regulatory factor 3 by Theiler's virus leader protein. *J Gen Virol* 90:177-186.
76. Bardina MV*, et al.* (2009) Mengovirus-induced rearrangements of the nuclear pore complex: Hijacking cellular phosphorylation machinery. *J Virol* 83:3150-3161.
77. Borghese F & Michiels T (2011) The leader protein of cardioviruses inhibits stress granule assembly. *J. Virol.* 85(18):9614-9622.
78. Ng CS*, et al.* (2013) Encephalomyocarditis virus disrupts stress granules, the critical platform for triggering antiviral innate immune responses. *JVI* 87(17):9511-9522.
79. Roos RP, Stein S, Ohara Y, Fu J, & Semler BL (1989) Infectious cDNA clones of DA strain of Theiler's murine encephalomyelitis virus. *J.Virol.* 63:5492-5496.
80. van Eyll O & Michiels T (2000) Influence of the Theiler's virus L* protein on macrophage infection, viral persistence, and neurovirulence. *J VIrol.* 74(19):9071-9077.
81. Kong WP & Roos RP (1991) Alternative translation initiation site in the DA strain of Theiler's murine encephalomyelitis virus. *J.Virol.* 65:3395-3399.
82. Obuchi M*, et al.* (2000) L* Protein of Theiler's Murine Encephalomyelitis Virus Is Required for Virus Growth in a Murine Macrophage-Like Cell Line. *J Virol.* 74(10):4898-4901.
83. Himeda T*, et al.* (2005) A lentiviral expression system demonstrates that L* protein of Theiler's murine encephalomyelitis virus (TMEV) is essential for virus growth in a murine macrophage-like cell line. *Virus Res.* 108(1-2):23-28.
84. Asakura K, Murayama H, Himeda T, & Ohara Y (2002) Epitope-tagged L* protein of Theiler's murine encephalomyelitis virus is expressed in the central nervous system in the acute phase of infection. *J Virol.* 76(24):13049-13054.
85. Hahn H & Palmenberg AC (2001) Deletion mapping of the encephalomyocarditis virus 2A protein and the adjacent primary cleavage site. *J.Virol.* 75:7215-7218.
86. Bedard KM & Semler BL (2004) Regulation of picornavirus gene expression. *Microbes Infect.* 6(7):702-713.

87. Groppo R, Brown BA, & Palmenberg AC (2011) Mutational analysis of EMCV 2A protein identifies a nuclear localization signal and an eIF4E binding site. *Virology* 410:257-267.
88. Groppo R & Palmenberg A (2007) Cardiovirus 2A protein associates with 40S but not 80S ribosome subunits during infection. *J. Virol.* 81:13067-13074.
89. Aminev AG, Amineva SP, & Palmenberg AC (2003) Encephalomyocarditis virus (EMCV) proteins 2A and 3BCD localize to nuclei and inhibit cellular mRNA transcription but not rRNA transcription. *Virus Research* 95:59-73.
90. Aminev AG, Amineva SP, & Palmenberg AC (2003) Encephalomyocarditis viral protein 2A localizes to nucleoli and inhibits cap-dependent mRNA translation. *Virus Research* 95:45-57.
91. Medvedkina OA, Scarlat IV, Kalinina NO, & Agol VI (1974) Virus-specific proteins associated with ribosomes of Krebs-II cells infected with encephalomyocarditis virus. *FEBS Lett.* 39:4-9.
92. Svitkin YV, Hahn H, Gingras AC, Palmenberg AC, & Sonenberg N (1998) Rapamycin and wortmannin enhance replication of a defective encephalomyocarditis virus. *J.Virol.* 72:5811-5819.
93. Carocci M*, et al.* (2011) Encephalomyocarditis virus 2A protein is required for viral pathogenesis and inhibition of apoptosis. *JVI* 85(20):10741-10754.
94. Gabriel G, Herwig A, & Klenk HD (2008) Interaction of polymerase subunit PB2 and NP with importin alpha 1 is a determinant of host range of influenza a virus. *PLoS Pathog.* 4(2):e11.
95. Sasaki Y*, et al.* (2013) Importin α3/Qip1 is involved in multiplication of mutant influenza virus with alanine mutation at amino acid 9 independently of nuclear transport function. *PLoS One.* 8(1):e55765.
96. Tarendeau F*, et al.* (2007) Structure and nuclear import function of the C-terminal domain of influenza virus polymerase PB2 subunit. *Nat Struct Mol Biol.* 14(3):229-233.
97. Karlas A*, et al.* (2010) Genome-wide RNAi screen identifies human host factors crucial for influenza virus replication. *Nature* 463(7282):818-822.
98. Konig R*, et al.* (2010) Human host factors required for influenza virus replication. *Nature* 463(7282):813-817.
99. Watanabe T, Watanabe S, & Kawaoka Y (2010) Cellular networks involved in the influenza virus life cycle. *Cell Host Microbe.* 7(6):427-439.
100. Chase GP*, et al.* (2011) Influenza virus ribonucleoprotein complexes gain preferential access to cellular export machinery through chromatin targeting. *PLoS Pathog.* 7(9):e1002187.
101. Satterly N*, et al.* (2007) Influenza virus targets the mRNA export machinery and the nuclear pore complex. *PNAS* 104(6):1853-1858.
102. Rajani KR*, et al.* (2012) Complexes of vesicular stomatitis virus matrix protein with host Rae1 and Nup98 involved in inhibition of host transcription. *PLoS Pathog.* 8(9):e1002929.
103. Stojdl DF*, et al.* (2003) VSV strains with defects in their ability to shutdown innate immunity are potent systemic anti-cancer agents. . *Cancer Cell.* 4(4):263-275.
104. Shuai K & Liu B (2003) Regulation of JAK-STAT signaling in the immune system. *Nat Rev Immunol.* 3(11):900-911.

105. Kopecky-Bromberg SA, Martinez-Sobrido L, Frieman M, Baric RA, & Palese P (2007) Severe acute respiratory syndrome coronavirus open reading frame (ORF) 3b, ORF6, and nucleocapsids proteins function as interferon antagonists. *J Virol.* 81(2):548-557.
106. Frieman M*, et al.* (2007) Severe acute respiratory syndrome coronavirus ORF6 antagonizes STAT1 function by sequestering nuclear import factors on the rough endoplasmic reticulum/Golgi membrane. *J Virol.* 81(18):9812-9824.
107. Hall BE, Bar-Sagi D, & Nassar N (2002) The structural basis for the transition from Ras-GTP to Ras-GDP. *PNAS* 99(19):12138-12142.
108. Vieira AV, Lamaze C, & Schmid SL (1996) Control of EGF receptor signaling by clathrin-mediated endocytosis. *Science* 274(5295):2086-2089.
109. Ceresa BP, Kao AW, Santeler SR, & Pessin JE (1998) Inhibition of clathrin-mediated endocytosis selectively attenuates specific insulin receptor signal transduction pathways. *Mol Cell Biol.* 18(7):3862-3870.
110. Kranenburg O, Verlaan I, & Moolenaar WH (1999) Dynamin is required for the activation of mitogen-activated protein (MAP) kinase by MAP kinase kinase. *J Biol Chem.* 274:35301-35304.
111. Potenza N*, et al.* (2005) Replacement of K-Ras with H-Ras supports normal embryonic development despite inducing cardiovascular pathology in adult mice. *EMBO Rep.* 6(5):432-437.
112. Castellano E & Santos E (2011) Functional specificity of ras isoforms: so similar but so different. *Genes Cancer.* 2(3):216-231.
113. Vigil D, Cherfils J, Rossman KL, & Der CJ (2010) Ras superfamily GEFs and GAPs: validated and tractable targets for cancer therapy? *Nat Rev Cancer.* 10(12):842-857.
114. Scolnick EM & Parks WP (1974) Harvey sarcoma virus: a second murine type C sarcoma virus with rat genetic information. *J Virol.* 13(6):1211-1219.
115. Wortzel I & Seger R (2011) The ERK cascade: distinct functions with various subcellular organelles. *Genes Cancer.* 2(3):195-209.
116. Ranganathan A, Yazicioglu MN, & Cobb MH (2006) The nuclear localization of ERK2 occurs by mechanisms both independent of and dependent on energy. *J Biol Chem.* 281(23):15645-15652.
117. James BP, Bunch TA, Krishnamoorthy S, Perkins LA, & Brower DL (2007) Nuclear localization of the ERK MAP kinase mediated by Drosophila alphaPS2betaPS integrin and importin-7. *Mol Biol Cell.* 18(10):4190-4199.
118. Nishimoto S & Nishida E (2006) MAPK signalling: ERK5 versus ERK1/2. *EMBO Rep.* 7(8):782-786.
119. Khokhlatchev AV*, et al.* (1998) Phosphorylation of the MAP kinase ERK2 promotes its homodimerization and nuclear translocation. *Cell* 93(4):605-615.
120. Zarubin T & Jan J (2005) Activation and signaling of the p38 MAP kinase pathway. *Cell Res.* 15(1):11-18.
121. Remy G*, et al.* (2010) Differential activation of p38MAPK isoforms by MKK6 and MKK3. *Cell Signal.* 22(4):660-667.
122. Brancho D*, et al.* (2003) Mechanism of p38 MAP kinase activation in vivo. *Genes Dev.* 17(16):1969-1978.

123. Xu K & Shu HK (2007) EGFR activation results in enhanced cyclooxygenase-2 expression through p38 mitogen-activated protein kinase-dependent activation of the Sp1/Sp3 transcription factors in human gliomas. *Cancer Res.* 67(13):6121-6129.
124. Rubio N*, et al.* (2014) p38(MAPK)-regulated induction of p62 and NBR1 after photodynamic therapy promotes autophagic clearance of ubiquitin aggregates and reduces reactive oxygen species levels by supporting Nrf2-antioxidant signaling. *Free Radic Biol Med.* 67:292-303.
125. Barr AJ & Knapp S (2006) MAPK-specific tyrosine phosphatases: new targets for drug discovery? *Trends Pharmacol Sci.* 27(10):525-530.
126. Pearson G*, et al.* (2001) Mitogen-activated protein (MAP) kinase pathways: regulation and physiological functions. *Endocr Rev.* 22(2):153-183.
127. Manning AM & Davis RJ (2003) Targeting JNK for therapeutic benefit: from junk to gold? *Nat Rev Drug Discov.* 2(7):554-565.
128. Greenblatt MB, Shim JH, & Glimcher LH (2013) Mitogen-activated protein kinase pathways in osteoblasts. *Annu Rev Cell Dev Biol.* 29:63-79.
129. Li M, Wu ZM, Yang H, & Huang SJ (2011) NFκB and JNK/MAPK activation mediates the production of major macrophage- or dendritic cell-recruiting chemokine in human first trimester decidual cells in response to proinflammatory stimuli. *J Clin Endocrinol Metab.* 96(8):2502-2511.
130. Arthur JS & Ley SC (2013) Mitogen-activated protein kinases in innate immunity. *Nat Rev Immunol.* 13(9):679-692.
131. Shih VF, Tsui R, Caldwell A, & Hoffmann A (2011) A single NFκB system for both canonical and non-canonical signaling. *Cell Res.* 21(1):86-102.
132. Varfolomeev EE & Ashkenazi A (2004) Tumor necrosis factor: an apoptosis JuNKie? *Cell* 116(4):491-497.
133. Gradi A*, et al.* (2004) Cleavage of eukaryotic translation initiation factor 4GII within foot-and-mouth disease virus-infected cells: identification of the L-protease cleavage site in vitro. *J Virol.* 78(7):3271-3278.
134. Hinton TM, Ross-Smith N, Warner S, Belsham GJ, & Crabb BS (2002) Conservation of L and 3C proteinase activities across distantly related aphthoviruses. *J. Gen. Virol* 83:3111-3121.
135. Guarné A*, et al.* (1998) Structure of the foot-and-mouth disease virus leader protease: A papain-like fold adapted for self-processing and eIF4G recognition. *EMBO J.* 17:7469-7479.
136. Pringle CR (1999) Virus taxonomy at the XIth International Congress of Virology, Sydney, Australia. *Arch Virol* 144:2065-2070.
137. Wutz G*, et al.* (1996) Equine rhinovirus serotypes 1 and 2: relationship to each other and to aphthoviruses and cardioviruses. *J. Gen. Virol.* 77:1719-1730.
138. Hato SV*, et al.* (2010) Differential IFN-alpha/beta production suppressing capacities of the leader proteins of mengovirus and food-and-mouth disease virus. *Cell Microbiol* 12(3):310-317.
139. Castello A, Alvarez E, & Carrasco L (2011) The multifaceted poliovirus 2A protease: regulation of gene expression by picornavirus proteases. *J Biomed Biotechnol.* 2011(369648).

140. Park N, Katikaneni P, Skern T, & Gustin KE (2008) Differential targeting of nuclear pore complex protein in poliovirus-infected cells. *J Virol* 82:1647-1655.
141. Castello A, Izquierdo JM, Welnowska E, & Carrasco L (2009) RNA nuclear export is blocked by poliovirus 2A protease and is concomitant with nucleoporin cleavage. *J. Cell Science* 122:3799-3809.
142. Watters K & Palmenberg A (2011) Differential processing of nuclear pore complex proteins by rhinovirus 2A proteases from different species and serotypes. *J Virol* 85:10874-10883.
143. Zhang YZ*, et al.* (2013) The 2A protease of Enterovirus 71 cleaves nup62 to inhibit nuclear transport. *Bing Du Xue Bao.* 29(4):421-425.
144. Sharma R, Raychaudhuri S, & Dasgupta A (2004) Nuclear entry of poliovirus protease-polymerase precursor 3CD: implications for host cell transcription shut-off. *Virology* 320(2):195-205.
145. Amineva SP, Aminev AG, Palmenberg AC, & Gern JE (2004) Rhinovirus 3C protease precursors 3CD and 3CD' localize to the nuclei of infected cells. *J. Gen. Virol.* 85:2969-2979.
146. Ghildyal R*, et al.* (2009) Rhinovirus 3C protease can localize in the nucleus and alter active and passive nucleocytoplamic transport. *J. Virol.* 83:7349-7352.
147. Walker EJ*, et al.* (2013) Rhinovirus 3C protease facilitates specific nucleoporin cleavage and mislocalization of nuclear proteins in infected host cells. *PLoS One* 8(8):e71316.
148. Lidsky PL*, et al.* (2006) Nucleo-cytoplasmic traffic disorder induced by cardioviruses. *J. Virol.* 80:2705-2717.
149. Agol VI (2002) Picornavirus genome: an overview. *Molecular Biology of Picornaviruses*, eds Semler BL & Wimmer E (ASM Press, Washington, D.C.).
150. LaRue R*, et al.* (2003) A wild-type porcine encephalomyocarditis virus containing a short poly(C) tract is pathogenic to mice, pigs, and cynomolgus macaques. *J Virol.* 77(17):9136-9146.
151. Delhaye S, van Pesch V, & Michiels T (2004) The leader protein of Theiler's virus interferes with nucleocytoplasmic trafficking of cellular proteins. *J Virol* 78(8):4357-4362.
152. Romanova L*, et al.* (2009) Antiapoptotic activity of the cardiovirus leader protein, a viral "security" protein. *J Virol* 83:7273-7284.
153. Apriletti JW & Penhoet EE (1978) Cellular RNA synthesis in normal and mengovirus-infected L-929 cells. *J.Biol.Chem.* 253:603-611.
154. Gustin KE (2003) Inhibition of nucleo-cytoplasmic trafficking by RNA viruses: targeting the nuclear pore complex. . *Virus Res.* 95:35-44.
155. Crampton N, Kodiha M, Shrivastava S, Umar R, & Stochaj U (2009) Oxidative stress inhibits nuclear protein export by multiple mechanisms that target FG nucleoporins and Crm 1. *Mol Biol Cell* 20(24):5106-5116.
156. Moore MS & Blobel G (1994) Purification of a Ran-interacting protein that is required for protein import into the nucleus. *PNAS* 91(21):10212-10216.
157. Bischoff FR, Krebber H, Smirnova EA, Dong W, & Ponstingl H (1995) Co-activation of RanGTPase and inhibtion of GTP dissociation by Ran-GTP binding protein Ran BP1. *The EMBO Journal* 14(4):705-715.

158. Coutavas E, Ren M, Oppenheim JD, D'Eustachio P, & Rush MG (1993) Characterization of proteins that interact with the cell-cycle regulatory protein Ran/TC4. *Nature* 366(6455):585-587.
159. Li HY, Wirtz D, & Zheng Y (2003) A mechanism of coupling RCC1 mobility to RanGTP production on the chromatin in vivo. *J Cell Biol.* 160(5):635-644.
160. Cook A, Bono F, Jinek M, & Conti E (2007) Structural biology of nucleocytoplasmic transport. *Annu Rev Biochem.* 76:647-671.
161. Cornilescu CC, Porter FW, Zhao Q, Palmenberg AC, & Markley JL (2008) NMR structure of the Mengovirus leader protein zinc-finger domain. *FEBS Letters* 582:896-900.
162. Petty RV & Palmenberg AC (2013) Guanine-nucleotide exchange factor RCC1 facilitates a tight binding between EMCV Leader and cellular Ran GTPase. *J Virol.* 87:6517-6520.
163. Row PE & Gray JC (2000) The effect of amino acid-modifying reagents on chloroplast protein import and the formation of early import intermediates. *J. Exp. Bot.* 52(354):57-66.
164. Strong DS*, et al.* (2012) Purinergic neuromuscular transmission is selectively attenuated in ulcerated regions of inflamed guinea pig sital colon. *J. Physiol.* 588(5):847-859.
165. Baubichon-Cortay H, Broquet P, George P, & Louisot P (1989) Different reactivity of two brain sialyltransferases towards sulfhydrul reagents. Evidence for a thiol group involved in the nucleotide-sugar binding site of the NeuAC alpha 2-3Gal beta 1-3GalNAc alpha(2-6)sialyltransferase. . *Glycoconj J.* 6(1):115-127.
166. Toita R*, et al.* (2012) Fluorometric detection of protein kinase Cα activity based on phosphorylation-induced dissociation of the polyion complex. *Anal Biochem.* 424(2):130-136.
167. Arana JL & Vallejos RH (1981) Two different types of essential carboxyl groups in chloroplast coupling factors. *FEBS Letters* 123(1):103-106.
168. Gadda G, Beretta GL, & Pilone MS (1994) Chemical modification of lysyl residues of Rhodotorula gracilis D-amino acid oxidase. *Biochem Mol Biol Int.* 33(5):947-955.
169. Flügge UI*, et al.* (1991) The major chloroplast envelope polypeptide is the phosphate translocator and not the protein import receptor. *Nature* 353(1):364-367.
170. Holmgren A (1981) Selective N-bromosuccinimide oxidation of the nonfluorescent tryptophan-31 in the active center of thioredoxin from Escherichia coli. *Biochemistry* 20(11):3204-3207.
171. Friedman AL & Keegstra K (1989) Chloroplast protein import. Quantitative analysis of precursor binding. *Plant Physiology* 89(1):993-999.
172. Takahashi K (1968) The Reaction of Phenylglyoxal with Arginine Residues in Proteins. *Journal of Biological Chemistry* 243(23):6171-6179.
173. Miles EW (1977) Modification of histidyl residues in proteins by diethylpyrocarbonate. *Methods Enzymol.* 47(1):431-442.
174. Dominici P, Tancini B, & Voltattorni CB (1985) Chemical modification of pig kidney 3,4-dihydrophenylalanine decarboxylase with diethyl pyrocarbonate.

Evidence for an essential histidyl residue. . *Journal of Biological Chemistry* 260(1):10583-10589.
175. Mann M*, et al.* (2002) Analysis of protein phosphorylation using mass spectrometry: deciphering the phosphoproteome. *Trends Biotechnol* 20(6):261-268.
176. Leitner A, Foettinger A, & Lindner W (2007) Improving fragmentation of poorly fragmenting peptides and phosphopeptides during collision-induced dissociation by malondialdehyde modification of arginine residues. *J Mass Spectrom.* 42(7):950-959.
177. Lounsbury KM, Richards SA, Carey KL, & Macara IG (1996) Mutations within the Ran/TC4 GTPase. Effects on regulatory factor interactions and subcellular localization. *J. Biol. Chem.* 271:32834-32841.
178. Sekimoto T, Nakajima K, Tachibana T, Hirano T, & Yoneda Y (1996) Interferon-gamma-dependent nuclear import of Stat1 is mediated by the GTPase activity of Ran/TC4. *J Biol Chem.* 271(49):31017-31020.
179. Nilsson J, Weis K, & Kjems J (2002) The C-terminal extension of the small GTPase Ran is essential for defining the GDP-bound form. *J. Mol. Biol.* 318(2):583-593.
180. Kehlenbach RH, Assheuer R, Kehlenbach A, Becker J, & Gerace L (2001) Stimulation of nuclear export and inhibition of nuclear import by a Ran mutant deficient in binding to Ran-binding protein 1. *J Biol Chem* 276(17):14524-14531.
181. Nilsson J, Askjaer P, & Kjems J (2001) A role for the basic patch and the C terminus of RanGTP in regulating the dynamic interactions with importin beta, CRM1, and RanBP1. *J Mol Biol* 305(2):231-243.
182. Neuwald A (2009) The glycine brace: a component of Rab, Rho, and Ran GTPases associated with hinge regions of guanine- and phosphate-binding loops. *BMC Structural Biology* 9(11).
183. Guttler T & Gorlich D (2011) Ran-dependent nuclear export mediators: a structural perspective. *EMBO J.* 30(17):3457-3474.
184. Eisenthal R (1974) A New Graphical Procedure for Estimating Enzyme Kinetic Parameters. *Biochem. J.* 139:715-720.
185. Kanjee U & Houry WA (2010) An assay for measuring the activity of Escherichia coli inducible lysine decarboxylase. *J Vis Exp.* 46.
186. Basle E, Joubert N, & Pucheault M (2010) Protein Chemical Modification on Endogenous Amino Acids. *Chemistry & Biology* 17(3):213-227.
187. Laemmli UK (1970) Cleavage of Structural Proteins during the Assembly of the Head of Bacterophage T4. *Nature* 227:680-685.
188. Patridge J & Schwartz T (2009) Crystallographic and biochemical analysis of the Ran-binding zinc finger domain. *J Mol Biol* 391(2):375-389.
189. Tovchigrechko A & Vakser I (2005) Development and testing of an automated approach to proein docking. *Proteins* 60(2):296-301.
190. Tovchigrechko A & Vakser I (2006) GRAMM-X public web server for protein-protein docking. *Nucleic Acids Res* 34(2):W310-W314.
191. Bibak N, Paul RM, Freymann DM, & Yaseen NR (2004) Purification of RanGDP, RanGTP, and RanGMPPNP by ion exchange chromatography. *Analytical Biochemistry* 333(1):57-64.

192. Hall A & Lalli G (2010) Rho and Ras GTPases in axon groth, guidance, and branching. *Cold Spring Harb Perspect Biol* 2(2):a001818.
193. Walker JE, Saraste M, Runswick MJ, & Gay NJ (1982) Distantly related sequences in the alpha- and beta-subunits of ATP synthase, myosin, kinases and other ATP-requiring enzymes and a common nucleotide binding fold. *EMBO* 1(8):945-951.
194. Ramakrishnan C, Dani VS, & Ramasarma T (2002) A conformational analysis of Walker motif A [GXXXXGKT (S)] in nucleotide-binding and other proteins. *Protein Eng.* 15(10):783-798.
195. Overmeyer JH, Wilson AL, Erdman RA, & Maltese WA (1998) The putative "switch 2" domain of the Ras-related GTPase, Rab1B, plays an essential role in the interaction with Rab escort protein. *Mol Biol Cell* 9:223-235.
196. Gremer L*, et al.* (2010) Duplication of Glu37 in the switch I region of HRAS impairs effector/GAP binding and underlies Costello syndrome by promoting enhanced growth factor-dependent MAPK and AKT activation. *Hum Mol Genet* 19:790-802.
197. Rout MP*, et al.* (2000) The yeast nuclear pore complex: composition, architecture, and transport mechanism. *J Cell Biol.* 148:635-652.
198. Otsuka S, Iwasaka S, Yoneda Y, Takeyasu K, & Yoshimura SH (2008) Individual binding pockets of importin-beta for FG-nucleoporins have different binding properties and different sensitivities to RanGTP. *PNAS* 105:16101-16106.
199. Oka M*, et al.* (2010) The mobile FG nucleoporin Nup98 is a cofactor for Crm1-dependent protein export. *Mol Biol Cell* 21:1885-1896.
200. Askjaer P*, et al.* (1999) RanGTP-regulated interactions of CRM1 with nucleoporins and a shuttling DEAD-box helicase. *Mol Cell Biol* 19:6276-6285.
201. Lonhienne TG*, et al.* (2009) Importin-beta is a GDP-to-GTP exchange factor of Ran: implications for the mechanism of nuclear import. *J Biol Chem.* 284:22549-22558.
202. Bischoff FR & Ponstingl H (1991) Catalysis of guanine nucleotide exchange on Ran by the mitotic regulator RCC1. *Nature* 354(6348):80-82.
203. Seino H, Hisamoto N, Uzawa S, Sekigushi T, & Nishimoto T (1992) DNA-binding domain of RCC1 protein is not essential for coupling mitosis with DNA replication. *J Cell Sci* 102:393-400.
204. Seki T, Hayashi N, & Nishimoto T (1996) RCC1 in the Ran Pathway. *J. Biochem.* 120:207-214.
205. Nemergut ME & Macara IG (2000) Nuclear import of the ran exchange factor, RCC1, is mediated by at least two distinct mechanisms. *J Cell Biol.* 149(4):835-850.
206. Renault L, Kuhlmann J, Henkel A, & Wittinghofer A (2001) Structural basis for guanine nucleotide exchange on Ran by the regulator of chromosome condensation (RCC1). *Cell* 105:245-255.
207. Makde RD, England JR, Yennawar HP, & Tan S (2010) Structure of RCC1 chromatin factor bound to the nucleosome core particle. *Nature* 467(7315):562-566.
208. Seewald MJ, Korner C, Wittinghofer A, & Vetter IR (2002) RanGAP mediates GTP hydrolysis without an arginine finger. *Nature* 415:662-666.

209. Stewart M, Kent HM, & McCoy AJ (1998) Structural basis for molecular recognition between nuclear transport factor 2 (NTF2) and the GDP-bound form of the Ras-family GTPase Ran. *J. Mol. Biol.* 277:635-646.
210. Bacot-Davis VR & Palmenberg AC (2013) Encephalomyocarditis virus Leader protein hinge domain is responsible for interactions with Ran GTPase. *Virology* 443:177-185.
211. Delaglio F*, et al.* (1995) NMRPipe: a multidimensional spectral processing system based on UNIX pipes. *J Biomo NMR* 6:277-293.
212. Keller RLJ (2004) The computer aided resonance assignment tutorial. *Institute for Molecular Biology and Biophysics*
The Swiss Federal Institute of Technology. 1(1):1-73.
213. Goddard TD & Kneller DG (2008) SPARKY 3. *University of California, San Francisco*.
214. Shen Y, Delaglio F, Cornilescu G, & Bax A (2009) TALOS+: a hybrid method for predicting protein backbone torsion angles from NMR chemical shifts. *J Biomol NMR* 44:213-223.
215. Guntert P (2004) Automated NMR structure calculation with CYANA. *Methods Mol Biol* 278:353-378.
216. Bilbao-Cortes D, Hetzer M, Langst G, Becker PB, & Mattaj I (2002) Ran binds to chromatin by two distinct mechanisms. *Curr Biol.* 12:1151-1156.
217. Zhang C, Goldberg MW, Moore WJ, Allen TD, & Clarke PR (2002) Concentration of Ran on chromatin induces decondensation, nuclear envelope formation and nuclear pore complex assembly. *Eur J Cell Biol.* 81:623-633.
218. Smith SJM & Rittinger K (2002) Preparation of GTPases for structural and biophysical analysis. *GTPase Protocols: The Ras Superfamily.*, eds Manser EJ & Leung T (Humana Press Inc., Totowa, N.J.), Vol 189, pp 13-24.
219. Smith MJ, Neel BG, & Ikura M (2013) NMR-based functional profiling of RASopathies and oncogenic RAS mutations. *PNAS* 110:4574-4579.
220. Plafker SM & Macara IG (2002) Ribosomal protein L12 uses a distinct nuclear import pathway mediated by importin 11. *Mol Cell Biol.* 22:1266-1275.
221. Vetter IR, Nowak C, Nishimoto T, Kuhlmann J, & Wittinghofer A (1999) Structure of a Ran-binding domain complexes with Ran bound to a GTP analogue: implications for nuclear transport. *Nature* 398(1):39-46.
222. Bischoff FR & Gorlich D (1997) RanBP1 is crucial for the release of RanGTP from imporin beta-related nuclear transport factors. *FEBS Lett.* 419:249-254.
223. Sarić M*, et al.* (2007) Structural and biochemical characterization of the Importin-beta.Ran.GTP.RanBD1 complex. *FEBS Lett.* 581:1369-1376.
224. Nevo R*, et al.* (2003) A molecular switch between alternative conformational states in the complex of Ran and importin beta1. *Nat Struct Biol.* 10:553-557.
225. Boriack-Sjodin PA, Margarit SM, Bar-Sagi D, & Kuriyan J (1998) The structural basis of the activation of Ras by Sos. *Nature* 394:337-343.
226. Cherfils J & Chardin P (1999) GEFs: structural basis for their activation of small GTP-binding proteins. *Trends Biochem Sci.* 24:306-311.
227. Araki M*, et al.* (2011) Solution structue of the state 1 confomer of GTP-bound H-Ras protein and distinct dynamic properties between the state 1 and state 2 conformers. *J Biol Chem.* 286:39644-39653.

228. Hieda M*, et al.* (1999) A monoclonal antibody to the COOH-terminal acidic portion of Ran inhibits both the recycling of Ran and nuclear protein import in living cells. *J Cell Biol* 144(4):645-655.
229. Rueckert RR & Wimmer E (1984) Systematic nomenclature of picornavirus proteins. *J.Virol.* 50:957-959.
230. van Pesch V, van Eyll O, & Michiels T (2001) The leader protein of Theiler's virus inhibits immediate-early alpha/beta interferon production *J. Virol.* 75:7811-7817.
231. Hato SV*, et al.* (2007) The mengovirus leader protein blocks interferon-alpha/beta gene transcription and inhibits activation of interferon regulatory factor 3. (Translated from eng) *Cell Microbiol* 9:2921-2930 (in eng).
232. Cherfils J & Zeghouf M (2013) Regulation of small GTPases by GEFs, GAPs, and GDIs. *Physiol Rev.* 93(1):269-239.
233. de Vries SJ, van Dijk M, & Bonvin AMJJ (2010) The HADDOCK web server for data-driven biomolecular docking. *Nature Protocols* (5):883-897.
234. Gorlich D, Pante N, Kutay U, Aebi U, & Bischoff FR (1996) Identification of different roles for RanGDP and RanGTP in nuclear protein import. *EMBO J* 15(20):5584-5594.
235. Karalyan ZA*, et al.* (2013) Changes in the nuclei of infected cells at early stages of infection with EMCV. *CellBio* 2(3):125-130.
236. Monecke T*, et al.* (2009) Crystal Structure of the nuclear Export Receptor CRM1 in Complex with Snurportin 1 and RanGTP. *Science* 324:1087-1091.
237. Askjaer P, Jensen TH, Nilsson J, Englmeier L, & Kjems J (1998) The Specificity of the CRM1-Rev Nuclear Export Signal Interaction is Mediated by RanGTP. *J Biol Chem.* 273:33414-33422.
238. Schwieters CD & Clore GM (2001) The VMD-XPLOR visualization package for NMR structure refinement. *J Magn Reson* 149:239-244.
239. Davis IW*, et al.* (2007) MolProbity: all-atom contacts and structure validation for proteins and nucleic acids. *Nucleic Acids Res.*:W375-383.
240. Chen VB*, et al.* (2010) MolProbity: all-atom structure validation for macromolecular crystallography. *Acta Crystallogr D Biol Crystallogr.* 66:12-21.
241. Tina KG, Bhadra R, & Srinivasan N (2007) PIC: Protein Interactions Calculator. *Nucleic Acids Res.* (35):W473-476.
242. Anonymous (2008) The PyMOL Molecular Graphics System (DeLano Scientific LLC), 1.1r1.
243. Pettersen EF*, et al.* (2004) UCSF Chimera - A visualization system for exploratory research and analysis. *J Comput Chem* 25(13):1605-1612.
244. Kosako H & Imamoto N (2010) Phosphorylation of nucleoporins. *Nucleus* 1:309-313.
245. Zoll J, Galama JMD, van Kuppeveld FJM, & Melchers WJG (1996) Mengovirus leader is involved in the inhibition of host cell protein synthesis. *J.Virol.* 70:4948-4958.
246. Gingras AC, Svitkin Y, Belsham GJ, Pause A, & Sonenberg N (1996) Activation of the translational suppressor 4E-BP1 following infection with encephalomyocarditis virus and polio. *Proc.Natl.Acad.Sci.U.S.A.* 93:5578-5583.
247. Conti E, Muller CW, & Stewart M (2006) Karyopherin flexibility in nucleocytoplasmic transport. *Curr Opin Struct Biol.* 16(2):237-244.

248. Chook YM & Blobel G (2001) Karyopherins and nuclear import. *Current Opinion in Structural Biology* 11:703-715.
249. Roy S, Wyse B, & Hancock JF (2002) H-Ras signaling and K-Ras signaling are differentially dependent on endocytosis. *Mol Cell Biol.* 22(14):5128-5140.
250. Kim MS, Lee EJ, Kim HR, & Moon A (2003) p38 kinase is a key signaling molecule for H-Ras-induced cell motility and invasive phenotype in human breast epithelial cells. *Cancer Res.* 63(17):5454-5461.
251. Pamonsinlapatham P*, et al.* (2009) p120-Ras GTPase activating protein (RasGAP): a multi-interacting protein in downstream signaling. *Biochimie* 91(3):320-328.
252. Nassar N, Singh K, & Garcia-Diaz M (2010) Structure of the dominant negative S17N mutant of Ras. *Biochemistry* 49(9):1970-1974.
253. Muraoka S*, et al.* (2012) Crystal structures of the state 1 conformations of the GTP-bound H-Ras protein and its oncogenic G12V and Q61L mutants. *FEBS Lett.* 586(12):1715-1718.
254. White MA*, et al.* (1995) Multiple Ras functions can contribute to mammalian cell transformation. *Cell* 80(5):533-541.
255. Palacios I, Hetzer M, Adam SA, & Mattaj IW (1997) Nuclear import of U snRNPs requires importin beta. *EMBO* 16(22):6783-6792.
256. Joseph J, Tan SH, Karpova TS, McNally JG, & Dasso M (2002) SUMO-1 targets RanGAP1 to kinetochores and mitotic spindles. *J Cell Biol.* 156(4):595-602.
257. Terada K, Kaziro Y, & Satoh T (1995) Ras is not required for the interleukin 3-induced proliferation of a mouse pro-B cell line, BaF3. *J Biol Chem* 270(46):27880-27886.
258. Bustelo XR, Suen KL, Leftheris K, Meyers CA, & Barbacid M (1994) Vav cooperates with Ras to transform rodent fibroblasts but is not a Ras GDP/GTP exchange factor. *Oncogene* 9(8):2405-2413.
259. Luo RZ*, et al.* (2003) ARHI is a Ras-related small G-protein with a novel N-terminal extension that inhibits growth of ovarian and breast cancers. *Oncogene* 22(19):2897-2909.
260. Kim MJ*, et al.* (2000) Direct interaction of SOS1 Ras exchange protein with the SH3 domain of phospholipase C-gamma 1. *Biochemistry* 39(29):8674-8682.
261. Si X*, et al.* (2005) Stress-activated protein kinases are involved in Coxsackievirus B3 viral progeny release. *J Virol* 79:13875-13881.
262. Marchant D*, et al.* (2009) ERK MAP kinase-activated Arf6 trafficking directs coxsackievirus type B3 into an unproductive compartment during virus host-cell entry. *J. Gen Virol.* 90(4):854-862.
263. Wang B, Zhang H, Zhu M, Luo Z, & Peng Y (2012) MEK1-ERKs signal cascade is required for the replication of Enterovirus 71 (EV71). *Antiviral Res.* 93(1):110-117.
264. Plafker K & Macara IG (2000) Facilitated nucleocytoplasmic shuttling of the Ran binding protein RanBP1. *Mol Cell Biol.* 20(10):3510-3521.
265. Le Sage V & Mouland AJ (2013) Viral subversion of the nuclear pore complex. *Viruses* (5):2019-2042.
266. Yarbrough ML, Mata MA, Sakthivel R, & Fontoura BM (2014) Viral subversion of nucleocytoplasmic trafficking. *Traffic* 15(2):127-140.

267. Krupina KA, Sheval EV, & Lidsky PV (2010) Variability in inhibition of host RNA synthesis by entero- and cardioviruses. *J. General Virology* (91):1239-1244.
268. Thomas GM & Huganir RL (2004) MAPK cascade signaling and synaptic plasticity. *Nat Rev Neurosci.* 5(3):173-183.
269. Flores K & Seger R (2013) Stimulated nuclear import by β-like importins. *F1000Prime Rep.* 5(41).
270. Julien C, Coulombe P, & Meloche S (2003) Nuclear export of ERK3 by a CRM1-dependent mechanism regulates its inhibitory action on cell cycle progression. *J Biol Chem.* 278(43):42615-42624.
271. Hayakawa K, Arai K, & Lo EH (2010) Role of ERK map kinase and CRM1 in IL-1beta-stimulated release of HMGB1 from cortical astrocytes. *Glia.* 58(8):1007-1015.
272. Martin SF, Tatham MH, Hay RT, & Samuel ID (2008) Quantitative analysis of multi-protein interactions using FRET: application to the SUMO pathway. *Protein Sci.* 17(4):777-784.
273. Shyu YJ, Suarez CD, & Hu CD (2008) Visualization of ternary complexes in living cells by using a BiFC-based FRET assay. *Nat Protoc.* 3(11):1693-1702.
274. Yoon JW, Onodera T, & Notkins AL (1977) Virus-induced diabetes mellitus. VIII. Passage of encephalomyocarditis virus and severity of diabetes in susceptible and resistant strains of mice. *J.Gen.Virol.* 37:225-232.
275. Patrick AK, Oleszak EL, Leibowitz JL, & Rodriguez M (1990) Persistent infection of a glioma cell line generates a Theiler's virus variant which fails to induce demyelinating disease in SJL/J mice. *J.Gen.Virol.* 71:2123-2132.
276. Jones MS, Lukashov VV, Ganac RD, & Schnurr DP (2007) Discovery of a novel human picornavirus in a stool sample from a pediatric patient presenting with fever of unknown origin. *J. Clin. Microbiol.* 45(7):2144-2150.
277. Hertzler S, Liang Z, Treso B, & Lipton HL (2011) Adaptation of Saffold virus 2 for high-titer growth in mammalian cells. *Journal of virology* 85(21543476):7411-7418.
278. Chen H-H, Kong W-P, & Roos RP (1995) The leader peptide of Theiler's murine encephalomyelitis virus is a zinc-binding protein. *J.Virol.* 69:8076-8078.
279. Hahn H & Palmenberg AC (1995) Encephalomyocarditis viruses with short poly(C) tracts are more virulent than their Mengo virus counterparts. *J.Virol.* 69:2697-2699.
280. Takano-Maruyama M, Ohara Y, Asakura K, & Okuwa T (2006) Theiler's murine encephalomyelitis virus leader protein amino acid residue 57 regulates subgroup-specific virus growth on BHK-21 cells. *J. Virol.* 80:12025-12031.
281. Ho DT, Shayan H, & Murphy TH (1997) Okadaic acid induces hyperphosphorylation of tau independently of mitogen-activated protein kinase activation. *J Neurochem.* 68:106-111.
282. Hollinger S & Hepler JR (2004) Methods for measuring RGS protein phosphorylation by G protein-regulated kinases. *Methods Mol Biol.* 237:205-219.
283. Larkin M*, et al.* (2007) Clustal W and Clustal X version 2.0. *Bioinformatics (Oxford, England)* 23(21):2947-2948.

284. Blom N, Gammeltoft S, & Brunak S (1999) Sequence and structure-based prediction of eukaryotic protein phosphorylation sites. *Journal of molecular biology* 294(10600390):1351-1362.
285. Amanchy R*, et al.* (2007) A curated compendium of phosphorylation motifs. *Nature biotechnology* 25(17344875):285-286.
286. Gnad F, Gunawardena J, & Mann M (2011) PHOSIDA 2011: the posttranslational modification database. *Nucleic acids research* 39(Database):D253-D260.
287. Crooks GE, Hon G, Chandonia J-M, & Brenner SE (2004) WebLogo: A Sequence Logo Generator. *Genome Res* 14(6):1188-1190.
288. Melese T & Xue Z (1995) The nucleolus: an organelle formed by the act of building a ribosome. *Curr.Opin.Cell Biol.* 7:319-324.
289. Mócsai A, Ruland J, & Tybulewiza VL (2010) The SYK tyrosone kinase: a crucial player in diverse biological functions. *Nat Rev Immunol.* 10(6):387-402.
290. Forwood JK*, et al.* (1999) The 37-amino-acid interdomain of dengue virus NS5 protein contains a functional NLS and inhibitory CK2 site. *Biochemical and biophysical research communications* 257(10208852):731-737.
291. Keating J & Striker R (2011) Phosphorylation events during viral infections provide potential therapeutic targets. *Reviews in medical virology* 22(3):166-181.
292. Grankowski N, Boldyreff B, & Issinger OG (1991) Isolation and characterization of recombinant human casein kinase II subunits alpha and beta from bacteria. *European journal of biochemistry / FEBS* 198(2040287):25-30.
293. Wang Y & Roach PJ (1993) Inactivation of rabbit muscle glycogen synthase by glycogen synthase kinase-3. Dominant role of the phosphorylation of Ser-640 (site-3a). *The Journal of biological chemistry* 268(8226927):23876-23880.
294. Fiol CJ, Wang A, Roeske RW, & Roach PJ (1990) Ordered multisite protein phosphorylation. Analysis of glycogen synthase kinase 3 action using model peptide substrates. *The Journal of biological chemistry* 265(2156841):6061-6065.
295. Hornbeck P*, et al.* (2012) PhosphoSitePlus: a comprehensive resource for investigating the structure and function of experimentally determined post-translational modifications in man and mouse. *Nucleic acids research* 40(D1):D261-D270.
296. Luz S*, et al.* (2011) Contribution of Casein Kinase 2 and Spleen Tyrosine Kinase to CFTR Trafficking and Protein Kinase A-Induced Activity. *Molecular and cellular biology* 31(22):4392-4404.